Unlocking Iminium Catalysis in Artificial Enzymes to Create a Friedel-Crafts Alkylase

Reuben B. Leveson-Gower[1], Zhi Zhou[1], Ivana Drienovská[1,2], Gerard Roelfes[1]*

[1]Stratingh Institute for Chemistry, University of Groningen, 9747 AG, Groningen, The Netherlands. [2]Current address: Department of Chemistry and Pharmaceutical Sciences, VU Amsterdam, De Boelelaan 1108, 1081 HZ Amsterdam, The Netherlands

* j.g.roelfes@rug.nl

ABSTRACT

The construction and engineering of artificial enzymes consisting of abiological catalytic moieties incorporated into protein scaffolds is a promising strategy to realise new mechanisms in biocatalysis. Here, we show that incorporation of the non-canonical amino acid para-aminophenylalanine (pAF) into the non-enzymatic protein scaffold LmrR creates a proficient and stereoselective artificial enzyme (LmrR_pAF) for the vinylogous Friedel-Crafts alkylation between α,β-unsaturated aldehydes and indoles. pAF acts as a catalytic residue, activating enal substrates towards conjugate addition via the formation of intermediate iminium ion species, whilst the protein scaffold provides rate acceleration and enantio-induction. Improved LmrR_pAF variants were identified by low-throughput directed evolution advised by alanine-scanning to obtain a triple mutant that provided higher yields and enantioselectivities for a range of aliphatic enals and substituted indoles. Analysis of Michaelis-Menten kinetics of LmrR_pAF and evolved mutants reveals that new activities emerge via evolutionary pathways that diverge from one another and specialise catalytic reactivity. Translating this iminium-based catalytic mechanism into an enzymatic context will enable many new biocatalytic transformations inspired by organocatalysis.

INTRODUCTION

The enantioselective Friedel-Crafts alkylation of arenes is an important reaction in both synthetic chemistry and biosynthesis.[1–4] The use of enzymes as catalysts for this transformation is of great appeal due to their mild, efficient, benign and highly selective nature, however relatively few enzymes are known to perform this chemistry.[4–7] Notable examples are tryptophan synthase (TrpB),[8] a promiscuous enzyme involved cylindrocyclophane biosynthesis (CylK),[9,10] as well as enzymes which catalyse Friedel-Crafts acylation (*Pp*ATase) (Figure 1(a)).[11,12] Catalytic machinery in these enzymes includes nucleophilic cysteine residues as well as pyridoxal phosphate, each powerful chemical motifs which have inspired biomimetic catalysis strategies.[13,14] Artificial enzymes have also been employed for Friedel-Crafts alkylation reactions by Cu^{II} Lewis acid activation of α,β-unsaturated imidazole ketones, employing proteins or DNA as a scaffold to afford rate acceleration and enantioselectivity.[15,16] An effective chemocatalytic strategy for Friedel-Crafts alkylation of arenes employs secondary-amine organocatalysts (e.g. MacMillan imidazolidinone catalysts) to activate α,β-unsaturated aldehydes as iminium ions (Figure 1(b)).[1,17,18] The iminium ion species is a highly versatile reaction intermediate[19] which has previously been exploited in designer enzymes featuring catalytic lysine or N-terminal proline residues, and in artificial enzymes with secondary-amine-containing unnatural cofactors.[20–25] However, Friedel-Crafts alkylation via an iminium ion species has not been demonstrated in these contexts, and is a distinct reaction pathway from those employed by natural enzymes for this reaction. We saw great potential in unlocking iminium catalysis to create an artificial Friedel-Crafts alkylase by using expanded genetic code technology to provide an appropriate non-canonical catalytic residue.[26]

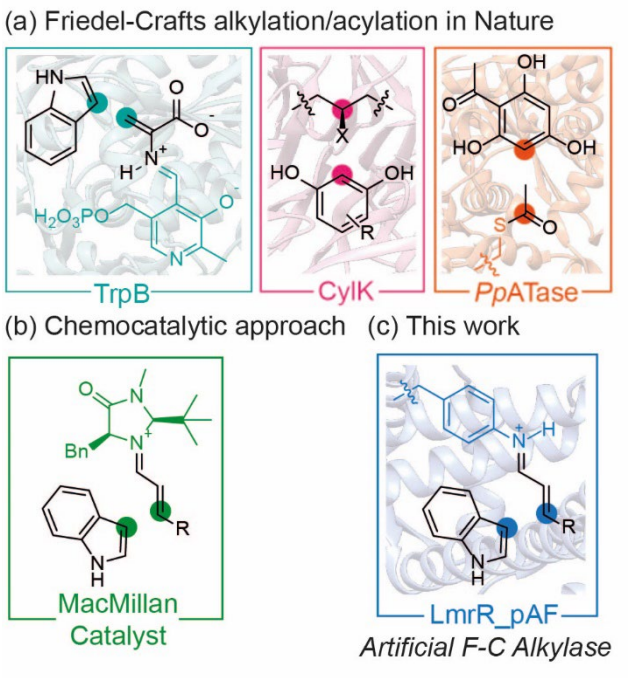

Figure 1: (a) biocatalytic strategies of natural enzymes which catalyse aromatic alkylation/acylation (b) organocatalytic approach to vinylogous Friedel-Crafts alkylation; (c) approach followed in this work: an artificial enzyme using expanded genetic code technology to incorporate a non-canonical catalytic residue which operates via *a non-natural mechanism.*

Artificial enzymes consist of an abiological catalyst incorporated into a protein scaffold which provides stereoselectivity and rate acceleration, as well as the opportunity for genetic optimisation.[27–29] Strategies to assemble these two components include covalent protein modification, supramolecular and 'trojan-horse' strategies.[30,31] Our group has recently pioneered the use of non-canonical amino acids (ncAAs) with inherent catalytic properties for artificial enzyme construction, where the catalytic component is incorporated directly into the protein's peptide-chain during biosynthesis using expanded genetic code technology.[26,32,33] Judicious choice of protein scaffold is also essential for success; in this study, as in our previous work, we employ the Lactococcal multidrug resistance regulatory (LmrR) protein. This homodimeric protein (15 kDa per monomer) has a unique structural feature, a large hydrophobic pocket situated at the dimer interface, which binds planar organic molecules in its physiological function, and affords rate-acceleration and enantio-induction of catalysis conducted inside it.[34–36] We incorporated the aniline containing ncAA para-aminophenylalanine (pAF) at position 15 in hydrophobic pocket of LmrR, creating LmrR_pAF, an artificial enzyme for the hydrazone formation reaction which acts *via* a trans-amination mechanism employing pAF as the catalytic residue.[34,35] A similar strategy has been employed by Green and coworkers, who showed that incorporation of N-methyl histidine into a protein scaffold could endow ester-hydrolase activity.[37] More recently, we also employed the pAF catalytic residue in a synergistic system, where α,β-unsaturated aldehydes were activated for conjugate addition by enolate nucleophiles activated by a Cu^{II} cofactor.[38] In this work we show LmrR_pAF as a means to translate the iminium catalysis mechanism from organocatalysis into a designer enzyme, facilitating a vinylogous Friedel-Crafts alkylation of indole substrates (Figure 1(c)). Situating the pAF residue within the LmrR microenvironment significantly enhances its inherent catalytic properties and paves a path towards further new-to-nature reactions.

RESULTS AND DISCUSSION

INITIAL CATALYSIS EXPERIMENTS

We initially explored the vinylogous Friedel-Crafts alkylation of 2-methyl-indole (**2a**) with trans-2-hexenal (**1a**) catalysed by LmrR_pAF to form product **3a** after *in situ* reduction with sodium borohydride, which makes the product amenable to HPLC analysis.[39] We found that with just 2 mol% loading, LmrR_pAF could catalyse the transformation of **1a** and **2a** to give **3a** with a moderate yield and enantioselectivity (Table 1, Entry 1). Without pAF incorporated, LmrR itself gives negligible yield and enantioselectivity under the same conditions (Table 1, Entry 2). Lysine, which is used as a catalytic residue in nature, e.g. aldolase A,[40] when incorporated at position V15 in LmrR fails to endow the protein with catalytic activity for this transformation (Table 1, Entry 3). Likewise, mutation of the same position to tyrosine, in effect, single-functional group mutagenesis of the amino moiety of pAF to the canonical hydroxy moiety, also abrogates catalytic activity demonstrating the necessity of the aniline functional group for catalysis (Table 1, Entry 4). Even at equimolar catalyst loadings, aniline itself affords only 8% yield of **3a**, demonstrating the importance of the chemical environment provided by the hydrophobic pocket of LmrR for rate acceleration (Table 1, Entry 5). Finally, we ruled out the efficacy of an artificial enzyme based on the supramolecular assembly between LmrR and aniline by combining these two catalysts in a ratio typically employed in supramolecular catalysis (Table 1, Entry 6).[15]

*Table 1: Initial results of LmrR_pAF catalysed formation of **3a** from **1a** and **2a**, and control reactions.*

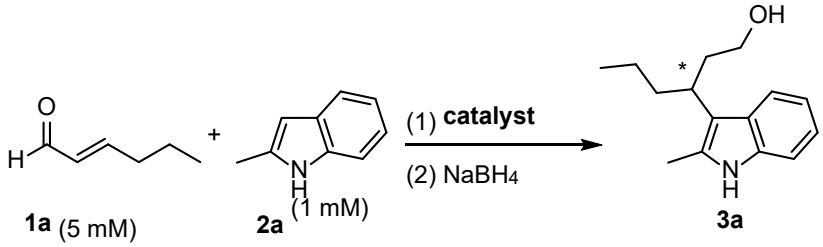

Entry	Catalyst	Yield (%)[a]	ee (%)[b]
1	LmrR_pAF (20 μM)	42 ± 4	45 ± 0
2	LmrR (20 μM)	2 ± 0	N.D.[c]
3	LmrR_V15K (20 μM)	3 ± 0	N.D. [c]
4	LmrR_V15Y (20 μM)	2 ± 0	N.D. [c]
5	Aniline (1 mM)	8 ± 0	-
6	LmrR (20 μM) + aniline (16 μM)	4 ± 0	N.D. [c]

*Reaction conditions: LmrR variants (20 μM dimer concentration) in phosphate buffer (50 mM, pH 6.5) containing NaCl (150 mM) and 8 vol% DMF, [**2a**] = 1 mM, [**1a**] = 5 mM, reaction time 16 hours at 4 °C with mixing by continuous inversion in 300 μL total volume. Reduction with $NaBH_4$ (60 μL, 20 mg mL^{-1} in 0.5 w/v% NaOH) afforded the alcohol product 3a. For each entry, two independent experiments were conducted, each in duplicate. Errors are the standard deviation of the results. [a]Yields determined by normal-phase HPLC (Chiralcel® OJ-H) with 3-(3-hydroxypropyl)indole as internal standard. [b]Enantiomeric excess determined by chiral normal-phase HPLC (Chiralcel® OJ-H). [c] N.D., not determined*

ALANINE SCANNING

With a good starting activity achieved by LmrR_pAF for the formation of **3a**, we sought to probe residues near the active site for their importance in catalysis by alanine scanning. Guided by the structure of LmrR_pAF we selected a total of twelve positions – E7, A11, L18, N19, K22, N88, M89, A92, F93, S95, S97 and D100 (Figure 2) choosing residues which we considered important for catalysis by LmrR-based artificial enzymes based on our previous studies, as well as several others which are close to the catalytic residue but are less well investigated.[41–43] We mutated these positions to alanine, except in the cases of A11 and A92 which are already alanine in the wild-type LmrR sequence, where we chose mutations which have previously proved beneficial for catalysis for LmrR-based artificial enzymes namely A11L and A92E.[41–43] We purified these twelve variants and assessed them in the production of **3a,** comparing the enantioselectivity and yield obtained with that obtained with LmrR_pAF (Figure 2, Supplementary Table S1).

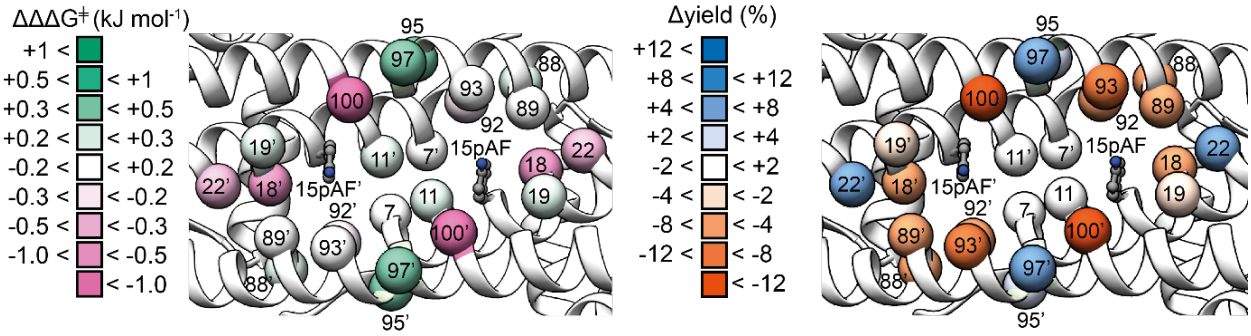

*Figure 2: analysis of the effects of mutations of residues close to the catalytic residue of LmrR_pAF in catalysis of the reaction of **1a** and **2a** to produce **3a**. The alpha-carbon atoms of residues mutated are shown as spheres in the crystal structure of LmrR_pAF (PDB: 6I8N. Reactions were conducted under the standard reaction conditions outlined in table 1. Enantioselectivity was visualized as the effect on relative Gibbs' free energies of the diastereomeric transition states leading to formation of the two enantiomers of **3a** which was calculated from the enantiomeric ratio according to the equation $\Delta\Delta\Delta G^{\ddagger} = -RT\ln(e.r.)$. The results are shown on a scale from green (increased e.r.) to pink (decreased e.r.). Δyield values are the differences in yields obtained when employing different mutants in catalysis for **3a** product under the standard conditions, relative to LmrR_pAF, and are shown on a scale from blue (increased yield) to orange (decreased yield).*

Of the twelve mutants tested, five (namely E7A, A11L, N19A, N88A and M89A) showed no significant effect on the catalytic results. One mutation, D100A, abrogated catalytic activity. Some of our previous work with LmrR-based enzymes also found this position to be immutable for catalysis, suggesting that it may be crucial for proper protein folding.[43,44] Mutations at the six remaining residues produced larger, positive or negative, effects on the yield and enantioselectivity obtained in catalysis, indicating a greater importance for catalytic activity. We also tested the twelve mutants in the cell-free extract (CFE), and observed a similar trend in the catalysis results to those obtained with purified proteins (Supplementary Table S2). Together, these results enabled a focussed directed evolution campaign by prioritising mutations at positions whose importance was highlighted by our alanine scanning as demonstrated in our previous work.[42]

DIRECTED EVOLUTION

We created randomised codon libraries at the six positions shown to be important for catalysis with alanine scanning (L18, K22, A92, F93, S95, S97).[45] We opted for the NDT codon, which encodes 12 amino acids with a good representation of the functional diversity of all 20 proteogenic amino acids.[46] The degenerate codon libraries were produced by QuikChange PCR and their qualities were confirmed with pooled plasmid sequencing.[47] Cell-free extracts obtained from the resultant libraries were screened by chiral-HPLC and mutants that had beneficial effects on enantioselectivity and yield were verified with purified protein (representative screening results presented in Supplementary Figure 1, summary of hits identified in Supplementary Table S3). After one round of screening, we found a few improved mutants, including L18R and S95G, which afford higher yield and enantioselectivity in production of **3a** relative to LmrR_pAF (Figure 3, Supplementary Table S4). Gratifyingly, these particular mutants produced a synergistic effect when combined, giving yet further improvements in the double mutant LmrR_pAF_L18R_S95G (Figure 3, Supplementary Table S4). In a similar manner, we continued with a second round of library screening, selecting five positions close to the catalytic residue for randomisation. This second round of screening identified one further improved mutant, LmrR_pAF_L18R_S95G_M89N (hereafter, LmrR_pAF_RGN) which affords the product **3a** with a yield of 74 % and an enantiomeric excess of 87 % under our standard reaction conditions (Figure 3, Supplementary Table S4). As with LmrR_pAF, mutation of the catalytic residue in LmrR_pAF_RGN to either lysine or tyrosine abrogates activity (Supplementary Table S4).

Whilst the nature of the contributions of these mutations towards efficient and selective catalysis is hard to rationalise, it is notable that both this directed evolution campaign and our previous campaign with LrmR_pAF found mutants with an arginine residue close to the catalytic residue (previously A92R was identified).[41] Positively charged residues in enzymes with catalytic lysine or proline residues are known to promote catalysis by perturbing pK_as in the active site, or stabilising negatively charged intermediates.[48–51] It is possible that R18 facilitates stereo selective iminium formation, shown to be the stereoselectivity determining step in the Friedel-Crafts reaction,[52] acting as a primitive oxyanion hole to promote hemiaminal formation or dehydration. Since the asparagine mutation at position M89 also introduces a new sidechain with hydrogen accepting properties this residue plausibly cooperates with R18 during iminium ion formation. Mutation of the S95 residue to glycine involves a significant shift in helical propensity[53] and thus may perturb the secondary structure in the particularly dynamic α4 helix,[36,54] thus shifting the conformational ensemble toward more catalytically productive states.[55,56]

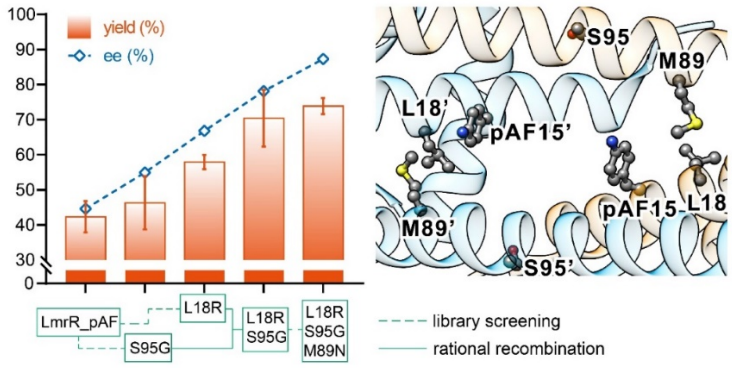

*Figure 3: Left: Yields and enantioselectivities of mutants obtained throughout directed evolution of LmrR_pAF for the formation of **3a**, results with purified protein under standard conditions outlined in table 1. Mutations were obtained by screening of degenerate codon libraries (dashed lines), or by rational recombination (solid lines). Right: positions of residues mutated in LmrR_pAF_RGN are shown in the crystal structure of LmrR_pAF (PDB: 6I8N).*

SUBSTRATE SCOPE

We assessed the performance of LmrR_pAF and LmrR_pAF_RGN with a variety of indole and enal substrates, finding that the evolved mutant outperformed the parent in both yields and enantioselectivities for almost all tested substrate combinations. Isopropyl and methyl groups in the beta-position of the enal afforded products **3b** and **3c** with moderate and excellent yields, respectively. In the case of **3b** only a small loss in enantioselectivity was observed when LmrR_pAF_RGN was used as catalyst, compared with product **3a**. Notably, cinnamaldehyde (product **3d**) was not tolerated well, giving very low yields with both LmrR_pAF and LmrR_pAF_RGN. However, using the same loading of LmrR (entry 5) did not afford product **3d**, suggesting that the pAF residue is involved in catalysis.

When different indole substrates were employed together with trans-2-hexenal **1a** the corresponding products were obtained with moderate to good yields, with LmrR_pAF_RGN showing improved results in each case. Using this evolved artificial enzyme, unsubstituted indole, 5-methyl-indole and 5-methoxy-indoles were converted to products **3e-3g** without any loss in enantioselectivity compared to the 2-methyl-indole substrate employed in our directed evolution. For products **3e** and **3g**, the major enantiomer can be tentatively assigned as *(S)*-configured based on comparison with order of elution on chiral normal-phase HPLC to the literature.[39] With the doubly substituted 5-methoxy-2-methyl-indole product **3i** was obtained with a good yield and with little loss in enantioselectivity compared to **3a**. The electron poor 5-bromo-indole proved unreactive under standard conditions (product **3h**), affording no product. In general, LmrR_pAF, but especially the evolved LmrR_pAF_RGN, maintain enantioselectivity with changes in the steric/electron properties of the substrate. This tolerance towards structurally diverse substrates highlights our evolved mutant as a promising lead for the generation of a highly selective and generally applicable biocatalyst for this Friedel-Crafts alkylation.

*Table 2: Substrate scope of indoles and enals converted to the corresponding Friedel-Crafts products **3a-3i** by LmrR_pAF and LmrR_pAF_RGN*

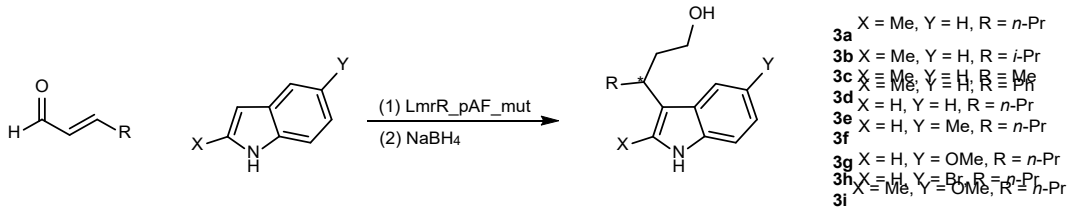

LmrR_pAF				LmrR_pAF_RGN			
Entry	**Product**	**Yield (%)[a]**	**ee (%)[b]**	**Entry**	**Product**	**Yield (%)[a]**	**ee (%)[b]**
1	**3a**	42 ± 4	45 ± 0	11	**3a**	74 ± 2	87 ± 0
2[c]	**3b**	24 ± 1	58 ± 0	12[c]	**3b**	34 ± 6	83 ± 2
3	**3c**	76 ± 7	33 ± 1	13	**3c**	95 ± 7	58 ± 1
4	**3d**	3 ± 0	20 ± 1	14	**3d**	4 ± 1	13 ± 9
5[d,e]	**3d**	< 1	-				
6[f]	**3e**	10 ± 1	50 ± 0	15[f]	**3e**	27 ± 2	89 ± 1
7[f]	**3f**	16 ± 1	41 ± 0	16[f]	**3f**	31 ± 3	89 ± 2
8[f]	**3g**	24 ± 2	55 ± 1	17[f]	**3g**	40 ± 3	89 ± 1
9[e]	**3h**	< 1	-	18[e]	**3h**	< 1	-
10	**3i**	62 ± 11	58 ± 0	19	**3i**	75 ± 9	82 ± 1

*Reaction conditions: LmrR variants (20 µM dimer concentration) in pH 6.5 buffer containing NaCl (150 mM) and NaH_2PO_4 (50 mM), 8 vol% DMF, [indole] = 1 mM, [enal] = 5 mM, reaction time 16 hours, reactions conducted at 4 °C with mixing by continuous inversion in 300 µL total volume. Reduction with $NaBH_4$ (60 µL, 20 mg mL^{-1} in 0.5 w/v% NaOH) afforded the alcohol products **3a-3i**. For each entry, two independent experiments were conducted, each in duplicate. Errors are the standard deviation of the results thus obtained. [a]Yields determined using normal phase HPLC using 3-(3-hydroxypropyl)indole as internal standard. [b]Enantiomeric excess determined using chiral normal-phase HPLC (Chiracel OJ-H (3a), AS-H (3b, 3c, 3f), OD-H (3d, 3e, 3h, 3i) or OB-H (3g)). [c] Reaction time 40 hours. [d] LmrR was used in place of LmrR_pAF. [e] No product could be detected. [f] 50 µM artificial enzyme (concentration of dimer) was used, reaction time 64 hours.*

KINETIC ANALYSIS

Having genetically optimised LmrR_pAF for both Friedel-Crafts alkylation and hydrazone formation[41] we wanted to assess if the mutations in each evolved variant promote catalysis by the pAF residue in a general, or reaction specific, manner.[57,58] In order to assess this, we selected three mutants for comparison, LmrR_pAF, LmrR_pAF_RGN, as well as the mutant with the highest k_{cat} for the hydrazone formation reaction studied in our previous work, LmrR_pAF_RMH.[41] We then determined the kinetic parameters for one substrate according to the Michaelis-Menten equation for both the transformation of **1a** and **2a** into **3a** (Table 3, Supplementary Figure S2) as well as the hydrazone formation reaction between **4** and **5** to give **6** (Table 4, Supplementary Figures S3 and S4).

Focusing on the Friedel-Crafts alkylation, we saw that the evolved mutant LmrR_pAF_RGN has a significantly decreased K_M for the enal **1a**, indicating increased affinity towards this substrate (Table 3). The k_{cat} for this mutant is also somewhat decreased relative to LmrR_pAF, which may be an expense paid for selecting based on enhanced stereoselectivity, and not on enhanced kinetic properties. An overall increase in catalytic efficiency (k_{cat}/K_M) of around 60% is obtained over the course of the evolution. Relative to LmrR_pAF, however, LmrR_pAF_RMH has a similar K_M for the enal **1a**, but a ~5 fold decrease in k_{cat}, and an overall ~8-fold loss in catalytic efficiency, demonstrating that increased activity for hydrazone formation emerges at the expense of a promiscuous activity (Table 3). Indeed, the same characteristic is observed with LmrR_pAF_RGN in the hydrazone forming reaction, it shows an increased K_M for the hydrazine **5**, and a ~2-fold loss in k_{cat} relative to LmrR_pAF, resulting in a ~3-fold drop in catalytic efficiency (Table 4). Directed evolution of this enzyme for the Friedel-Crafts reaction gave a more modest increase in catalytic efficiency compared to our previous directed evolution for hydrazone formation, but a smaller loss in the promiscuous activity not under selection is also observed.

*Table 3: Michaelis-Menten kinetic parameters calculated for a single substrate, **1a**, for the Friedel-Crafts reaction between **1a** and **2a** to give **3a**.*

Mutant	$K_{M\text{-}1a,\ app}$ (mM)	$k_{cat,\ app}$ (s^{-1}) x 10^2	$(k_{cat}/K_M)_{app}$ ($M^{-1}s^{-1}$)	vs. LmrR_pAF
LmrR_pAF	18.2 ± 2.8	1.45 ± 0.11	0.80 ± 0.06	1
LmrR_pAF_RGN	5.2 ± 0.9	0.64 ± 0.03	1.25 ± 0.17	1.56
LmrR_pAF_RMH	25.7 ± 6.6	0.27 ± 0.04	0.11 ± 0.02	0.14

*Determined at 25 °C in phosphate buffer (50 mM) containing NaCl (150 mM) and 5% (v/v) DMF at pH 6.5. **2a** was kept at a concentration of 1 mM and **1a** was varied between 2 mM and 30 mM.*

*Table 4: Michaelis-Menten kinetic parameters calculated for a single substrate, **5**, for the hydrazone formation reaction between **4** and **5** to give **6**.*

4 5 6

Mutant	$K_{M\text{-}5,\ app}$ (µM)	$k_{cat,\ app}$ (s^{-1}) x 10^3	$(k_{cat}/K_M)_{app}$ ($M^{-1}s^{-1}$)	vs. LmrR_pAF
LmrR_pAF[a]	122 ± 10	0.23 ±0.01	1.85 ± 0.08	1
LmrR_pAF_RGN	203 ± 87	0.11 ± 0.03	0.56 ± 0.17	0.30
LmrR_pAF_RMH[a]	38 ± 4	3.98 ± 0.16	105 ± 7	56.7

*Determined at 25 °C in phosphate buffer (50 mM) containing NaCl (150 mM) and 5% (v/v) DMF at pH 7.4. The estimated errors reflect the standard deviation from three independent experiments. **4** was kept at a constant concentration of 5 mM, the concentration of **5** was varied from 20 to 200 µM. [a]Data from ref. 41.*

Together these results show that in both this study and our previous work new activities in LmrR_pAF evolve at the expense of others, i.e. divergent evolution of function or "evolutionary trade-offs" (Figure 4). Such specialisation is often observed in natural and laboratory evolution[57,59] and may play an important role in the evolution of new enzyme function in nature after gene duplication.[60] In most cases in natural enzymes, losses in the activity not under selection pressure are significantly lower than gains in the selected activity, probably related to organism fitness retention, however our results show a more pronounced specialisation effect.[57] Specialisation through mutation has been employed to tune product distributions obtained from promiscuous natural enzymes,[61] and to unlock new-to-nature reactivities in engineered enzymes.[62] Here we have shown that we can exploit this effect in promiscuous enzymes that operate with non-canonical catalytic machinery in order to specialise them towards selective and useful transformations (Figure 4).

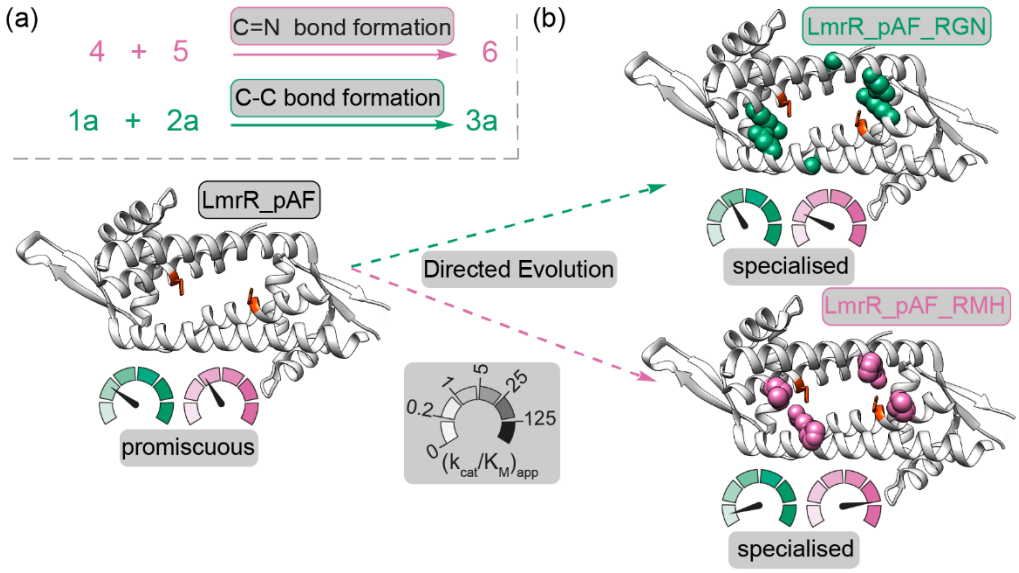

Figure 4: (a) Promiscuous transformations catalysed by LmrR_pAF. (b) Directed evolution has specialised LmrR_pAF, increasing catalytic efficiency for reaction selected for, whilst the promiscuous activity is concomitantly diminished, giving specialised variants LmrR_pAF_RMH and LmrR_pAF_RGN.

DISCUSSION AND IMPLICATIONS

Aniline and its derivatives are rather limited in their catalytic capabilities[63–65] which include hydrazone formation previously demonstrated with LmrR_pAF[32,41] but not the full breadth of iminium-based transformations catalysed by other amine catalysts.[19] Here we have demonstrated that the microenvironment provided by the LmrR scaffold expands the catalytic properties of the pAF residue beyond those inherent to the sidechain by itself, achieving catalysis normally associated with secondary amines. However, the lack of steric bulk about the amino moiety in pAF may also permit conversion of substrates which are challenging for secondary amine catalytic groups seen in other promiscuous and artificial enzymes.[23,66,67]

Compared to the earlier reported Cu(II) based artificial enzymes for Friedel-Crafts alkylation reactions,[68] the reaction developed herein is not only metal-free, but the need for a chelating group in the substrate is also obviated. Instead, both the enal substrate and the product contain aldehyde moieties, whose set of functional-group interconversions is extremely diverse, including the in-situ reduction to alcohol shown herein.[69] Whilst some natural and engineered enzymes are now known to catalyse Friedel-Crafts alkylation and acylation, the substrate scope of the arene component is limited to (poly)-hydroxylated resorcinol derivatives.[9–11] Secondary amine-based organocatalysts catalyse the Friedel-Crafts alkylation of activated arenes with α,β-unsaturated aldehydes.[1,17,18] However, often, high catalyst loadings, organic solvents and

cryogenic temperatures are required.[70] Here we demonstrate how this reaction can be conducted with reduced catalyst loadings, in aqueous media without significant change from ambient temperature with a catalyst that can be genetically optimised using the Darwinian algorithm.

CONCLUSIONS

Here we have shown how iminium-based mechanisms from organocatalysis can be translated into a biocatalytic context by creating artificial enzymes with non-canonical catalytic residues incorporated by expanded genetic code technology. The artificial enzyme described here stereoselectively constructs an important chemical linkage with a different approach to those employed by natural enzymes. Whilst small molecule catalysts often require empirical structural optimisation, this artificial enzyme could be optimised using the Darwinian algorithm through directed evolution. We envision that this new approach will enable many more enzymatic reactions *via* iminium ion reaction intermediates, thus expanding the biocatalytic repertoire to enable further reactions for green synthesis.[19,32,71]

ASSOCIATED CONTENT

Supporting Information: Complete experimental procedures and methods, Supplementary Figures S1-S4, Supplementary Tables S1-S4, Primer Sequences, Protein Mass Spectra, HPLC Chromatograms and NMR Spectra.

ACKNOWLEDGEMENT

This work was supported by the Netherlands Organisation for Scientific Research (NWO, project 724.013.003), the Netherlands Ministry of Education, Culture and Science (Gravitation program no. 024.001.035) and the European Research Council (ERC starting grant 280010 and ERC advanced grant 885396). We would like to thank Dr. Clemens Mayer for useful discussions and advice throughout this research.

AUTHOR INFORMATION

Corresponding Author:

Gerard Roelfes - Stratingh Institute for Chemistry, University of Groningen, 9747 AG, Groningen, The Netherlands; orcid.org/0000-0002-0364-9564; Email: j.g.roelfes@rug.nl

Authors:

Reuben B. Leveson-Gower - Stratingh Institute for Chemistry, University of Groningen, 9747 AG, Groningen, The Netherlands; orcid.org/0000-0001-7254-3950

Zhi Zhou - Stratingh Institute for Chemistry, University of Groningen, 9747 AG, Groningen, The Netherlands; orcid.org/0000-0001-7926-118X

Ivana Drienovská - Stratingh Institute for Chemistry, University of Groningen, 9747 AG, Groningen, The Netherlands; Current address - Department of Chemistry and Pharmaceutical Sciences, VU Amsterdam, De Boelelaan 1108, 1081 HZ Amsterdam, The Netherlands; orcid.org/0000-0003-1715-4236

Notes

The authors declare no competing financial interest.

REFERENCES

(1) Paras, N. A.; MacMillan, D. W. C. The Enantioselective Organocatalytic 1,4-Addition of Electron-Rich Benzenes to α,β-Unsaturated Aldehydes. *J. Am. Chem. Soc.* **2002**, *124*, 7894–7895.

(2) Bartoli, G.; Bencivenni, G.; Dalpozzo, R. Organocatalytic Strategies for the Asymmetric Functionalization of Indoles. *Chem. Soc. Rev.* **2010**, *39*, 4449-4465.

(3) Rueping, M.; Nachtsheim, B. J. A Review of New Developments in the Friedel-Crafts Alkylation - From Green Chemistry to Asymmetric Catalysis. *Beilstein J. Org. Chem.* **2010**, *6*, 1–24.

(4) Zetzsche, L. E.; Narayan, A. R. H. Broadening the Scope of Biocatalytic C–C Bond Formation. *Nat. Rev. Chem.* **2020**, *4*, 334–346.

(5) Sheldon, R. A.; Woodley, J. M. Role of Biocatalysis in Sustainable Chemistry. *Chem. Rev.* **2018**, *118*, 801–838.

(6) Sheldon, R. A.; Brady, D.; Bode, M. L. The Hitchhiker's Guide to Biocatalysis: Recent Advances in the Use of Enzymes in Organic Synthesis. *Chem. Sci.* **2020**, *11*, 2587–2605.

(7) Huffman, M. A.; Fryszkowska, A.; Alvizo, O.; Borra-Garske, M.; Campos, K. R.; Canada, K. A.; Devine, P. N.; Duan, D.; Forstater, J. H.; Grosser, S. T.; Halsey, H. M.; Hughes, G. J.; Jo, J.; Joyce, L. A.; Kolev, J. N.; Liang, J.; Maloney, K. M.; Mann, B. F.; Marshall, N. M.; McLaughlin, M.; Moore, J. C.; Murphy, G. S.; Nawrat, C. C.; Nazor, J.; Novick, S.; Patel, N. R.; Rodriguez-Granillo, A.; Robaire, S. A.; Sherer, E. C.; Truppo, M. D.; Whittaker, A. M.; Verma, D.; Xiao, L.; Xu, Y.; Yang, H. Design of an in Vitro Biocatalytic Cascade for the Manufacture of Islatravir. *Science* **2019**, *366*, 1255–1259.

(8) Watkins-Dulaney, E.; Straathof, S.; Arnold, F. Tryptophan Synthase: Biocatalyst Extraordinaire. *ChemBioChem* **2021**, *22*, 5–16.

(9) Nakamura, H.; Schultz, E. E.; Balskus, E. P. A New Strategy for Aromatic Ring Alkylation in Cylindrocyclophane Biosynthesis. *Nat. Chem. Biol.* **2017**, *13*, 916–921.

(10) Schultz, E. E.; Braffman, N. R.; Luescher, M. U.; Hager, H. H.; Balskus, E. P. Biocatalytic Friedel–Crafts Alkylation Using a Promiscuous Biosynthetic Enzyme. *Angew. Chem. Int. Ed.* **2019**, *58*, 3151–3155.

(11) Schmidt, N. G.; Pavkov-Keller, T.; Richter, N.; Wiltschi, B.; Gruber, K.; Kroutil, W. Biocatalytic Friedel–Crafts Acylation and Fries Reaction. *Angew. Chem. Int. Ed.* **2017**, *56*, 7615–7619.

(12) Sheng, X.; Kazemi, M.; Żądło-Dobrowolska, A.; Kroutil, W.; Himo, F. Mechanism of Biocatalytic Friedel–Crafts Acylation by Acyltransferase from *Pseudomonas Protegens*. *ACS Catal.* **2020**, *10*, 570–577.

(13) Handoko; Satishkumar, S.; Panigrahi, N.; Arora, P. S. Rational Design of an Organocatalyst for Peptide Bond Formation. *J. Am. Chem. Soc.* **2019**, *141*, 15977–15985.

(14) Chen, J.; Gong, X.; Li, J.; Li, Y.; Ma, J.; Hou, C.; Zhao, G.; Yuan, W.; Zhao, B. Carbonyl Catalysis Enables a Biomimetic Asymmetric Mannich Reaction. *Science* **2018**, *360*, 1438–1442.

(15) Bos, J.; Browne, W. R.; Driessen, A. J. M.; Roelfes, G. Supramolecular Assembly of Artificial Metalloenzymes Based on the Dimeric Protein LmrR as Promiscuous Scaffold. *J. Am. Chem. Soc.* **2015**, *137*, 9796–9799.

(16) Boersma, A. J.; Feringa, B. L.; Roelfes, G. Enantioselective Friedel-Crafts Reactions in Water Using a DNA-Based Catalyst. *Angew. Chem. Int. Ed.* **2009**, *48*, 3346–3348.

(17) Paras, N. A.; MacMillan, D. W. C. New Strategies in Organic Catalysis: The First Enantioselective Organocatalytic Friedel−Crafts Alkylation. *J. Am. Chem. Soc.* **2001**, *123*, 4370–4371.

(18) Austin, J. F.; MacMillan, D. W. C. Enantioselective Organocatalytic Indole Alkylations. Design of a New and Highly Effective Chiral Amine for Iminium Catalysis. *J. Am. Chem. Soc.* **2002**, *124*, 1172–1173.

(19) Erkkilä, A.; Majander, I.; Pihko, P. M. Iminium Catalysis. *Chem. Rev.* **2007**, *107*, 5416–5470.

(20) Garrabou, X.; Wicky, B. I. M.; Hilvert, D. Fast Knoevenagel Condensations Catalyzed by an Artificial Schiff-Base-Forming Enzyme. *J. Am. Chem. Soc.* **2016**, *138*, 6972–6974.

(21) Obexer, R.; Godina, A.; Garrabou, X.; Mittl, P. R. E. E.; Baker, D.; Griffiths, A. D.; Hilvert, D. Emergence of a Catalytic Tetrad during Evolution of a Highly Active Artificial Aldolase. *Nat. Chem.* **2017**, *9*, 50–56.
(22) Garrabou, X.; Macdonald, D. S.; Wicky, B. I. M. M.; Hilvert, D. Stereodivergent Evolution of Artificial Enzymes for the Michael Reaction. *Angew. Chem. Int. Ed.* **2018**, *57*, 5288–5291.
(23) Nödling, A. R.; Świderek, K.; Castillo, R.; Hall, J. W.; Angelastro, A.; Morrill, L. C.; Jin, Y.; Tsai, Y.-H.; Moliner, V.; Luk, L. Y. P. Reactivity and Selectivity of Iminium Organocatalysis Improved by a Protein Host. *Angew. Chem. Int. Ed.* **2018**, *57*, 12478–12482.
(24) Guo, C.; Saifuddin, M.; Saravanan, T.; Sharifi, M.; Poelarends, G. J. Biocatalytic Asymmetric Michael Additions of Nitromethane to α,β-Unsaturated Aldehydes via Enzyme-Bound Iminium Ion Intermediates. *ACS Catal.* **2019**, *9*, 4369–4373.
(25) Xu, G.; Crotti, M.; Saravanan, T.; Kataja, K. M.; Poelarends, G. J. Enantiocomplementary Epoxidation Reactions Catalyzed by an Engineered Cofactor-Independent Non-natural Peroxygenase. *Angew. Chem. Int. Ed.* **2020**, *59*, 10374–10378.
(26) Drienovská, I.; Roelfes, G. Expanding the Enzyme Universe with Genetically Encoded Unnatural Amino Acids. *Nat. Catal.* **2020**, *3*, 193–202.
(27) Yu, Y.; Hu, C.; Xia, L.; Wang, J. Artificial Metalloenzyme Design with Unnatural Amino Acids and Non-Native Cofactors. *ACS Catal.* **2018**, *8*, 1851–1863.
(28) Schwizer, F.; Okamoto, Y.; Heinisch, T.; Gu, Y.; Pellizzoni, M. M.; Lebrun, V.; Reuter, R.; Köhler, V.; Lewis, J. C.; Ward, T. R. Artificial Metalloenzymes: Reaction Scope and Optimization Strategies. *Chem. Rev.* **2018**, *118*, 142–231.
(29) Markel, U.; Sauer, D. F.; Schiffels, J.; Okuda, J.; Schwaneberg, U. Towards the Evolution of Artificial Metalloenzymes—A Protein Engineer's Perspective. *Angew. Chem. Int. Ed.* **2018**, *58*, 4454–4464.
(30) Rosati, F.; Roelfes, G. Artificial Metalloenzymes. *ChemCatChem* **2010**, *2*, 916–927.
(31) Raines, D. J.; Clarke, J. E.; Blagova, E. V.; Dodson, E. J.; Wilson, K. S.; Duhme-Klair, A.-K. Redox-Switchable Siderophore Anchor Enables Reversible Artificial Metalloenzyme Assembly. *Nat. Catal.* **2018**, *1*, 680–688.
(32) Drienovská, I.; Mayer, C.; Dulson, C.; Roelfes, G. A Designer Enzyme for Hydrazone and Oxime Formation Featuring an Unnatural Catalytic Aniline Residue. *Nat. Chem.* **2018**, *10*, 946–952.
(33) Zhao, J.; Burke, A. J.; Green, A. P. Enzymes with Noncanonical Amino Acids. *Curr. Opin. Chem. Biol.* **2020**, *55*, 136–144.
(34) Agustiandari, H.; Lubelski, J.; Saparoea, H. B. van den B. van; Kuipers, O. P.; Driessen, A. J. M. LmrR Is a Transcriptional Repressor of Expression of the Multidrug ABC Transporter LmrCD in Lactococcus Lactis. *J. Bacteriol.* **2008**, *190*, 759–763.
(35) Roelfes, G. LmrR: A Privileged Scaffold for Artificial Metalloenzymes. *Acc. Chem. Res.* **2019**, *52*, 545–556.
(36) Villarino, L.; Splan, K. E.; Reddem, E.; Alonso-Cotchico, L.; Lledós, A.; Gutiérrez de Souza, C.; Thunnissen, A.-M. W. H.; Maréchal, J.-D.; Roelfes, G. An Artificial Heme Enzyme for Cyclopropanation Reactions. *Angew. Chem. Int. Ed.* **2018**, *57*, 7785–7789.
(37) Burke, A. J.; Lovelock, S. L.; Frese, A.; Crawshaw, R.; Ortmayer, M.; Dunstan, M.; Levy, C.; Green, A. P. Design and Evolution of an Enzyme with a Non-Canonical Organocatalytic Mechanism. *Nature* **2019**, *570*, 219–223.
(38) Zhou, Z.; Roelfes, G. Synergistic Catalysis in an Artificial Enzyme by Simultaneous Action of Two Abiological Catalytic Sites. *Nat. Catal.* **2020**, *3*, 289–294.
(39) Jin, S.; Li, C.; Ma, Y.; Kan, Y.; Zhang, Y. J.; Zhang, W. Highly Efficient Asymmetric Organocatalytic Friedel-Crafts Alkylation of Indoles with α,β-Unsaturated Aldehydes. *Org. Biomol. Chem.* **2010**, *8*, 4011–4015.
(40) Lorentzen, E.; Siebers, B.; Hensel, R.; Pohl, E. Mechanism of the Schiff Base Forming Fructose-1,6-Bisphosphate Aldolase: Structural Analysis of Reaction Intermediates. *Biochemistry* **2005**, *44*, 4222–4229.

(41) Mayer, C.; Dulson, C.; Reddem, E.; Thunnissen, A.-M. W. H.; Roelfes, G. Directed Evolution of a Designer Enzyme Featuring an Unnatural Catalytic Amino Acid. *Angew. Chem. Int. Ed.* **2019**, *58*, 2083–2087.
(42) Chordia, S.; Narasimhan, S.; Lucini Paioni, A.; Baldus, M.; Roelfes, G. In Vivo Assembly of Artificial Metalloenzymes and Application in Whole-Cell Biocatalysis. *Angew. Chem. Int. Ed.* **2021**. https://doi.org/10.1002/anie.202014771.
(43) Villarino, L.; Chordia, S.; Alonso-Cotchico, L.; Reddem, E.; Zhou, Z.; Thunnissen, A. M. W. H.; Maréchal, J.-D.; Roelfes, G. Cofactor Binding Dynamics Influence the Catalytic Activity and Selectivity of an Artificial Metalloenzyme. *ACS Catal.* **2020**, *10*, 11783–11790.
(44) Drienovská, I.; Alonso-Cotchico, L.; Vidossich, P.; Lledós, A.; Maréchal, J.-D.; Roelfes, G. Design of an Enantioselective Artificial Metallo-Hydratase Enzyme Containing an Unnatural Metal-Binding Amino Acid. *Chem. Sci.* **2017**, *8*, 7228–7235.
(45) Reetz, M. T.; Carballeira, J. D. Iterative Saturation Mutagenesis (ISM) for Rapid Directed Evolution of Functional Enzymes. *Nat. Protoc.* **2007**, *2*, 891–903.
(46) Kille, S.; Acevedo-Rocha, C. G.; Parra, L. P.; Zhang, Z.-G.; Opperman, D. J.; Reetz, M. T.; Acevedo, J. P. Reducing Codon Redundancy and Screening Effort of Combinatorial Protein Libraries Created by Saturation Mutagenesis. *ACS Synth. Biol.* **2013**, *2*, 83–92.
(47) Sullivan, B.; Walton, A. Z.; Stewart, J. D. Library Construction and Evaluation for Site Saturation Mutagenesis. *Enzyme Microb. Technol.* **2013**, *53*, 70–77.
(48) Westheimer, F. H. Coincidences, Decarboxylation, and Electrostatic Effects. *Tetrahedron* **1995**, *51*, 3–20.
(49) Highbarger, L. A.; Gerlt, J. A.; Kenyon, G. L. Mechanism of the Reaction Catalyzed by Acetoacetate Decarboxylase. Importance of Lysine 116 in Determining the p K_a of Active-Site Lysine 115. *Biochemistry* **1996**, *35*, 41–46.
(50) Poelarends, G. J.; Almrud, J. J.; Serrano, H.; Darty, J. E.; Johnson, W. H.; Hackert, M. L.; Whitman, C. P. Evolution of Enzymatic Activity in the Tautomerase Superfamily: Mechanistic and Structural Consequences of the L8R Mutation in 4-Oxalocrotonate Tautomerase. *Biochemistry* **2006**, *45*, 7700–7708.
(51) Zühlsdorf, M.; Werten, S.; Klupp, B. G.; Palm, G. J.; Mettenleiter, T. C.; Hinrichs, W. Dimerization-Induced Allosteric Changes of the Oxyanion-Hole Loop Activate the Pseudorabies Virus Assemblin PUL26N, a Herpesvirus Serine Protease. *PLoS Pathog* **2015**, *11*, e1005045.
(52) Gordillo, R.; Carter, J.; Houk, K. N. Theoretical Explorations of Enantioselective Alkylation Reactions of Pyrroles and Indoles Organocatalyzed by Chiral Imidazolidinones. *Adv. Synth. Catal.* **2004**, *346*, 1175–1185.
(53) Pace, N. C.; Scholtz, M. J. A Helix Propensity Scale Based on Experimental Studies of Peptides and Proteins. *Biophys. J.* **1998**, *75*, 422–427.
(54) Alonso-Cotchico, L.; Rodríguez-Guerra Pedregal, J.; Lledós, A.; Maréchal, J.-D. The Effect of Cofactor Binding on the Conformational Plasticity of the Biological Receptors in Artificial Metalloenzymes: The Case Study of LmrR. *Front. Chem.* **2019**, *7*, 1–12.
(55) Otten, R.; Pádua, R. A. P.; Bunzel, H. A.; Nguyen, V.; Pitsawong, W.; Patterson, M.; Sui, S.; Perry, S. L.; Cohen, A. E.; Hilvert, D.; Kern, D. How Directed Evolution Reshapes the Energy Landscape in an Enzyme to Boost Catalysis. *Science* **2020**, *370*, 1442–1446.
(56) Broom, A.; Rakotoharisoa, R. V.; Thompson, M. C.; Zarifi, N.; Nguyen, E.; Mukhametzhanov, N.; Liu, L.; Fraser, J. S.; Chica, R. A. Ensemble-Based Enzyme Design Can Recapitulate the Effects of Laboratory Directed Evolution in Silico. *Nat. Commun.* **2020**, *11*, 4808.
(57) Soskine, M.; Tawfik, D. S. Mutational Effects and the Evolution of New Protein Functions. *Nat. Rev. Genet.* **2010**, *11*, 572–582.
(58) Aharoni, A.; Gaidukov, L.; Khersonsky, O.; Gould, S. M.; Roodveldt, C.; Tawfik, D. S. The "evolvability" of Promiscuous Protein Functions. *Nat. Genet.* **2005**, *37*, 73–76.
(59) Khersonsky, O.; Tawfik, D. S. Enzyme Promiscuity: A Mechanistic and Evolutionary Perspective. *Annu. Rev. Biochem.* **2010**, *79*, 471–505.

(60) Rueffler, C.; Hermisson, J.; Wagner, G. P. Evolution of Functional Specialization and Division of Labor. *Proc. Natl. Acad. Sci. U.S.A.* **2012**, *109*, 1830–1831.
(61) Yoshikuni, Y.; Ferrin, T. E.; Keasling, J. D. Designed Divergent Evolution of Enzyme Function. *Nature* **2006**, *440*, 1078–1082.
(62) Coelho, P. S.; Wang, Z. J.; Ener, M. E.; Baril, S. A.; Kannan, A.; Arnold, F. H.; Brustad, E. M. A Serine-Substituted P450 Catalyzes Highly Efficient Carbene Transfer to Olefins in Vivo. *Nat. Chem. Biol.* **2013**, *9*, 485–487.
(63) Lv, J.; Zhang, Q.; Cai, M.; Han, Y.; Luo, S. Aromatic Aminocatalysis. *Chem. Asian J.* **2018**, *13*, 740–753.
(64) Cordes, E. H.; Jencks, W. P. Nucleophilic Catalysis of Semicarbazone Formation by Anilines. *J. Am. Chem. Soc.* **1962**, *84*, 826–831.
(65) Crisalli, P.; Kool, E. T. Water-Soluble Organocatalysts for Hydrazone and Oxime Formation. *J. Org. Chem.* **2013**, *78*, 1184–1189.
(66) Xu, L.-W.; Luo, J.; Lu, Y. Asymmetric Catalysis with Chiral Primary Amine-Based Organocatalysts. *Chem. Commun.* **2009**, 1807-1821.
(67) Zandvoort, E.; Geertsema, E. M.; Baas, B.-J.; Quax, W. J.; Poelarends, G. J. Bridging between Organocatalysis and Biocatalysis: Asymmetric Addition of Acetaldehyde to β-Nitrostyrenes Catalyzed by a Promiscuous Proline-Based Tautomerase. *Angew. Chem. Int. Ed.* **2012**, *51*, 1240–1243.
(68) Bos, J.; Fusetti, F.; Driessen, A. J. M.; Roelfes, G. Enantioselective Artificial Metalloenzymes by Creation of a Novel Active Site at the Protein Dimer Interface. *Angew. Chem. Int. Ed.* **2012**, *51*, 7472–7475.
(69) Hammer, S. C.; Kubik, G.; Watkins, E.; Huang, S.; Minges, H.; Arnold, F. H. Anti-Markovnikov Alkene Oxidation by Metal-Oxo–Mediated Enzyme Catalysis. *Science* **2017**, *358*, 215–218.
(70) van der Helm, M. P.; Klemm, B.; Eelkema, R. Organocatalysis in Aqueous Media. *Nat. Rev. Chem.* **2019**, *3*, 491–508.
(71) Leveson-Gower, R. B.; Mayer, C.; Roelfes, G. The Importance of Catalytic Promiscuity for Enzyme Design and Evolution. *Nat. Rev. Chem.* **2019**, *3*, 687–705.

Supporting Information

Unlocking Iminium Catalysis in Designer Enzymes to Create an Artificial Friedel-Crafts Alkylase

Reuben B. Leveson-Gower[1], Zhi Zhou[1], Ivana Drienovská[1,2], Gerard Roelfes[1]*

[1]Stratingh Institute for Chemistry, University of Groningen, 9747 AG, Groningen, The Netherlands. [2]Current address: Department of Chemistry and Pharmaceutical Sciences, VU Amsterdam, De Boelelaan 1108, 1081 HZ Amsterdam, The Netherlands

* j.g.roelfes@rug.nl

Contents

1. Supplementary Figures

Supplementary Figure S1: Representative results from library screening

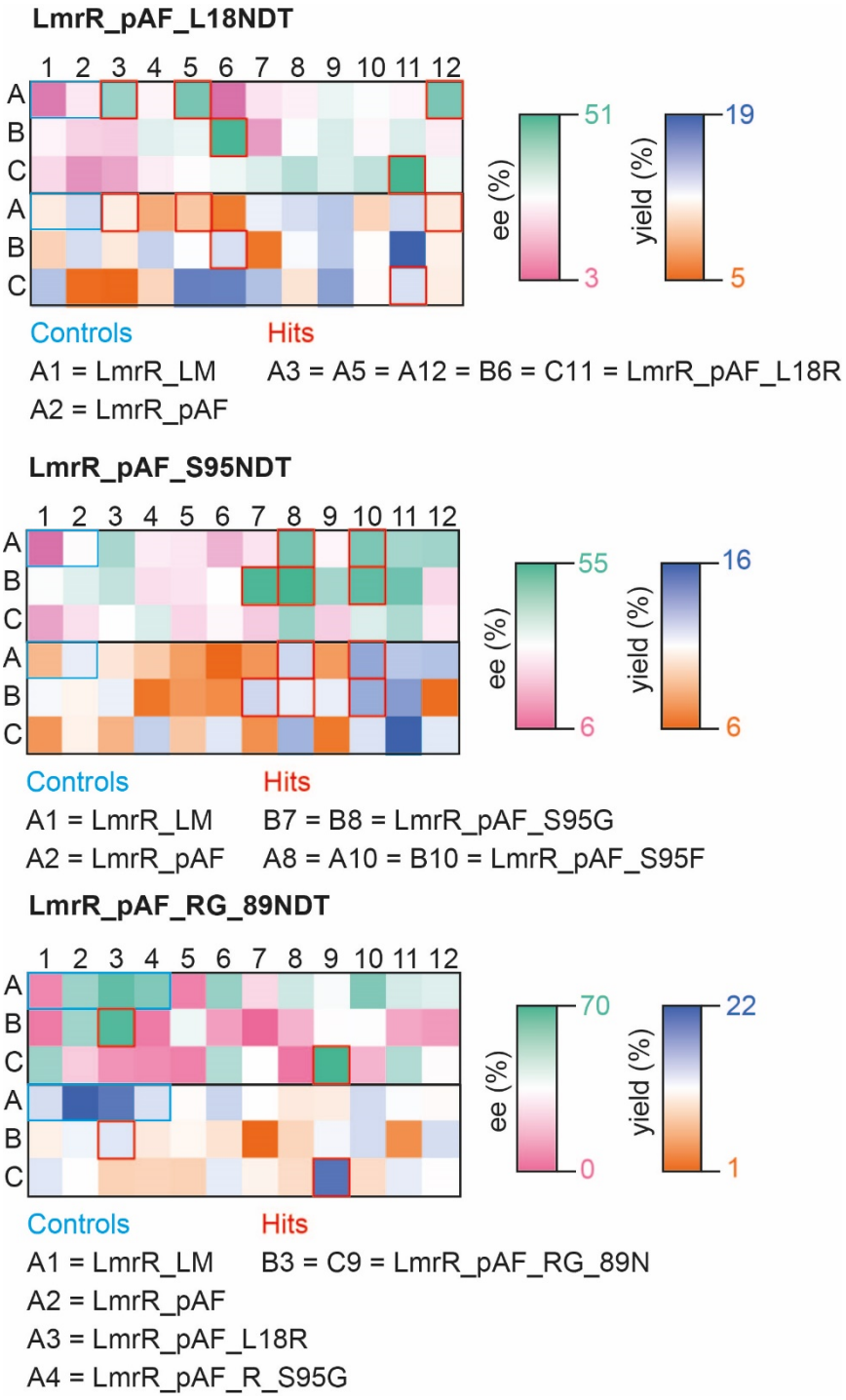

Supplementary Figures S2-S4: Plots of Michaelis-Menten Kinetics

Supplementary Figure S2: Apparent Michaelis-Menten kinetics of the Friedel-Crafts alkylation of 2-methylindole with trans-2-hexenal for LmrR_pAF, LmrR_pAF_RMH (evolved mutant for hydrazone formation) and LmrR_pAF_RGN (evolved mutant for Friedel-Crafts alkylation). Conditions: 50 mM NaH_2PO_4, 150 mM NaCl, pH 6.5, 1-5 µM protein (dimer) concentration, 1 mM 2-methylindole, 5% DMF, 25 °C. Values are an average of three experiments including both biological and technical replicates. Some error bars are too small to be shown.

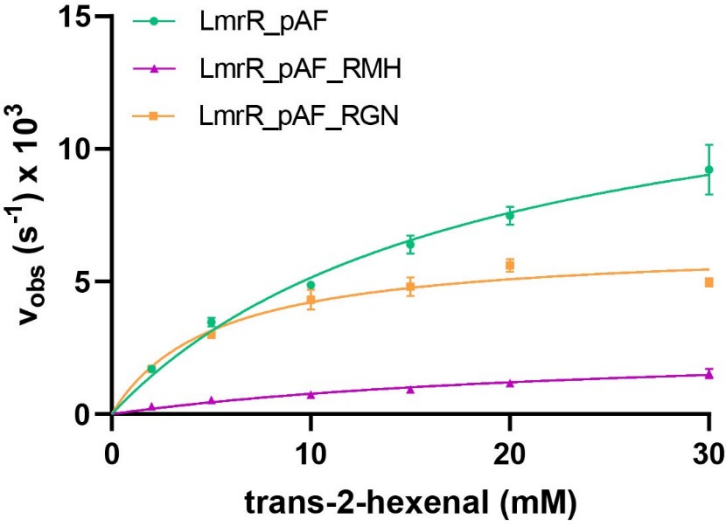

Supplementary Figure S3: Apparent Michaelis-Menten kinetics of the hydrazone formation of 4-hydroxybenzaldehyde with NDB-H for LmrR_pAF, LmrR_pAF_RMH (evolved mutant for hydrazone formation) and LmrR_pAF_RGN (evolved mutant for Friedel-Crafts alkylation). Conditions: 50 mM NaH_2PO_4, 150 mM NaCl, pH 7.4, 2 µM protein (dimer) concentration, 1-5 µM protein (dimer) concentration, 5 mM 4-hydroxybenzaldehyde, 5% DMF, 25 °C. Values are an average of three experiments including both biological and technical replicates. Some error bars are too small to be shown. This graph includes previously obtained data (Mayer et al., *Angew. Chem. Int. Ed.,* 2019, 2083-2087)

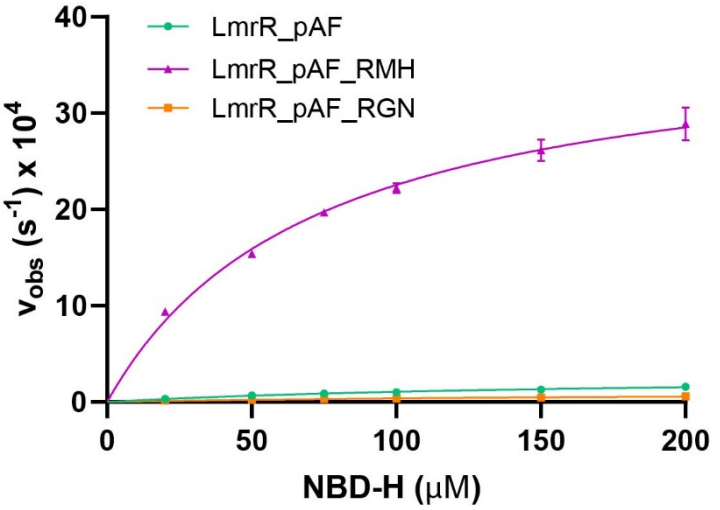

Supplementary Figure S4: Cropped view of Supplementary Figure S3 to more clearly show the data for LmrR_pAF and LmrR_pAF_RGN. Some error bars are too small to be shown. This graph includes previously obtained data (Mayer et al., *Angew. Chem. Int. Ed.,* 2019, 2083-2087).

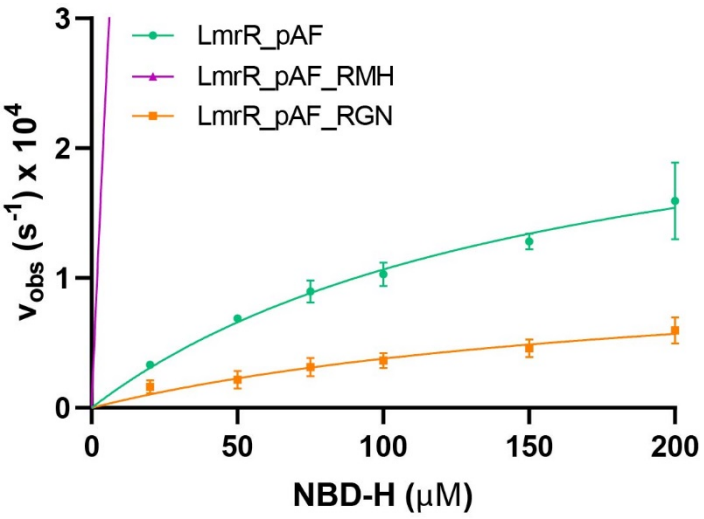

2. Supplementary Tables

Supplementary Table S1: Friedel-Crafts catalysis with purified LmrR_pAF (alanine) mutants and control mutants

Mutant	**Yield (%) ± S.D.**	**Δ_{yield} (%)[a]**	***ee* (%) ± S.D.**	**Δ_{ee} (%)[b]**
LmrR	2 ± 0	-	N.D.	-
LmrR_V15Y	2 ± 0	-	N.D.	-
LmrR_V15K	3 ± 0	-	N.D.	-
LmrR_V15pAF	42 ± 4	-	45 ± 0	-
LmrR_V15pAF_E7A	39 ± 1	-3	45 ± 1	0
LmrR_V15pAF_A11L	40 ± 2	-2	49 ± 0	+4
LmrR_V15pAF_L18A	**35 ± 5**	**-7**	**29 ± 5**	**-16**
LmrR_V15pAF_N19A	39 ± 7	-3	49 ± 0	+4
LmrR_V15pAF_K22A	**46 ± 3**	**+4**	**36 ± 1**	**-9**
LmrR_V15pAF_N88A	36 ± 6	-6	49 ± 4	+4
LmrR_V15pAF_M89A	37 ± 4	-5	47 ± 2	+2
LmrR_V15pAF_A92E	**35 ± 1**	**-9**	**41 ± 0**	**-4**
LmrR_V15pAF_F93A	**30 ± 4**	**-12**	**47 ± 0**	**+2**
LmrR_V15pAF_S95A	**38 ± 4**	**-4**	**50 ± 0**	**+5**
LmrR_V15pAF_S97A	**46 ± 3**	**+4**	**52 ± 1**	**+7**
LmrR_V15pAF_D100A	22 ± 11	-20	10 ± 0	-35

Reaction conditions: 50 mM NaH_2PO_4, 150 mM NaCl, pH 6.5, 1 mM 2-methyl-indole, 5 mM trans-2-hexenal, 8% DMF, 20 μM protein (dimer) concentration, 4 °C and 16 hours reaction time. Values are the average of at least two independent experiments, each conducted in duplicate, errors given are the standard deviation of the results thus obtained. [a] change in *ee* and yields obtained w.r.t. those obtained with LmrR_V15pAF was used to classify the effects of mutations on catalysis. Entries in bold signify positions chosen as targets for directed evolution.

Supplementary Table S2: Friedel-Crafts catalysis with LmrR_pAF (alanine) mutants and control mutants in cell-free extract

Mutant	**Δ_{ee} (%)[a]**	**Δ_{yield} (%)[a]**
LmrR	-25 ± 6	-9 ± 3
LmrR_V15Y	-25 ± 6	-10 ± 3
LmrR_V15pAF	0	0
LmrR_V15pAF_E7A	-1 ± 1	-3 ± 1
LmrR_V15pAF_A11L	-4 ± 3	-3 ± 0
LmrR_V15pAF_L18A	**+1 ± 1**	**0 ± 1**
LmrR_V15pAF_N19A	+1 ± 1	-2 ± 0
LmrR_V15pAF_K22A	**-5 ± 3**	**-3 ± 1**
LmrR_V15pAF_N88A	+2 ± 2	-1 ± 2
LmrR_V15pAF_M89A	-16 ± 5	-6 ± 2
LmrR_V15pAF_A92E	**-8 ± 4**	**-3 ± 1**
LmrR_V15pAF_F93A	**-5 ± 0**	**-5 ± 1**
LmrR_V15pAF_S95A	**+1 ± 2**	**+2 ± 1**
LmrR_V15pAF_S97A	**0 ± 3**	**-2 ± 1**
LmrR_V15pAF_D100A	-24 ± 5	-7 ± 2

Reaction conditions: Cell free extract (see methods) 50 mM NaH_2PO_4, 150 mM NaCl, pH 6.5, 1 mM 2-methyl-indole, 15 mM trans-2-hexenal, 8% DMF, 4 ºC and 16 hours reaction time. Values are the average of two independent experiments, each conducted in duplicate, errors given are the standard deviation of the results thus obtained. [a] change in *ee* and yields obtained w.r.t. those obtained with LmrR_V15pAF was used to classify the effects of mutations on catalysis. Absolute yield and enantioselectivity values vary for each independent culture, presumably due to varying expression levels, and thus only the differences with the LmrR_pAF positive control are shown.

Supplementary Table S3: Summary of library screening results

Round	**Library**	**Hits**
1	LmrR_pAF_L18NDT	L18R
1	LmrR_pAF_K22NDT	-
1	LmrR_pAF_A92NDT	A92F
1	LmrR_pAF_F93NDT	-
1	LmrR_pAF_S95NDT	S95F, S95G
1	LmrR_pAF_S97NDT	S97F, S97D
2	LmrR_pAF_L18R_K22NDT	-
2	LmrR_pAF_L18R_A92NDT	-
2	LmrR_pAF_L18R_S95G_M8NDT	-
2	LmrR_pAF_L18R_S95G_A11NDT	-
2	LmrR_pAF_L18R_S95G_N19NDT	-
2	LmrR_pAF_L18R_S95G_M89NDT	M89N
2	LmrR_pAF_L18R_S95G_A92NDT	-

Supplementary Table S4: Friedel-Crafts catalysis with purified LmrR_pAF library hits and recombined mutants and control mutants

Mutant	**Yield (%) ± S.D.**	***ee* (%) ± S.D.**
LmrR_V15pAF	42 ± 4	45 ± 0
LmrR_V15pAF_L18R	58 ± 2	67 ± 0
LmrR_V15pAF_A92F[a]	60	70
LmrR_V15pAF_A92Y[a]	54	57
LmrR_V15pAF_S95F[a]	50	57
LmrR_V15pAF_S95G	46 ± 7	55 ± 1
LmrR_V15pAF_S97F[a]	46	44
LmrR_V15pAF_S97D[a]	36	54
LmrR_V15pAF_L18R_A92F[a]	67	54
LmrR_V15pAF_L18R_S95F[a]	40	17
LmrR_V15pAF_L18R_S95G	70 ± 8	78 ± 0
LmrR_V15pAF_L18R_S95G_M89N	74 ± 2	87 ± 0
LmrR_V15Y_L18R_S95G_M89N	1 ± 0	N.D.
LmrR_V15K_L18R_S95G_M89N	2 ± 0	N.D.

Reaction conditions: 50 mM NaH_2PO_4, 150 mM NaCl, pH 6.5, 1 mM 2-methyl-indole, 5 mM trans-2-hexenal, 8% DMF, 20 μM protein (dimer) concentration, 4 °C and 16 hours reaction time. Values are the average of at least two independent experiments, each conducted in duplicate, except where noted. Errors given are the standard deviation of the results thus obtained. [a] average result from a duplicate experiment

3. Materials and Equipment

Chemicals were purchased from commercial suppliers (Sigma (UK), Acros (Germany), TCI (Belgium/Japan) and Flurochem (UK)) and used without further purification unless specified. Flash column chromatography was performed on silica gel (Silica-P flash silica gel from Silicycle, 0.040-0.063 mm, 230-400 mesh). The unnatural amino acid pAzF was purchased as racemic mixture from Bachem (Switzerland) or as the enantiopure hydrochloride salt from Iris-Biotech (Germany). NMR ^{1}H-NMR and ^{13}C-NMR spectra were recorded on a Varian 400 (400 MHz) spectrometer in $CDCl_3$ or $(CD_3)_2SO$. Chemical shifts values (δ) are denoted in ppm using residual solvent peaks as the internal standard ($CHCl_3$: δ 7.26 for ^{1}H; 77.16 for ^{13}C. $(CD_3)_2SO$: δ 2.50 for ^{1}H; 39.52 for ^{13}C). HPLC analysis was conducted using a Shimadzu LC-10ADVP HPLC equipped with a Shimadzu SPD-M10AVP diode array detector. Plasmids pEVOL-pAzF was obtained from Addgene (pEvol-pAzF was a gift from Prof. Peter Schultz (The Scripps Research Institute)). *E. coli* strains, NEB5-alpha, NEB10-beta and BL21(DE3) (New England Biolabs) were used for cloning and expression. Primers were synthesized by Eurofins MWG Operon (Germany) and Sigma-Aldrich (UK). Plasmid Purification Kits were obtained from QIAGEN (Germany) and DNA sequencing carried out by GATC-Biotech (Germany). Phusion polymerase and DpnI were purchased from New England Biolabs. Gibson cloning was conducted using NEBuilder® HiFi DNA Assembly Master Mix (New England Biolabs). Strep-tactin columns (Strep-Tactin® Superflow® high capacity) and Desthiobiotin were purchased from IBA-Lifesciences (Germany). Concentrations of DNA and protein solutions were determined based on the absorption at 260 nm or 280 nm on a Thermo Scientific Nanodrop 2000 UV-Vis spectrophotometer. UV/Vis absorption spectra and kinetic assays were recorded at 25 ºC on a Jasco V-660 spectrophotometer. UPLC/MS analysis was performed on Waters Acquity Ultra Performance LC with Acquity TQD detector. Water (solvent A) and acetonitrile (solvent B) containing 0.1% formic acid by volume, were used as the mobile phase at a flow rate of 0.3 mL/min. Gradient: 90% A for 2 min, linear gradient to 50% A in 2 min, linear gradient to 20% A in 5 min, followed by 2 min at 5% A. Re-equilibration of the column with 2 min at 90% A.

4. Methods

4.1 Protein Purification

LmrR_pAF variants were produced and purified as previously described[1]. The identity and purity of proteins and the successful reduction of pAzF were determined by mass spectrometry. Protein concentration was determined by correcting the calculated extinction coefficients for LmrR variants for the absorbance of pAF (ε_{280} = 1333 M^{-1} cm^{-1})

4.2 Alanine mutant construction

Where mutations were far separated from position V15 in the LmrR gene, we used previously prepared mutated LmrR plasmids[2] and introduced the V15TAG mutation, in other cases we incorporated the desired mutations into the LrmR_V15TAG gene. Primers are described in section 5, and Phusion polymerase was used. The following PCR protocol was used: (1) initial denaturation at 95 °C for 1 min, (2) 16 cycles of denaturation at 98 °C for 30 s, annealing at 56-68 °C for 30 s, and extension at 72 °C for 5 min, (3) a final extension at 72 °C for 10 min. The resulting PCR product was digested with DpnI for 2 hours at 37 °C and subsequently purified (PCR purification kit, Qiagen). The obtained PCR product (100-200 ng) was transformed into chemically-competent *E. coli* NEB5α cells and spread onto LB agar plates containing ampicillin (100 μg/mL). The plates were incubated at 37 °C overnight and individual colonies were grown in 5 mL LB containing ampicillin (100 μg/mL) overnight. The plasmid DNA was isolated (miniprep kit, Qiagen) and sent for sequencing (GATC Biotech) to confirm correct mutation. The isolated plasmid was then co-transformed with pEVOL_pAzF into chemically-competent *E. coli* BL21(DE3) cells which were spread onto LB agar plates containing ampicillin (100 μg/mL) and chloramphenicol (34 μg/mL). Single colonies from these plates were used for protein expression.

4.3 Library Construction

The previously described pET17b_LmrR_V15X plasmid was used as template for the library construction[1,3]. In addition to an in-frame TAG stop codon at position V15, this variant also features mutations of two lysines (K55D and K59Q), which abrogate the natural DNA-binding ability of LmrR. Randomization at residues lining the active site was achieved by site-directed mutagenesis (QuikChange, Agilent Technologies) starting from pET17b_LmrR_V15X and appropriate primer pairs and Phusion polymerase (see Section 5 of the Supporting Information). The following PCR protocol was used: (1) initial denaturation at 95 °C for 1 min, (2) 16 cycles of denaturation at 98 °C for 30 s, annealing at 56-68 °C for 30 s, and extension at 72 °C for 5 min, (3) a final extension at 72 °C for 10 min. The resulting PCR product was digested with DpnI for 2 hours at 37 °C and subsequently purified (PCR purification kit, Qiagen). The obtained PCR product (100-200 ng) was transformed into chemically-competent *E. coli* NEB10-beta cells (prepared by the Inoue method[4]) and spread onto LB agar plates containing ampicillin (100 μg/mL). The colonies obtained (>100) were scraped off with a Drigalski spatula into 5 mL fresh LB media containing ampicillin (100 μg/mL). The cultures thus obtained were incubated for 2 - 4 hours at 37 °C with 135 rpm shaking. The plasmid DNA was isolated (miniprep kit, Qiagen) and sent for sequencing (GATC Biotech) to confirm library quality. Once library quality was confirmed Q_{pool} ~ 0.6 or greater[5] the plasmid DNA was transformed into chemically-competent *E. coli* BL21 (DE3) cells containing the plasmid pEVOL-pAzF and spread onto LB agar plates containing ampicillin (100 μg/mL) and chloramphenicol (34 μg/mL). After incubation overnight at 37 °C, single colonies were picked and transferred into 96-well plates containing LB media with the same antibiotics. Before the second round the LmrR_V15X_L18R_S95G insert was cloned into the same vector using the Gibson method as described below.

4.4 Gibson Cloning

Before the construction of second-round libraries the LmrR_V15X_L18R_S95G insert was re-cloned into it a fresh vector to prevent the accumulation of detrimental mutations in areas of the plasmid that are not elucidated by sequencing with the T7 primer, after several sequential rounds of QuikChange. We amplified the LmrR_V15X_L18R_S95G insert and the vector from pET17b_LmrR6 using primers described in section 5, Phusion polymerase and the following PCR protocol: (1) initial denaturation at 95 °C for 1 min, (2) 30 cycles of denaturation at 98 °C for 30 s, annealing at 56 °C for 30 s, and extension at 72 °C for 5 min, (3) a final extension at 72 °C for 10 min. The resulting PCR product was digested with DpnI over-night at 37 °C and subsequently purified (PCR purification kit, Qiagen). The NEBuilder HiFi DNA Assembly Reaction was conducted with the PCR products thus obtained according to the manufacturer protocol. After assembly the product was transformed into chemical competent *E. Coli* NEB5α cells and spread on to LB agar plates containing ampicillin (100 μg/mL) and incubated at 37 °C overnight. Individual colonies were picked into 5 mL LB media with the same antibiotic and grown overnight at 37 °C. The plasmid DNA was isolated (miniprep kit, Qiagen) and sent for sequencing (GATC Biotech).

4.5 Preparation of Cell-Free Extracts in Deep-Well Format

Libraries were prepared as described above. (36 – n) colonies (where n = number of controls, 2 in first round, 4 in second round), obtained from the library preparation, were transferred into 1.5 mL deep well plates containing 500 μL LB media and appropriate antibiotics. In addition to library members, 2 or 4 wells were inoculated with glycerol stocks of controls (LmrR_pAF, LmrR, and LmrR_L18R and LmrR_pAF_R_S95G in the second round). The resulting deep well plates were incubated overnight at 37 °C while shaking at 950 rpm (Titramax 1000 & Incubator 1000, Heidolph). The next morning, 50 μL of the densely grown overnight cultures were transformed into fresh 96-deep well plates containing 1150 μL LB media and appropriate antibiotics. Glycerol (500 μL, 50 % with miliQ water) was added to the remaining overnight culture, mixed thoroughly and stored at - 70 °C. Bacteria were cultured at 37 °C for 5 - 6 hours while shaking at 950 rpm. Subsequently, protein production was induced by addition of 50 μL LB media, containing IPTG (1.2 μL of a 1 M stock solution), arabinose (1.2 μL of a 20% arabinose stock solution) and p-azidophenylalanine at a concentration of 15 mM (final concentrations: IPTG = 1 mM, arabinose = 0.02%, pAzF = 0.6 mM). To avoid precipitation of the unnatural amino acid, pAzF was dissolved by addition of 1 equivalent of base (1 M NaOH) prior to addition to the LB media. Plates were then incubated at 30 °C for 16 hours while shaking (950 rpm) and harvested by centrifugation (3,500 rpm at 4 °C for 15 minutes). After removing the supernatant, cells were washed by addition of 500 μL of buffer A (50 mM sodium phosphate, 150 mM NaCl, pH = 6.5), and the supernatant was again discarded after centrifugations (3,500 rpm for 10 minutes). For the preparation of cell-free extracts, bacteria were resuspended in 300 μL buffer A, containing protease inhibitor (Roche cOmplete), lysozyme (1 mg/mL). DNase I (0.1 mg/mL) and $MgSO_4$ (10 mM) to assist in cell lysis and prevent protein degradation. Resuspended cells were incubated for 2 hours at 30 °C at 800 rpm and then stored until further use at -20 °C. The lysates were defrosted and 30 μL of a TCEP stock solution (100 mM in buffer A, adjusted to pH 6.5 by addition of 6 M NaOH) was added to individual wells. The reduction was initially performed for 2 hours at 30 °C, after which incubation was continued overnight at 4 °C. Subsequently, cell debris was removed by centrifugation (4,000 rpm, 1 hour, 4 °C) and 276 μL of cell-free lysate was transferred into 2 mL microcentrifuge tubes for catalysis, stored at 4 °C and used within 8 hours.

4.6 Friedel-Crafts Catalysis with Cell-Free Extracts and Purified Proteins

Reactions were conducted in 300 μL total volume in a 2 mL microcentrifuge tube. Stock solutions of protein in pH 6.5 PBS buffer (50 mM NaCl, 150 mM NaH_2PO_4) to give the specified final concentration

and the same buffer was added to make up 276 μL volume. For screening of degenerate codon libraries, 276 μL of cell-free lysate was used instead. Stock solutions of indole (25 mM in DMF, 12 μL added, final concentration 1 mM) and enal (125 mM or 675 mM when using cell-free lystate, 12 μL added to give final concentrations of 5 mM or 15 mM with cell free lysate) substrates were added. The microcentrifuge tubes were then mixed by continuous inversion in a cold room as 4 °C for the specified reaction time. After the reaction time had elapsed, $NaBH_4$ solution (60 μL, 20 mg/mL in 0.5 w/v % NaOH) and 3-(3-hydroxyindole) internal standard solution (12 μL, 5 mM in DMF) were added. The micro-centrifuge tubes were mixed by continuous inversion for a further 30 minutes. The reaction products and internal standard were then extracted by vortex mixing with EtOAc (1 mL) and the organic extract was dried over Na_2SO_4, filtered and evaporated to dryness. The residue thus obtained was redissolved by vortex mixing with HPLC grade solvent (heptane:isopropanol 4:1, 90 μL) and analysed by normal phase HPLC to determine yield and enantioselectivity with a 20 μL injection volume.

4.7 Kinetic Characterisation – Hydrazone Formation

Conducted as previously described[3]. One measurement with LmrR_pAF was repeated to obtain results within the error previously determined. Measurements with LmrR_pAF_RGN were conducted in triplicate, one of the triplicate measurements utilised an independently expressed batch of enzyme.

4.8 Kinetic Characterisation – Friedel-Crafts Alkylation

Reactions were conducted as described for catalysis but with 1 mL total volume with a total of 5 vol% DMF, with 1 mM 2-methylindole concentration and varying concentrations of trans-2-hexenal (2 mM, 5 mM, 10 mM, 15 mM, 20 mM and 30 mM) which was distilled by kugelrohr apparatus prior to use. Enzyme concentrations were adjusted so that no reaction aliquot produced a yield above 10 % for any given enzyme mutant and substrate concentration (2 – 20 μM). The microcentrifuge tubes were incubated in an orbital shaker at 25 °C and 300 μL aliquots were removed at three time points (between 15 and 90 minutes depending on the enzyme mutant and enal concentration) and quenched by vortex mixing following addition of $NaBH_4$ solution (60 μL, 20 mg/mL in 0.5 w/v % NaOH) and 3-(3-hydroxyindole) internal standard solution (12 μL, 5 mM in DMF). Products and internal standard were extracted as described for catalysis and the yield was determined in the same manner by normal phase HPLC. Each reaction was conducted in triplicate, one of these triplicate reactions was also conducted using an independently expressed batch of enzyme.

5. Primer List

Primer	Sequence
V15TAG_fw	ACCAAT**TAG**ATCCTGCTGAATGTCC
V15TAG_rv	GCAGGAT**CTA**ATTGGTTTGAGCAC
L18A_fw	ATCCTG**GCG**AATGTCCTGAAACAA
L18A_rv	GGACATT**CGC**CAGGATCTAATTGG
N19A_fw	CTGCTG**GCG**GTCCTGAAACAAGGC
N19A_rv	TCAGGAC**CGC**CAGCAGGATCTAATTGGT
K22A_fw	GTCCTG**GCC**CAAGGCGATAACTATGTGT
K22A_rv	GCCTTG**CGG**CAGGACATTCAGCAG
L18NDT_fw	GATCCTG**NDT**AATGTCCTGAAACAAG
L18NDT_rv	GACATT**AHN**CAGGATCTAATTGGTTTGA
K22NDT_fw	TGTCCTG**NDT**CAAGGCGATAACTATGTG
K22NDT_rv	GCCTTG**AHN**CAGGACATTCAGCAG
A92NDT_fw	CGCCTG**NDT**TTCGAATCCTGGAGTCGTG
A92NDT_rv	ATTCGAA**AHN**CAGGCGCATGTTTTCATGGC
F93NDT_fw	GAAAACATGCGTCTGGCC**NDT**GAATCCT
F93NDT_rv	ACACGACTCCAGGATTC**AHN**GGCCAG
S95NDT_fw	CGCCTGGCGTTCGAA**NDT**TGGAGT
S95NDT_rv	TGTCCACACGACTCCA**AHN**TTCGAACG
S97NDT_fw	GCGTTCGAATCCTGG**NDT**CGTGTG
S97NDT_rv	CAATGATTTTGTCCACACG**AHN**CCAGGAT
L18R_K22NDT_fw	TGTCCTG**NDT**CAAGGCGATAACTATGTG
L18R_K22NDT_rv	GCCTTG**AHN**CAGGACATTACGCAG
A11NDT_fw	CTGCGT**NDT**CAAACCAATTAGATCCTG
A11NDT_rv	TGGTTTG**AHN**ACGCAGCATTTCTT
L18R_fw	GATCCTG**CGC**AATGTCCTGAAACAAG
L18R_rv	GGACATT**GCG**CAGGATCTAATTGGTTTG
Gibson_vector_fw	CACCCGCAGTTCGAAAAATAAAAGCTT
Gibson_vector_rv	GGGATTTCGGCACCCATATGTATATCTC
Gibson_insert_fw	GAGATATACATATGGGTGCCGAAATCCC
Gibson_insert_rv	AAGCTTTTATTTTTCGAACTGCGGGTG
L18R_N19NDT_fw	CTGCGT**NDT**GTCCTGAAACAAGGC
L18R_N19NDT_rv	TCAGGAC**AHN**ACGCAGGATCTAATTGG
S95G_M89NDT_fw	TGAAAAC**NDT**CGTCTGGCGTTCGAAG
S95G_M89NDT_rv	CCAGACG**AHN**GTTTTCATGGCCGATT
S95G_A92NDT_fw	CGCCTG**NDT**TTCGAAGGTTGGAGTCGTG
S95G_A92NDT_rv	CTTCGAA**AHN**CAGGCGCATGTTTTCATGGC
L18R_V15K_fw	ACCAAT**AAA**ATCCTGCGCAATGTCC
L18R_V15K_rv	GCAGGAT**TTT**ATTGGTTTGAGCACG
L18R_V15Y_fw	ACCAAT**TAT**ATCCTGCGCAATGTCC
L18R_V15Y_rv	GCAGGAT**ATA**ATTGGTTTGAGCACG

6. Protein Mass Spectrometry

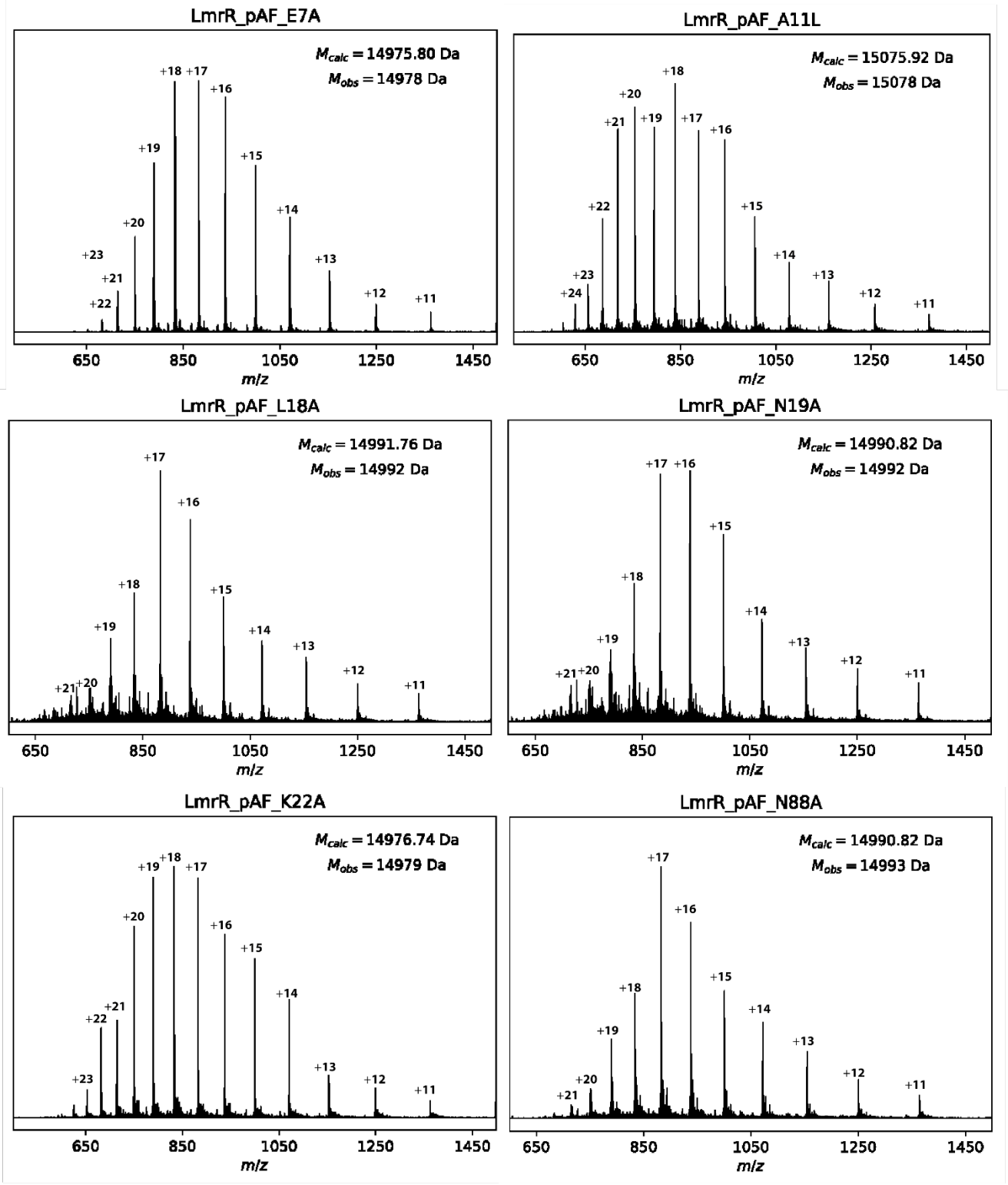

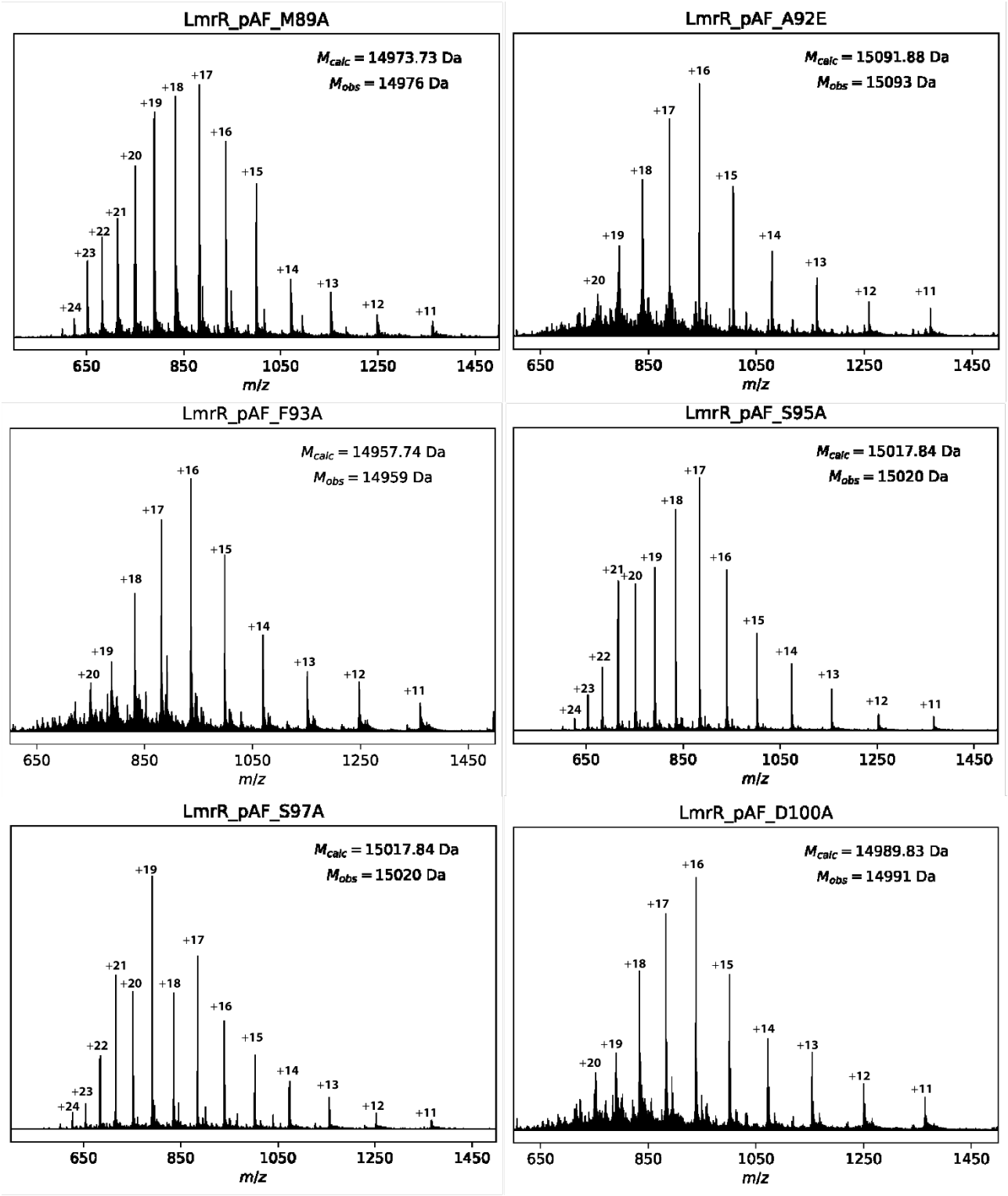
LmrR_pAF_M89A
M_{calc} = 14973.73 Da
M_{obs} = 14976 Da
LmrR_pAF_A92E
M_{calc} = 15091.88 Da
M_{obs} = 15093 Da
LmrR_pAF_F93A
M_{calc} = 14957.74 Da
M_{obs} = 14959 Da
LmrR_pAF_S95A
M_{calc} = 15017.84 Da
M_{obs} = 15020 Da
LmrR_pAF_S97A
M_{calc} = 15017.84 Da
M_{obs} = 15020 Da
LmrR_pAF_D100A
M_{calc} = 14989.83 Da
M_{obs} = 14991 Da
m/z

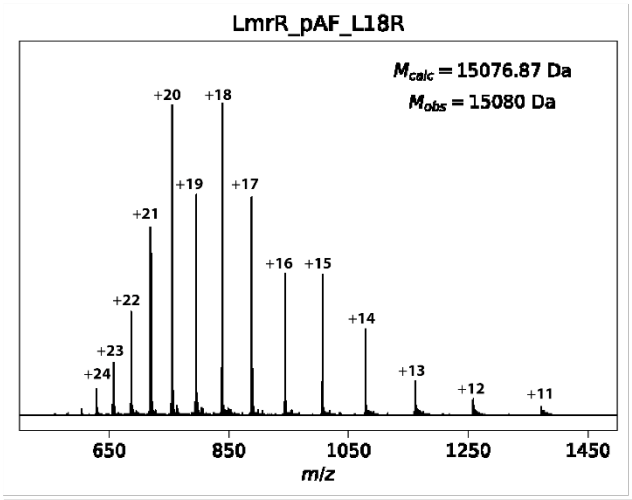
LmrR_pAF_L18R
M_{calc} = 15076.87 Da
M_{obs} = 15080 Da
+24
+23
+22
+21
+20
+19
+18
+17
+16
+15
+14
+13
+12
+11
650
850
1050
1250
1450
m/z

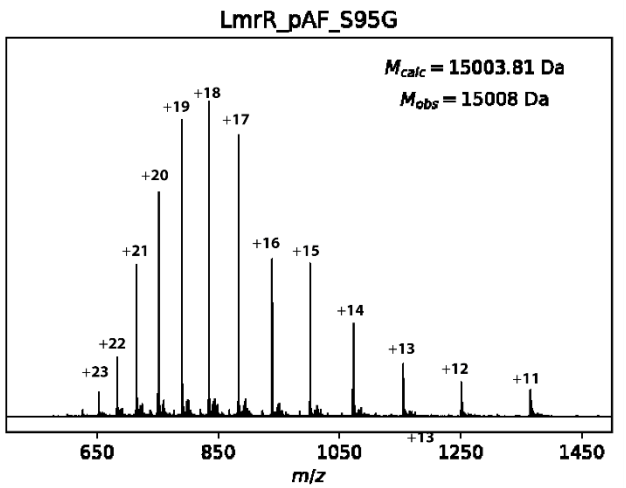
LmrR_pAF_S95G
M_{calc} = 15003.81 Da
M_{obs} = 15008 Da
+23
+22
+21
+20
+19
+18
+17
+16
+15
+14
+13
+12
+11
650
850
1050
1250
1450
m/z

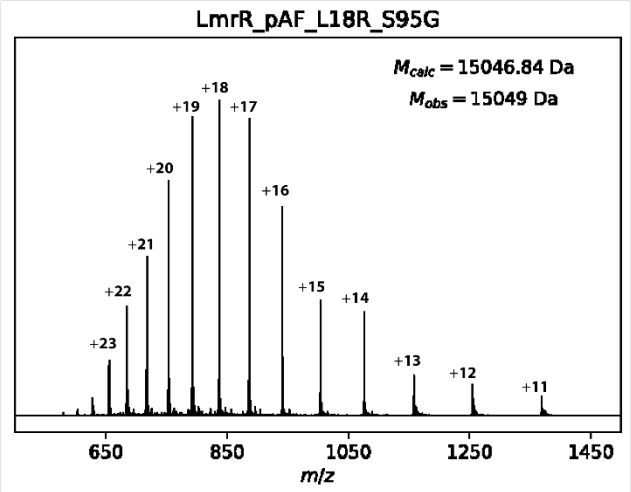
LmrR_pAF_L18R_S95G
M_{calc} = 15046.84 Da
M_{obs} = 15049 Da
+23
+22
+21
+20
+19
+18
+17
+16
+15
+14
+13
+12
+11
650
850
1050
1250
1450
m/z

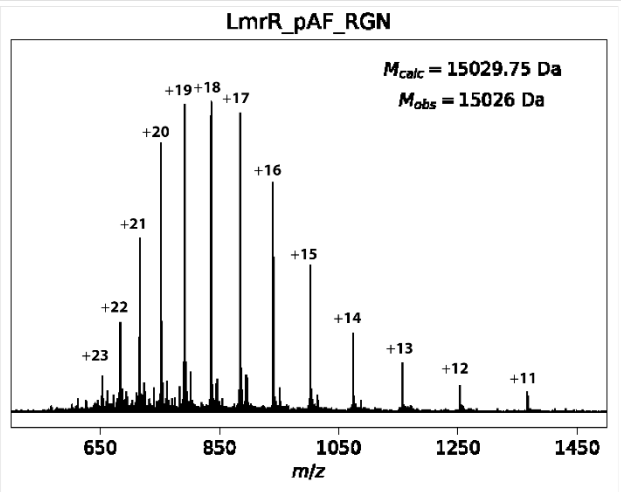
LmrR_pAF_RGN
M_{calc} = 15029.75 Da
M_{obs} = 15026 Da
+23
+22
+21
+20
+19
+18
+17
+16
+15
+14
+13
+12
+11
650
850
1050
1250
1450
m/z

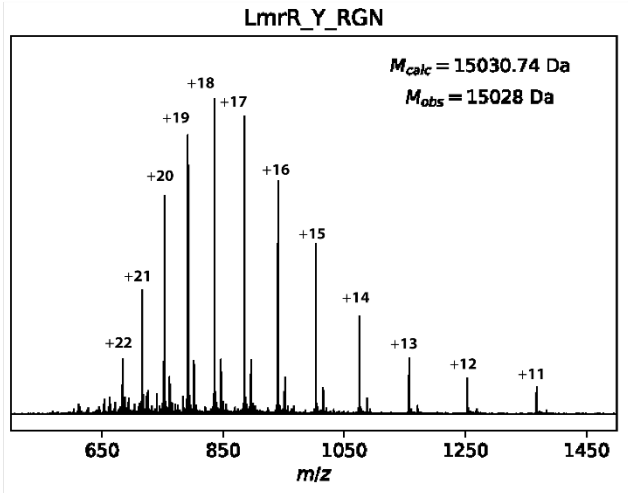
LmrR_Y_RGN
M_{calc} = 15030.74 Da
M_{obs} = 15028 Da
+22
+21
+20
+19
+18
+17
+16
+15
+14
+13
+12
+11
650
850
1050
1250
1450
m/z

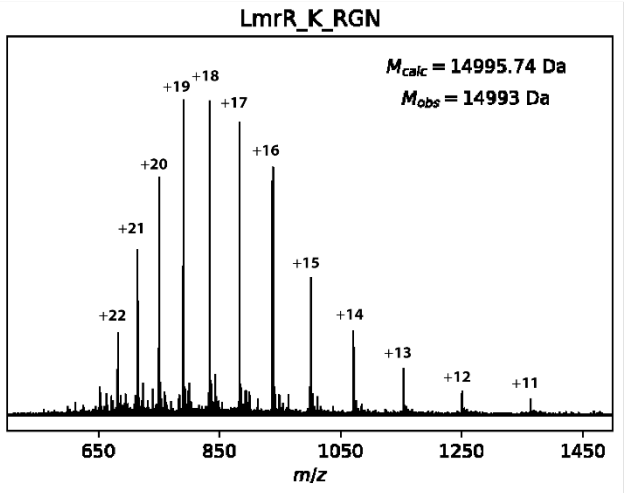
LmrR_K_RGN
M_{calc} = 14995.74 Da
M_{obs} = 14993 Da
+22
+21
+20
+19
+18
+17
+16
+15
+14
+13
+12
+11
650
850
1050
1250
1450
m/z

7. Preparation and Characterisation of Reference Products

7.1 Comment on Preparation of reference products

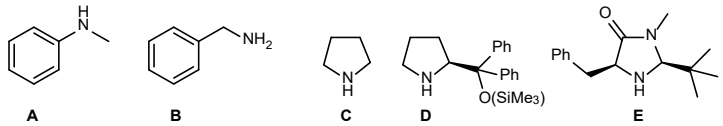

In our hands, racemic reference products could not be efficiently prepared using achiral primary or secondary amines **A**, **B** or **C**. The resulting reaction mixtures obtained using the procedure below with 20 mol % of these catalysts resulted in a complex mixture and an abundance of residual indole as evidenced by TLC. Similar difficulties have been reported elsewhere[6]. Instead, we prepared reference compounds using chiral secondary amines **D** or **E** and diminished the enantioselectivity of the reaction by heating to 50 °C to obtain a mixture of both enantiomers. We demonstrated the separation of the product enantiomers thus obtained on two different chiral stationary phases with normal phase HPLC, measuring very comparable ee in each case, and used these products to prepare calibration curves. We also prepared the racemic products in a crude form without purification using benzylamine **B** and analysed them with the HPLC method used to analyse enzyme catalysed reactions.

7.2 General Procedure for Preparation of Reference Products

Indole derivatives (0.5 mmol) and enal derivatives (1.5 mmol) and secondary amine **D** (16 mg, 0.05 mmol, general procedure **I**) or secondary amine **E** (12 mg, 0.05 mmol, general procedure **II**) were dissolved in MeOH (2 mL) in a 4 mL dram vial. The reaction mixtures were stirred at 50 °C (general procedure **II**) or ambient temperature (general procedure **I**) and monitored by TLC. After indole consumption was achieved, the reaction was cooled in an ice-bath and $NaBH_4$ (114 mg, 3 mmol) was added portion-wise with stirring. After the addition was complete, the reaction was stirred at ambient temperature for a further 30 minutes. The reaction was extracted with EtOAc (2 x 2 mL) and water/brine (2 mL) and the combined organic extracts were washed with brine (2 mL) and dried over Na_2SO_4. The EtOAc was removed *in vacuo* and the resulting extracts were purified by silica-gel chromatography (heptane:ethyl acetate 6:1-3:1, or pentane:ethyl acetate 3:1). The organic solvent was removed from product containing fractions from the column *in vacuo* to obtain the pure reference products.

7.3 General Procedure for Preparation of Crude Racemic Reference Products

Indole derivatives (0.167 mmol) and enal derivatives (0.5 mmol) and benzylamine **B** (4 μL, 0.033 mmol) were dissolved in methanol (0.7 mL) in a 4 mL dram vial. The reaction mixtures were stirred at 50 °C for 16-21 hr (compounds **3a, 3b, 3c, 3e, 3f, 3g, 3h, 3i**) or 2.5 hr (**3d**) after which time the reaction was cooled to 0 °C in an ice bath and $NaBH_4$ (37 mg, 1 mmol) was added portionwise, after which the reaction was stirred at room temperature for a further 30 minutes. The reaction was extracted with EtOAc (2 x 1 mL) and water/brine (1 mL) and the organic extract was washed with brine (1 mL) and dried over Na_2SO_4. The EtOAc was removed *in vacuo* and the resulting crude product was analysed by HPLC.

7.4 Characterisation of Reference Products

3-(2-methyl-1H-indol-3-yl)hexan-1-ol (3a)

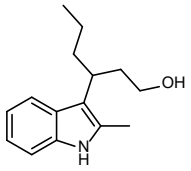

Prepared via general procedure **I** from 2-methyl-indole and trans-2-hexenal, isolated as a pale yellow oil. ^{1}H NMR (400 MHz, $CDCl_3$) δ 7.73 (s, 1H), 7.59 (d, *J* = 7.8 Hz, 1H), 7.26 (d, *J* = 8.0 Hz, 1H), 7.14 – 7.06 (m, 1H), 7.06 – 6.98 (m, 1H), 3.62 – 3.42 (m, 2H), 3.03 – 2.88 (m, 1H), 2.37 (s, 3H), 2.19 – 2.07 (m, 1H), 2.07 – 1.85 (m, 2H), 1.75 – 1.65 (m, 1H), 1.29 – 1.11 (m, 2H), 0.84 (t, *J* = 7.3 Hz, 3H). ^{13}C NMR (101 MHz, $CDCl_3$) δ 135.8, 131.4, 127.5, 120.8, 119.5, 118.9, 113.8, 110.5, 62.1, 38.2, 38.0, 33.6, 21.3, 14.3, 12.3. HRMS (ESI+) calc'd for $C_{15}H_{22}NO$ ($[M+H]^+$) 232.1696; found 232.1695. HPLC Chiracel® OJ-H (heptane:isopropanol 80:20 1 mL/min) 5.7 min (minor); 6.4 min (major) (22 % ee). Chiralcel® AS-H (heptane:isopropanol 90:10 1 mL/min) 5.5 min (minor); 6.1 min (major) (23 % ee).

4-methyl-3-(2-methyl-1H-indol-3-yl)pentan-1-ol (3b)

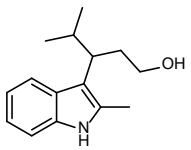

Prepared via general procedure **II** from 2-methyl-indole and 4-methyl-2-pentenal, isolated as a pale yellow oil. ^{1}H NMR (400 MHz, $(CD_3)_2SO$) δ 10.60 (s, 1H), 7.43 (d, *J* = 7.9 Hz, 1H), 7.20 (d, *J* = 7.9 Hz, 1H), 6.96 – 6.89 (m, 1H), 6.88 – 6.82 (m, 1H), 4.17 (t, *J* = 5.0 Hz, 1H), 3.24 – 3.00 (m, 2H), 2.27 (s, 3H), 2.14 – 1.84 (m, 3H), 1.01 (d, *J* = 6.5 Hz, 3H), 0.65 (d, *J* = 6.6 Hz, 3H). ^{13}C NMR (101 MHz, $CDCl_3$) δ 135.7, 131.7, 127.8, 120.8, 119.7, 119.0, 113.5, 110.4, 62.5, 41.4, 34.9, 32.8, 21.9, 21.8, 12.4. HRMS (ESI+) calc'd for $C_{15}H_{22}NO$ ($[M+H]^+$) 232.1696; found 232.1697. HPLC Chiralcel® AS-H (heptane:isopropanol 90:10 0.5 mL/min) 11.2 min (minor); 12.9 min (major) (74 % ee). Chiracel® OJ-H (heptane:isopropanol 80:20 1 mL/min) 5.7 min (min); 8.4 min (maj) (73 % ee).

3-(2-methyl-1H-indol-3-yl)butan-1-ol (3c)

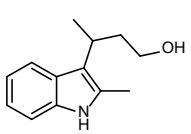

Prepared via general procedure **II** 2-methyl indole and crotonaldehyde, isolated as a colourless oil. ^{1}H NMR (400 MHz, $CDCl_3$) δ 7.72 (s, 1H), 7.60 (d, *J* = 7.8 Hz, 1H), 7.29 – 7.21 (m, 1H), 7.13 – 6.98 (m, 2H), 3.61 – 3.44 (m, 2H), 3.22 – 3.08 (m, 1H), 2.36 (s, 3H), 2.19 – 2.05 (m, 1H), 2.04 – 1.91 (m, 1H), 1.42 (d, *J* = 7.1 Hz, 3H). ^{13}C NMR (101 MHz, $CDCl_3$) δ 135.7, 130.4, 127.4, 120.9, 119.4, 119.0, 115.5, 110.5, 62.1, 39.6, 28.0, 21.5, 12.2. HRMS (ESI+) calc'd for $C_{13}H_{18}NO$ ($[M+H]^+$) 204.1383; found

204.1383. HPLC Chiracel® AS-H (heptane:isopropanol 90:10 0.5 mL/min) 12.8 min (minor); 14.1 min (major) (55 % ee). Chiracel® OJ-H (heptane:isopropanol 80:20 1 mL/min) 8.9 min (minor); 12.5 min (major) (57 % ee).

3-(2-methyl-1H-indol-3-yl)-3-phenylpropan-1-ol (3d)

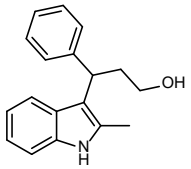

Prepared via general procedure **II** from 2-methyl-indole and cinnamaldehyde, isolated as a colourless oil. ^{1}H NMR (400 MHz, $CDCl_3$) δ 7.77 (s, 1H), 7.48 (d, J = 7.9 Hz, 1H), 7.37 – 7.32 (m, 2H), 7.25 – 7.19 (m, 3H), 7.17 – 6.93 (m, 3H), 4.41 (t, J = 8.0 Hz, 1H), 3.76 – 3.61 (m, 1H), 3.61 – 3.50 (m, 1H), 2.58 – 2.46 (m, 2H), 2.39 (s, 3H). ^{13}C NMR (101 MHz, $CDCl_3$) δ 145.1, 135.6, 131.7, 128.4, 127.9, 127.8, 125.9, 121.0, 119.5, 119.4, 113.5, 110.5, 61.8, 38.2, 37.0, 12.4.. HRMS (ESI+) calc'd for $C_{18}H_{20}NO$ ($[M+H]^+$) 266.1539; found 266.1540. HPLC Chiracel® OJ-H (heptane:isopropanol 80:20 1 mL/min) 10.5 min (minor); 12.8 min (major) (31 % ee). Chiracel® OD-H (heptane:isopropanol 85:15 1 mL/min) 25.7 min (major); 29.8 min (minor) (31 % ee).

3-(1H-indol-3-yl)hexan-1-ol (3e)

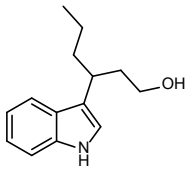

Prepared via general procedure **II** from indole and trans-2-hexenal, isolated as a colourless oil. ^{1}H NMR (400 MHz, $(CD_3)_2SO$) δ 10.74 (s, 1H), 7.53 (d, J = 7.9 Hz, 1H), 7.31 (d, J = 8.1 Hz, 1H), 7.05 (d, J = 2.3 Hz, 1H), 7.03 (ddd, J = 8.2, 6.9, 1.2 Hz, 1H), 6.92 (ddd, J = 8.0, 6.9, 1.1 Hz, 1H), 3.36 – 3.22 (m, 2H), 3.00 – 2.89 (m, 1H), 1.81 (q, J = 7.0 Hz, 2H), 1.73 – 1.55 (m, 2H), 1.22 – 1.11 (m, 2H), 0.81 (t, J = 7.4 Hz, 3H). ^{13}C NMR (101 MHz, $CDCl_3$) δ 136.7, 127.1, 122.0, 121.2, 119.8, 119.7, 119.2, 111.3, 61.9, 39.0, 38.7, 33.6, 20.9, 14.3. HRMS (APCI+) calc'd for $C_{14}H_{20}NO$ ($[M+H]^+$) 218.1539; found 218.1541. HPLC Chiracel® OD-H (heptane:isopropanol 85:15 1 mL/min) 12.0 min (major); 14.2 min (minor) (68 % ee). Chiracel® OJ-H (heptane:isopropanol 80:20 1 mL/min) 9.8 min (minor); 11.5 min (major) (67 % ee).

3-(5-methyl-1H-indol-3-yl)hexan-1-ol (3f)

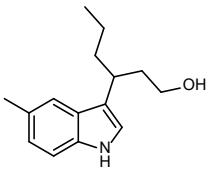

Prepared via general method **II** from 5-methyl-indole and trans-2-hexenal, isolated as a colourless oil. ^{1}H NMR (400 MHz, $CDCl_3$) δ 7.91 (s, 1H), 7.43 (s, 1H), 7.25 (d, J = 8.3 Hz, 1H), 7.01 (dd, J = 8.3, 1.6 Hz, 1H), 6.93 (d, J = 2.4 Hz, 1H), 3.65 – 3.50 (m, 2H), 3.10 – 2.93 (m, 1H), 2.46 (s, 3H), 2.06 – 1.95 (m, 2H), 1.81 – 1.66 (m, 2H), 1.31 – 1.21 (m, 2H), 0.87 (t, J = 7.4 Hz, 3H). ^{13}C NMR (101 MHz, $CDCl_3$) δ 135.1, 128.4, 127.3, 123.7, 121.4, 119.3, 119.2, 111.0, 61.9, 38.9, 38.7, 33.7, 21.7, 21.0, 14.3. HRMS (ESI+) calc'd for $C_{15}H_{22}NO$ ($[M+H]^+$) 232.1696; found 232.1698. HPLC Chiracel® AS-H

(heptane:isopropanol 90:10 0.5 mL/min) 12.2 min (minor); 13.1 min (major) (68 % ee). Chiracel® OD-H (heptane:isopropanol 85:15 1 mL/min) 10.5 min (major); 11.1 min (minor) (68 % ee).

3-(5-methoxy-1H-indol-3-yl)hexan-1-ol (3g)

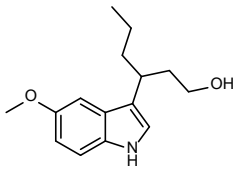

Prepared via general method **II** 5-methoxy-indole and trans-2-hexenal, isolated as a colourless oil. ^{1}H NMR (400 MHz, $CDCl_3$) δ 7.98 (s, 1H), 7.23 (d, *J* = 8.8 Hz, 1H), 7.10 (d, *J* = 2.4 Hz, 1H), 6.93 (d, *J* = 2.4 Hz, 1H), 6.86 (dd, *J* = 8.8, 2.4 Hz, 1H), 3.87 (s, 3H), 3.66 – 3.53 (m, 2H), 3.07 – 2.95 (m, 1H), 2.04 – 1.92 (m, 2H), 1.80 – 1.63 (m, 2H), 1.34 – 1.21 (m, 2H), 0.87 (t, *J* = 7.3 Hz, 3H). ^{13}C NMR (101 MHz, $CDCl_3$) δ 153.7, 131.9, 127.5, 122.1, 119.4, 112.0, 111.9, 101.8, 61.8, 56.1, 38.8, 38.6, 33.5, 20.9, 14.3. HRMS (ESI+) calc'd for $C_{15}H_{22}NO_2$ ($[M+H]^+$) 248.1645; found 248.1648. HPLC Chiracel® OD-H (heptane:isopropanol 85:15 1 mL/min) 13.9 min (major); 15.1 (minor) (68 % ee). Chiracel® OB-H (heptane:isopropanol 90:10 1 mL/min) 14.4 (major); 19.0 (minor) (69 % ee).

3-(5-bromo-1H-indol-3-yl)hexan-1-ol (3h)

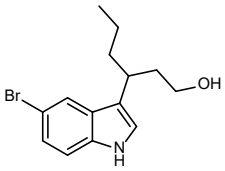

Prepared via general method **II** 5-bromo-indole and trans-2-hexenal, isolated as a colourless oil. ^{1}H NMR (400 MHz, $(CD_3)_2SO$) δ 11.00 (s, 1H), 7.67 (d, *J* = 1.9 Hz, 1H), 7.29 (d, *J* = 8.6 Hz, 1H), 7.17 – 7.10 (m, 2H), 3.35 – 3.21 (m, 2H), 2.99 – 2.87 (m, 1H), 1.87 – 1.69 (m, 2H), 1.68 – 1.54 (m, 2H), 1.23 – 1.09 (m, 2H), 0.81 (t, *J* = 7.3 Hz, 3H). ^{13}C NMR (101 MHz, $CDCl_3$) δ 135.3, 128.8, 124.9, 122.4, 122.2, 119.5, 112.8, 112.6, 61.7, 38.8, 38.6, 33.4, 20.9, 14.2. HRMS calc'd for $C_{14}H_{18}BrNO$ ($[M+H]^+$) 296.0645 and 298.0624; found 269.0655 and 298.0631. HPLC Chiracel® AS-H (heptane:isopropanol 90:10 0.5 mL/min) 14.0 min (minor); 15.3 min (major) (67 % ee). Chiracel® OD-H (heptane:isopropanol 85:15 1 mL/min) 10.2 min (major); 11.8 min (minor) (67 % ee).

3-(5-methoxy-2-methyl-1H-indol-3-yl)hexan-1-ol (3i)

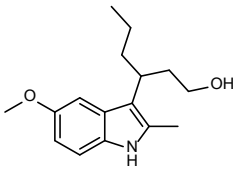

Prepared via general method **II** from 5-methoxy-2-methyl-indole and trans-2-hexenal, isolated as a colourless oil. ^{1}H NMR (400 MHz, $CDCl_3$) δ 7.63 (s, 1H), 7.15 (d, *J* = 8.7 Hz, 1H), 7.05 (d, *J* = 2.4 Hz, 1H), 6.75 (dd, *J* = 8.7, 2.4 Hz, 1H), 3.84 (s, 3H), 3.60 – 3.41 (m, 1H), 3.02 – 2.86 (m, 1H), 2.35 (s, 3H), 2.16 – 2.06 (m, 1H), 2.03 – 1.83 (m, 2H), 1.75 – 1.63 (m, 1H), 1.26 – 1.14 (m, 3H), 0.85 (t, *J* = 7.3 Hz, 3H). ^{13}C NMR (101 MHz, $CDCl_3$) δ 153.5, 132.4, 131.0, 128.0, 113.6, 110.9, 109.9, 102.6, 62.1, 56.2, 38.0, 37.8, 33.5, 21.3, 14.3, 12.4. HRMS calc'd for $C_{16}H_{24}NO_2$ ($[M+H]^+$) 262.1801; found 262.1804. HPLC Chiracel® OD-H (heptane:isopropanol 85:15 1 mL/min) 11.4 min (major); 17.7 min (minor) (64 % ee).

Chiracel® AS-H (heptane:isopropanol 90:10 0.5 mL/min) 12.3 min (minor); 14.1 min (major) (62 % ee).

8. Calibration Curves

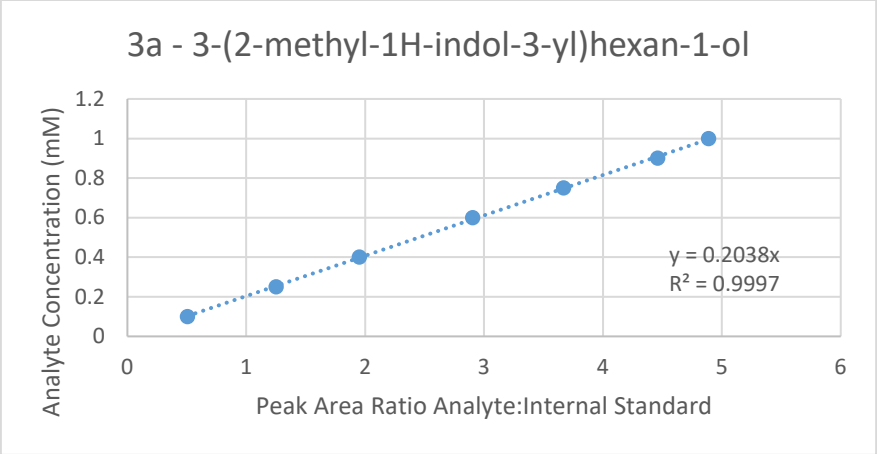

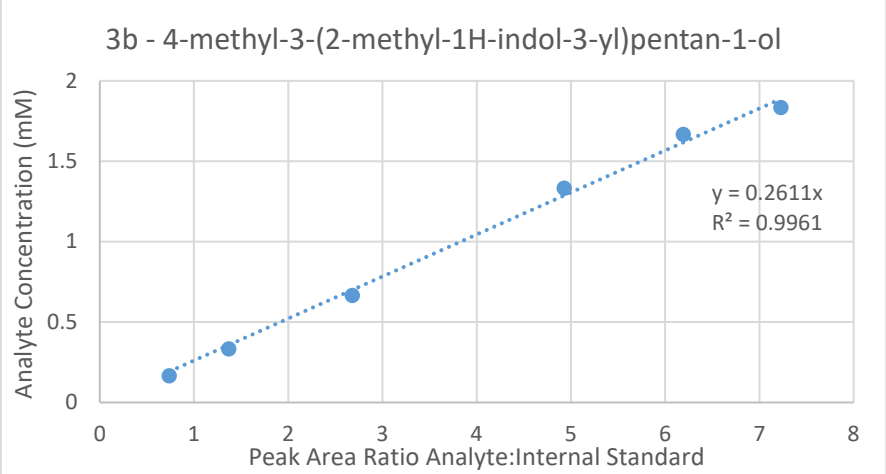

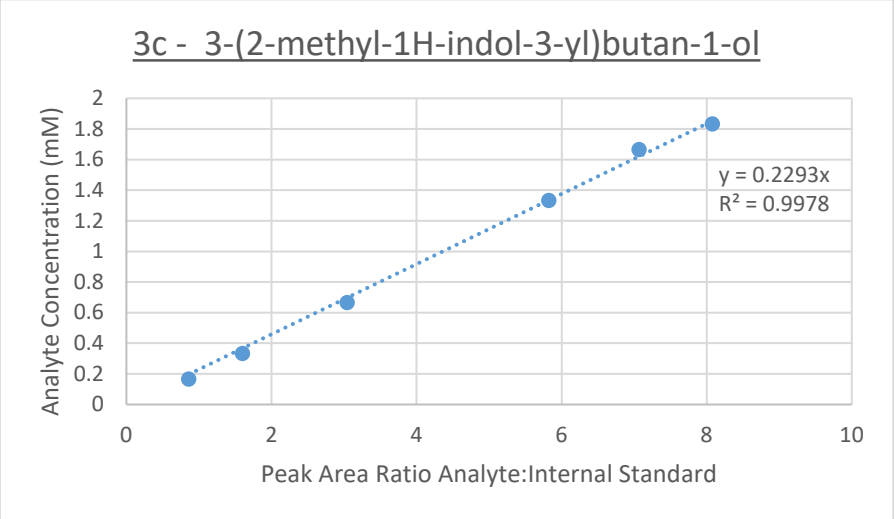

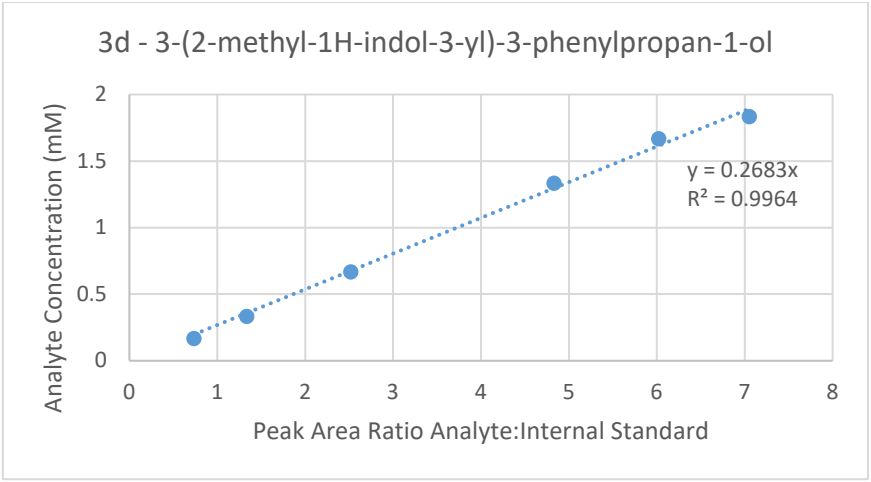
3d - 3-(2-methyl-1H-indol-3-yl)-3-phenylpropan-1-ol
Analyte Concentration (mM)
Peak Area Ratio Analyte:Internal Standard
y = 0.2683x
R² = 0.9964

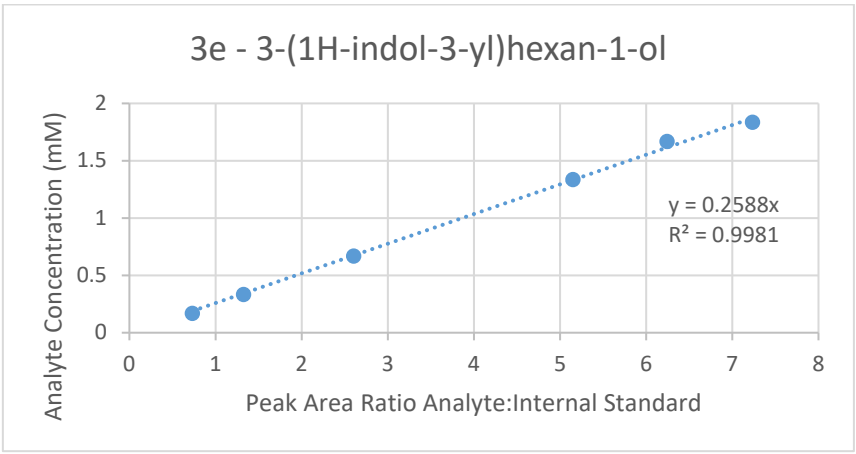
3e - 3-(1H-indol-3-yl)hexan-1-ol
Analyte Concentration (mM)
Peak Area Ratio Analyte:Internal Standard
y = 0.2588x
R² = 0.9981

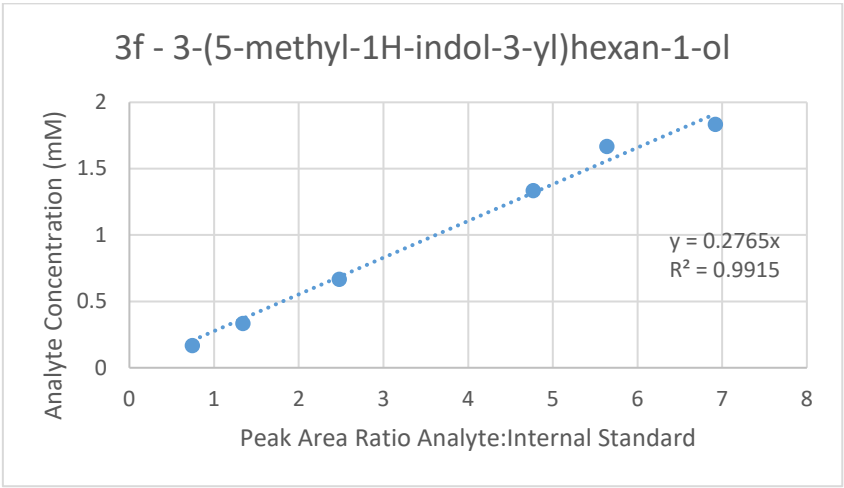
3f - 3-(5-methyl-1H-indol-3-yl)hexan-1-ol
Analyte Concentration (mM)
Peak Area Ratio Analyte:Internal Standard
y = 0.2765x
R² = 0.9915

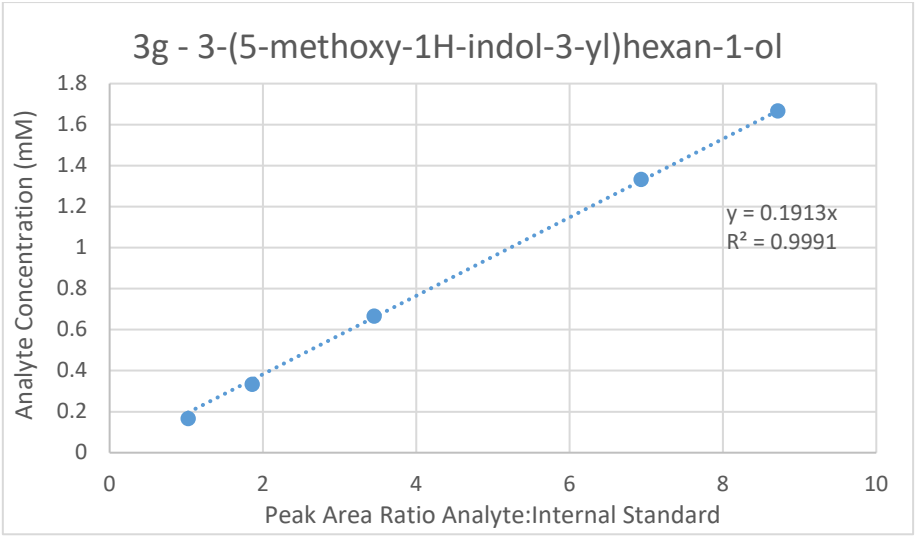
3g - 3-(5-methoxy-1H-indol-3-yl)hexan-1-ol
Analyte Concentration (mM)
Peak Area Ratio Analyte:Internal Standard
y = 0.1913x
R² = 0.9991

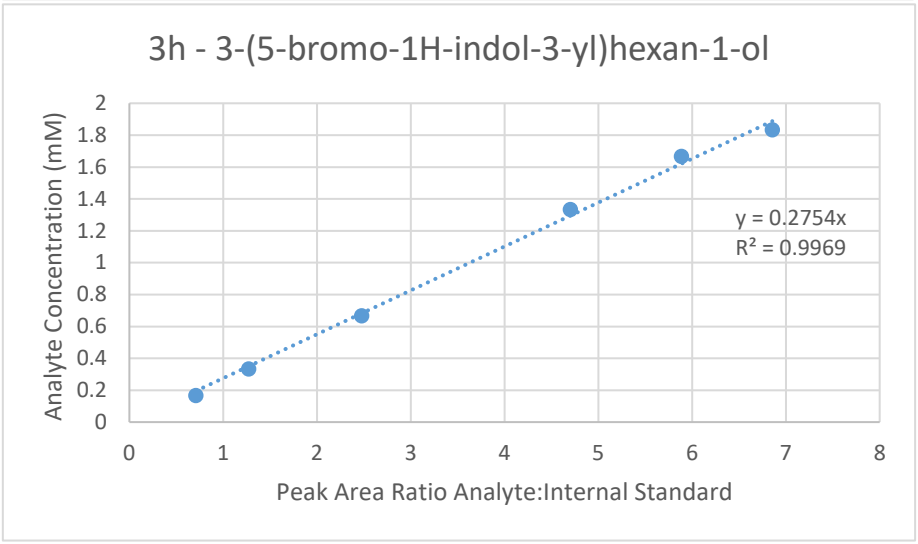
3h - 3-(5-bromo-1H-indol-3-yl)hexan-1-ol
Analyte Concentration (mM)
Peak Area Ratio Analyte:Internal Standard
y = 0.2754x
R² = 0.9969

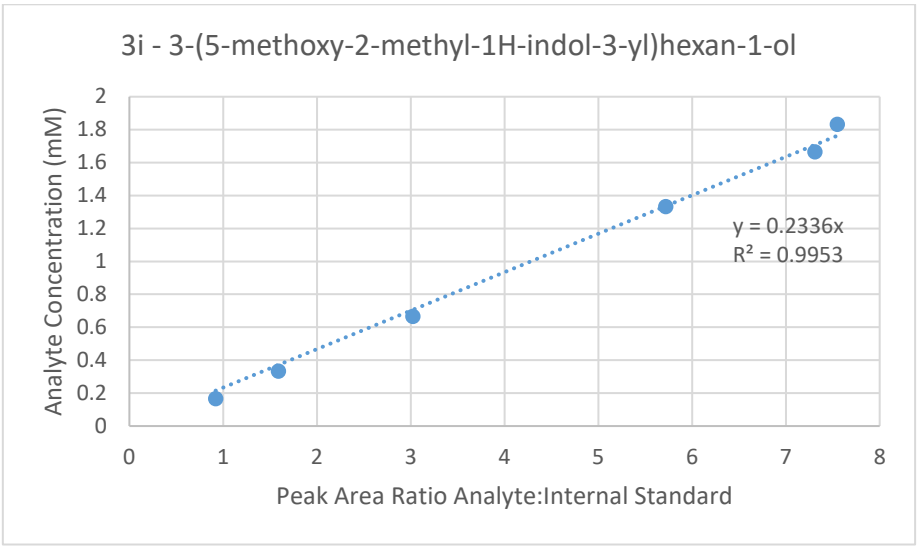
3i - 3-(5-methoxy-2-methyl-1H-indol-3-yl)hexan-1-ol
Analyte Concentration (mM)
Peak Area Ratio Analyte:Internal Standard
y = 0.2336x
R² = 0.9953

9. HPLC Chromatograms

3-(2-methyl-1H-indol-3-yl)hexan-1-ol (3a)

Reference compound and racemic crude product:

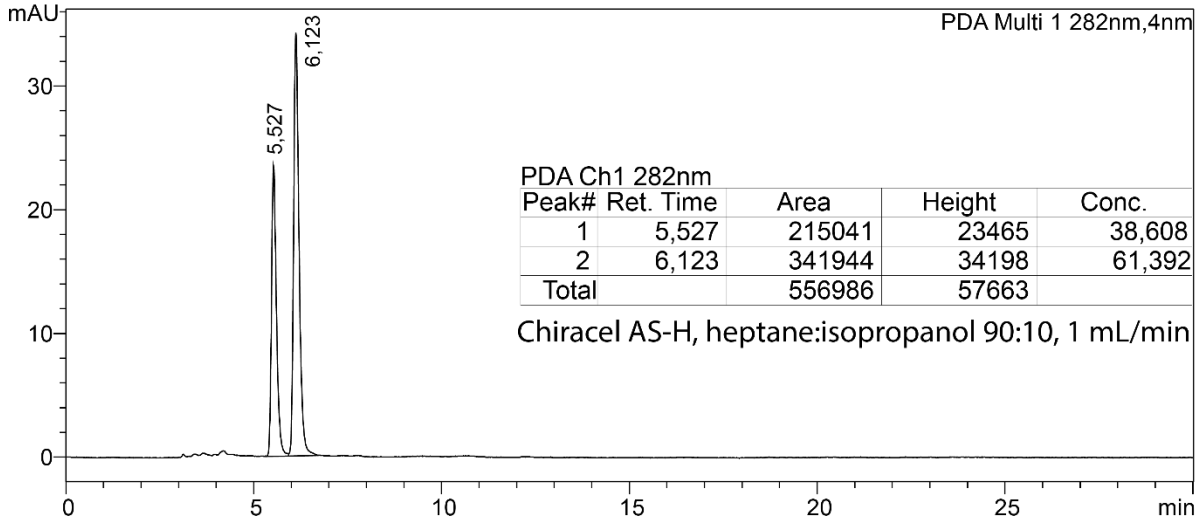

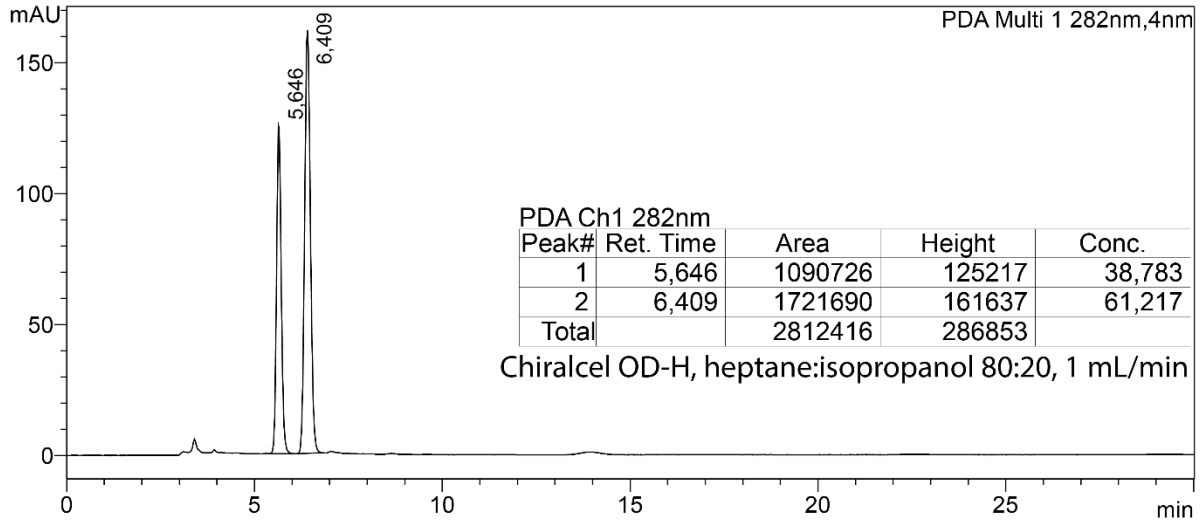

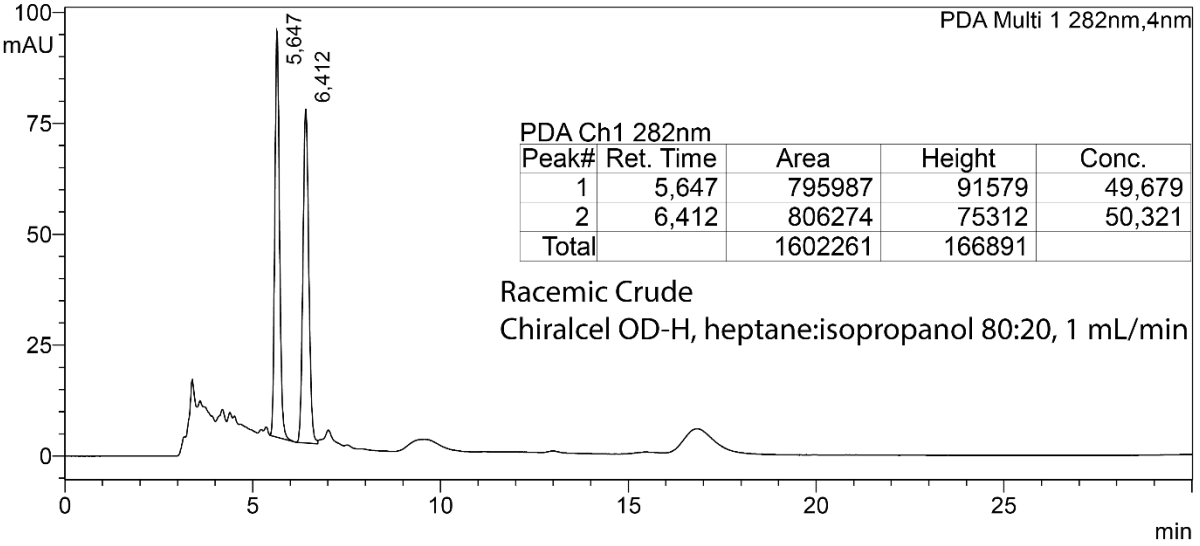

Artificial Enzyme catalysed reactions: Chiracel OJ-H, heptane isopropanol 80:20, 1 mL/min

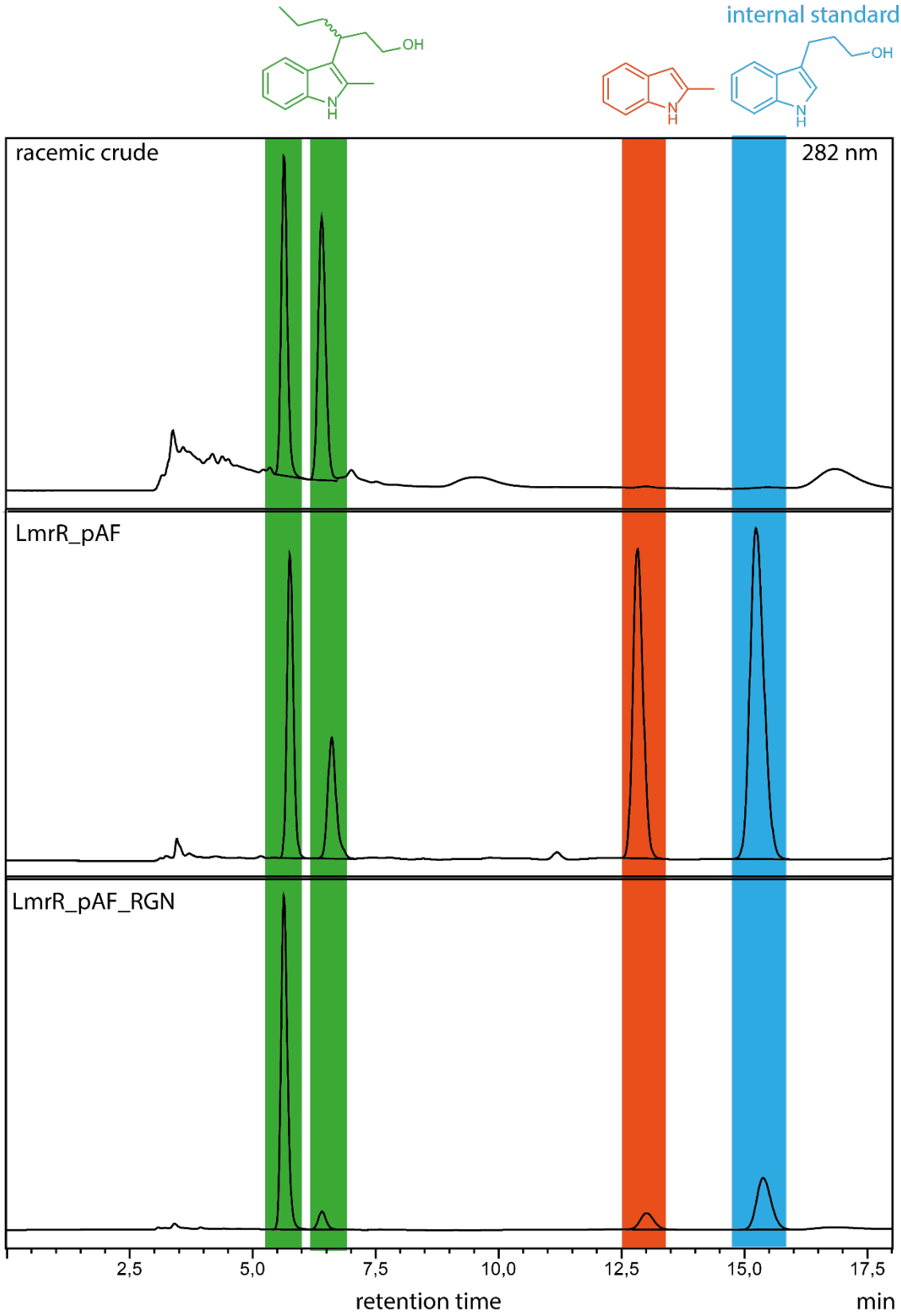

4-methyl-3-(2-methyl-1H-indol-3-yl)pentan-1-ol (3b)

Reference product and racemic crude product:

d

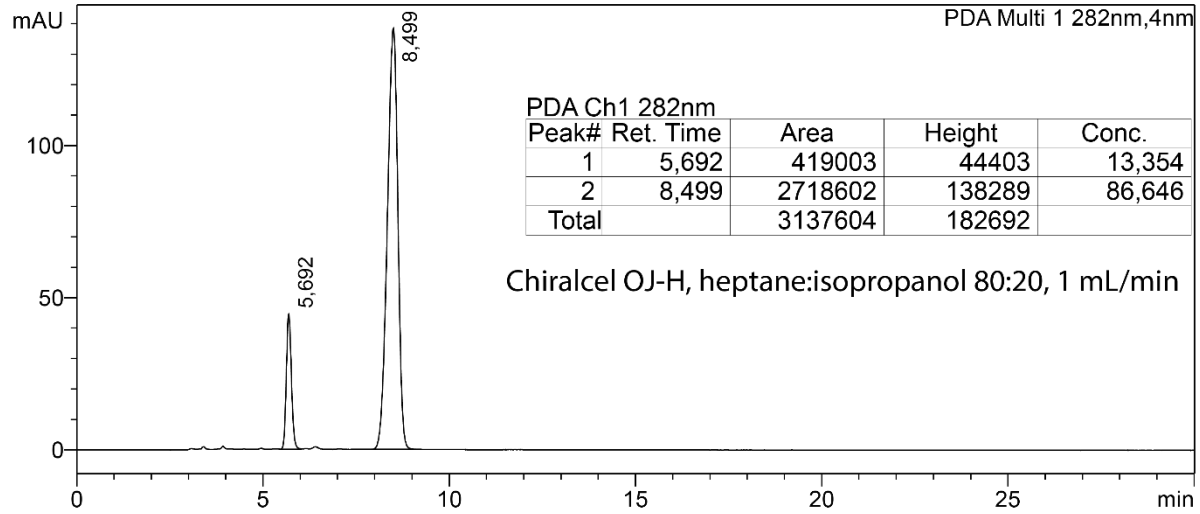

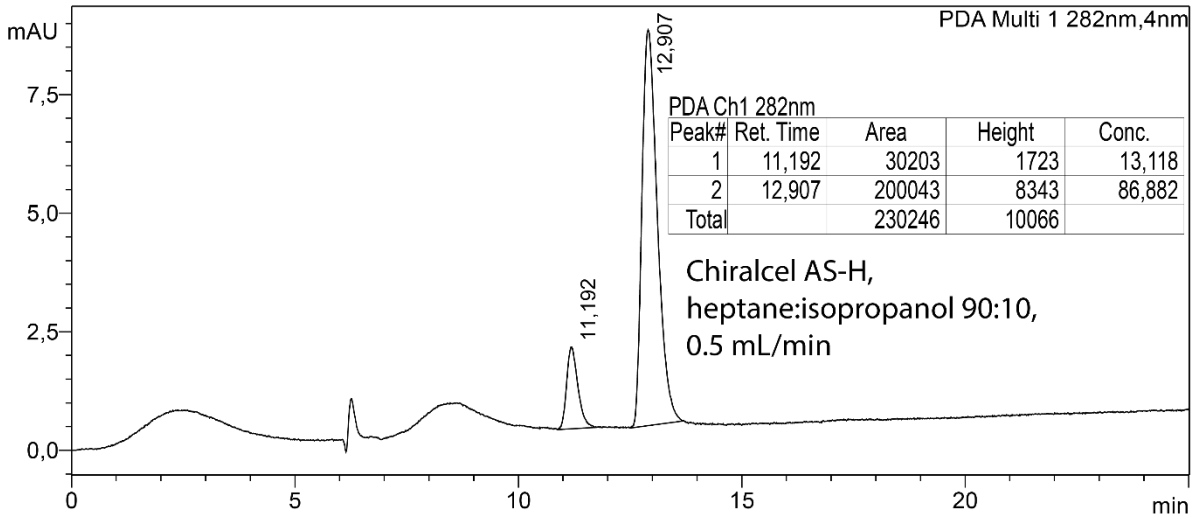

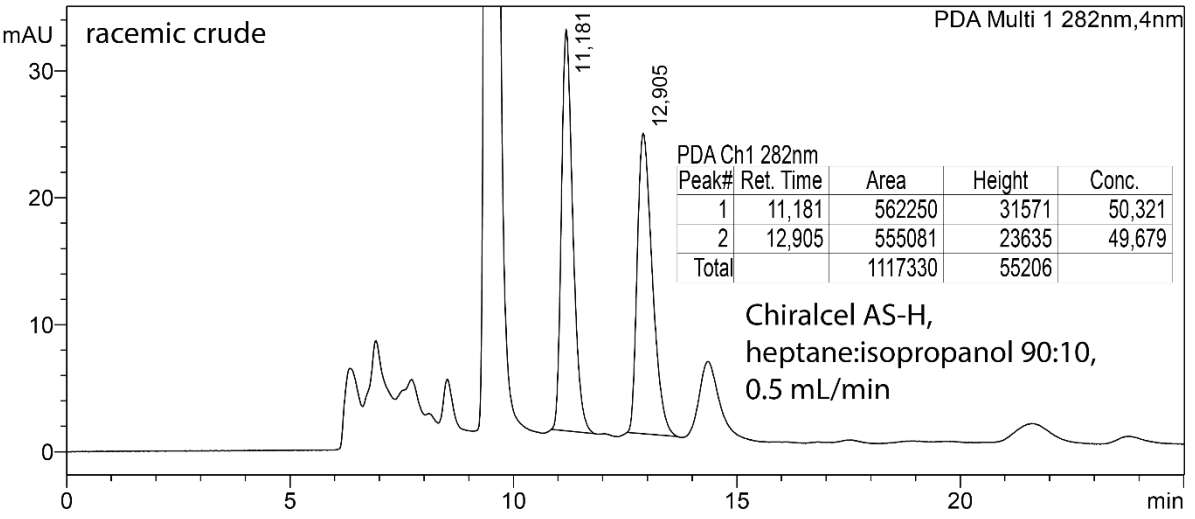

Artificial enzyme catalysed reactions: (Chiracel AS-H, heptane:isopropanol 90:10, 1 mL/min)

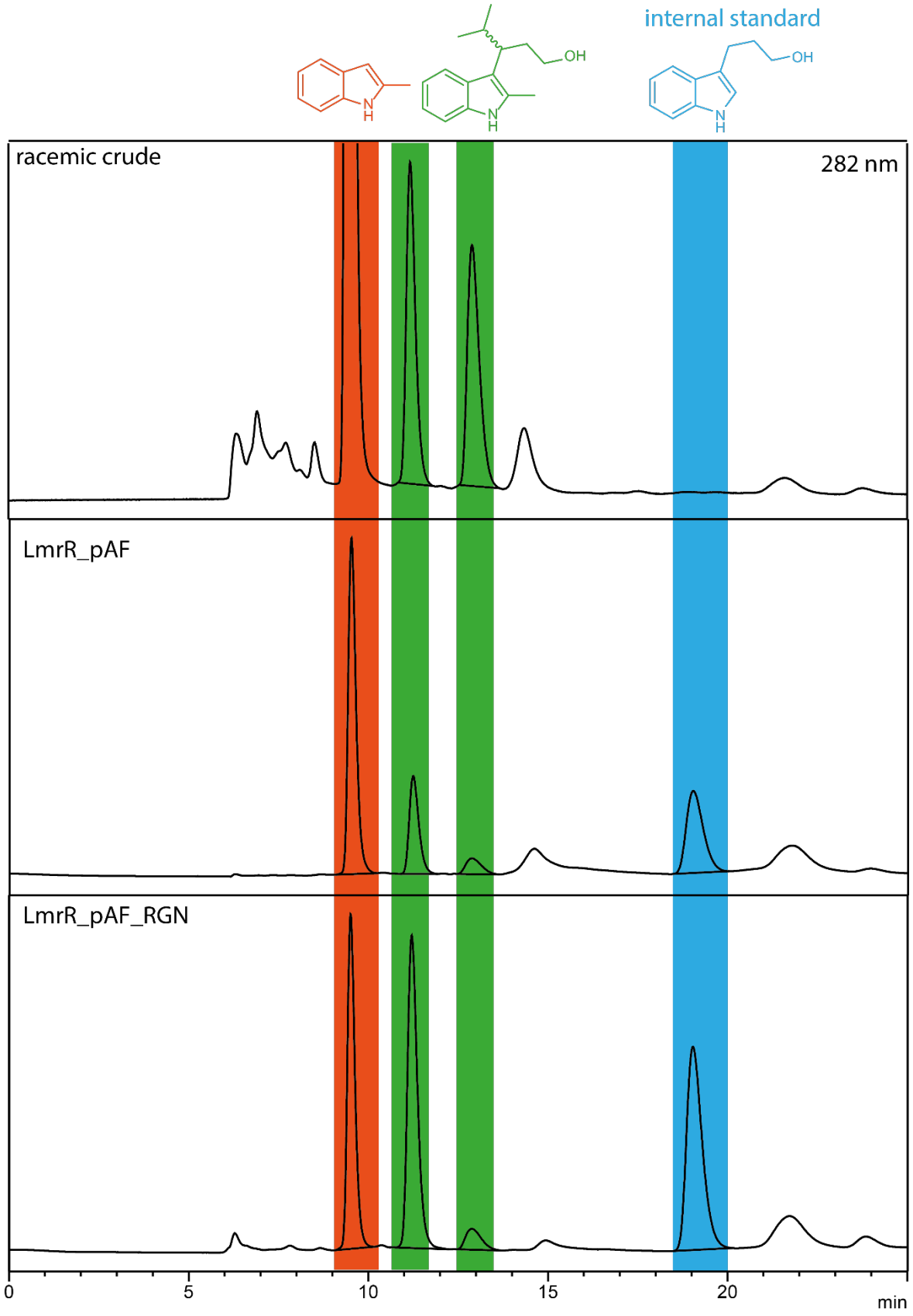

3-(2-methyl-1H-indol-3-yl)butan-1-ol (3c)

Reference compound and racemic crude product:

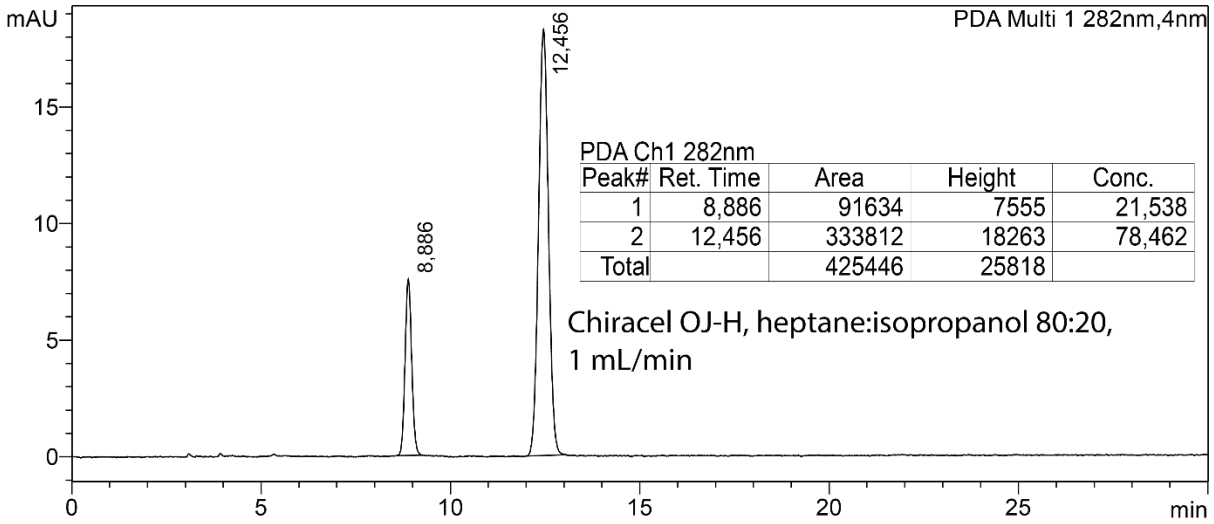

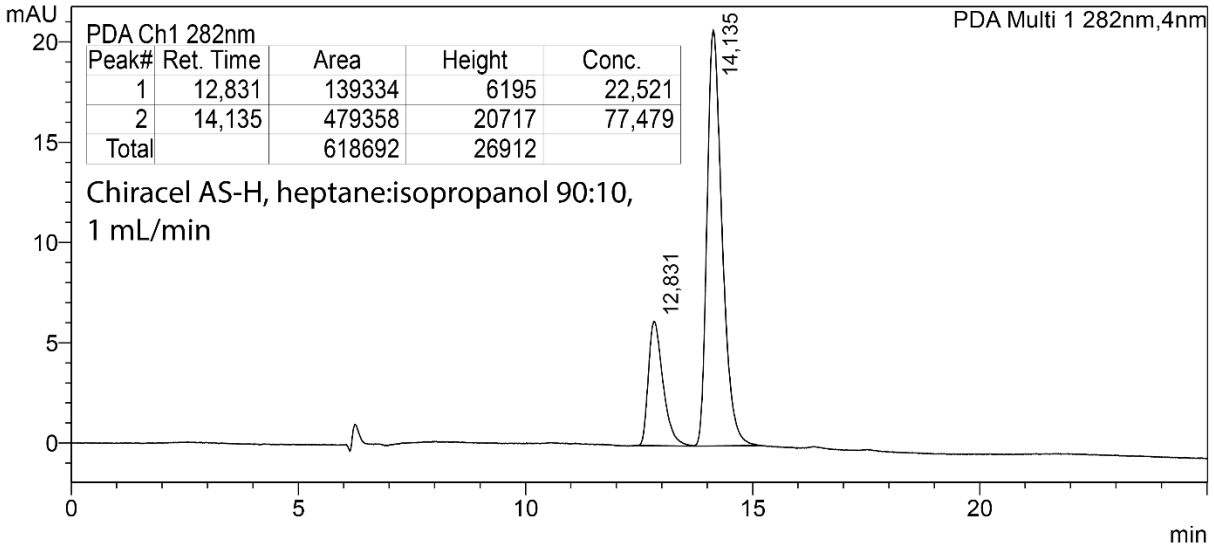

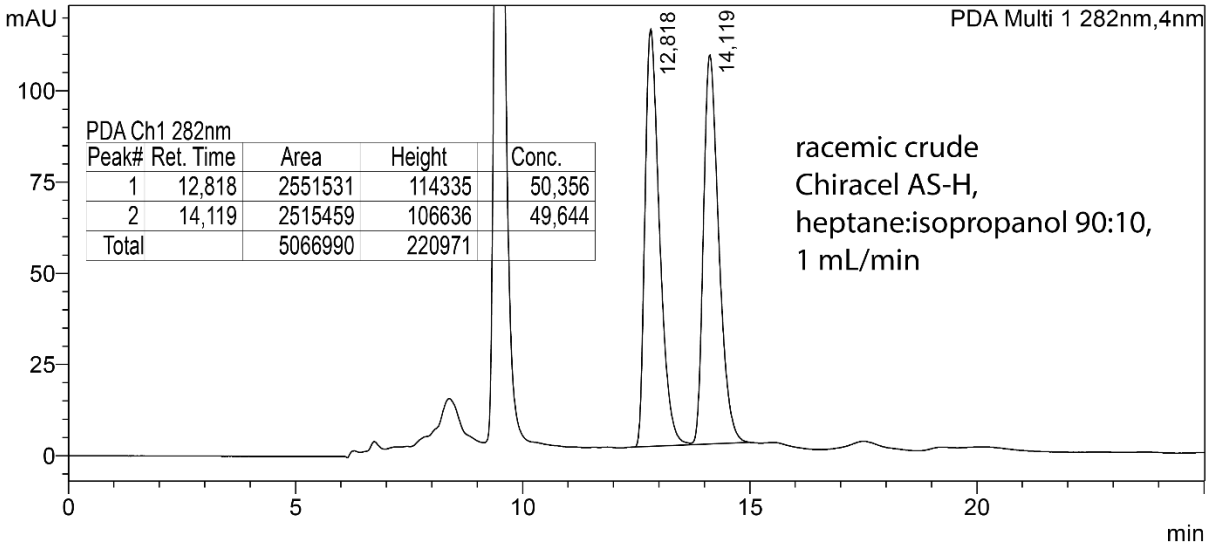

Artificial enzyme catalyzed reaction: (Chiracel AS-H, heptane:isopropanol 90:10, 0.5 mL/min)

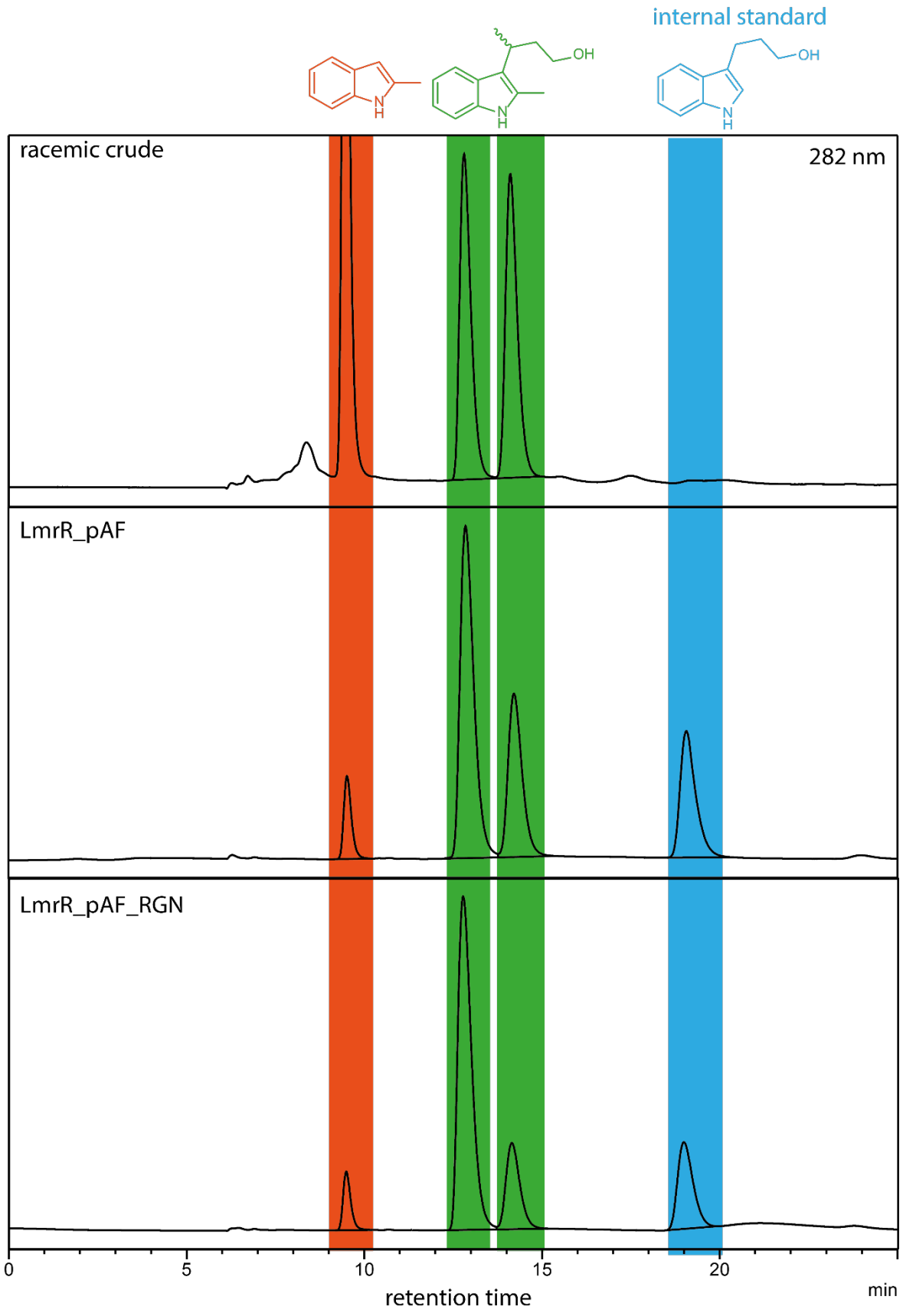

3-(2-methyl-1H-indol-3-yl)-3-phenylpropan-1-ol (3d)

Reference compound and racemic crude product:

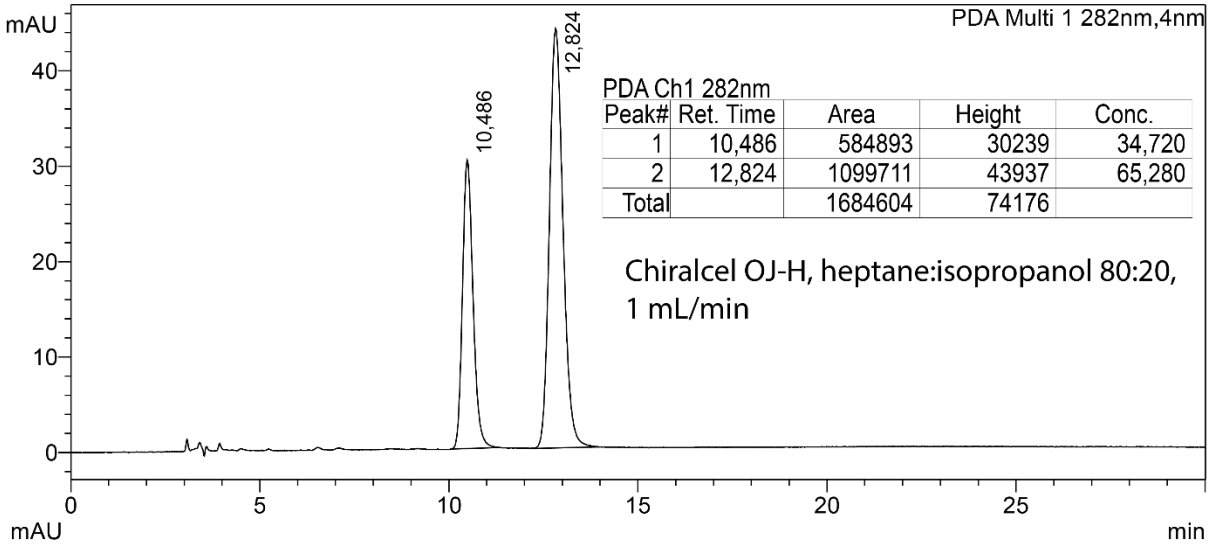

PDA Ch1 282nm

Peak#	Ret. Time	Area	Height	Conc.
1	10,486	584893	30239	34,720
2	12,824	1099711	43937	65,280
Total		1684604	74176	

Chiralcel OJ-H, heptane:isopropanol 80:20, 1 mL/min

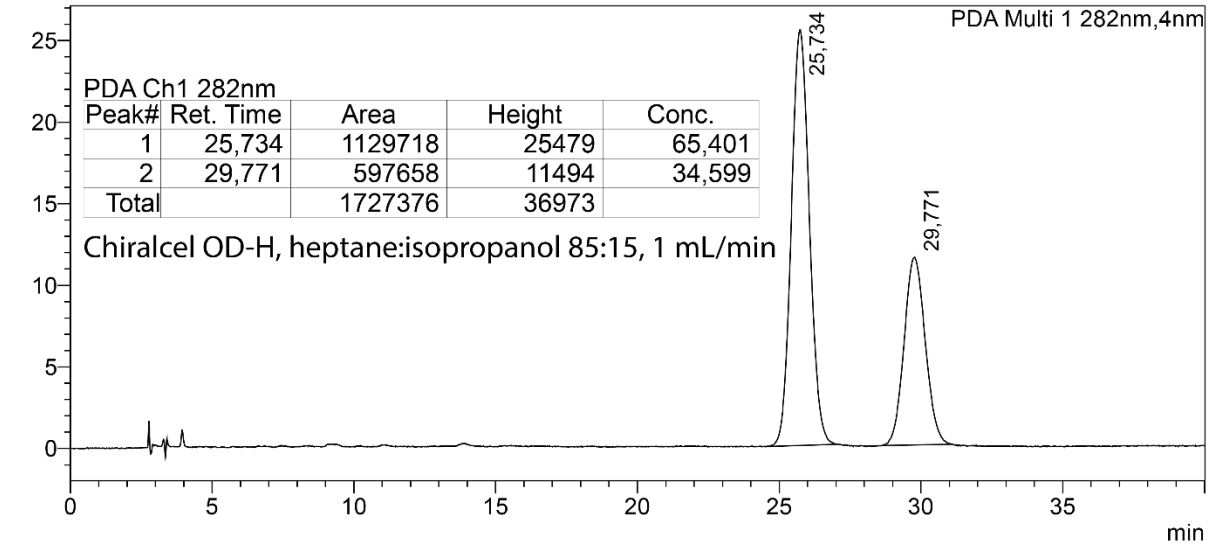

PDA Ch1 282nm

Peak#	Ret. Time	Area	Height	Conc.
1	25,734	1129718	25479	65,401
2	29,771	597658	11494	34,599
Total		1727376	36973	

Chiralcel OD-H, heptane:isopropanol 85:15, 1 mL/min

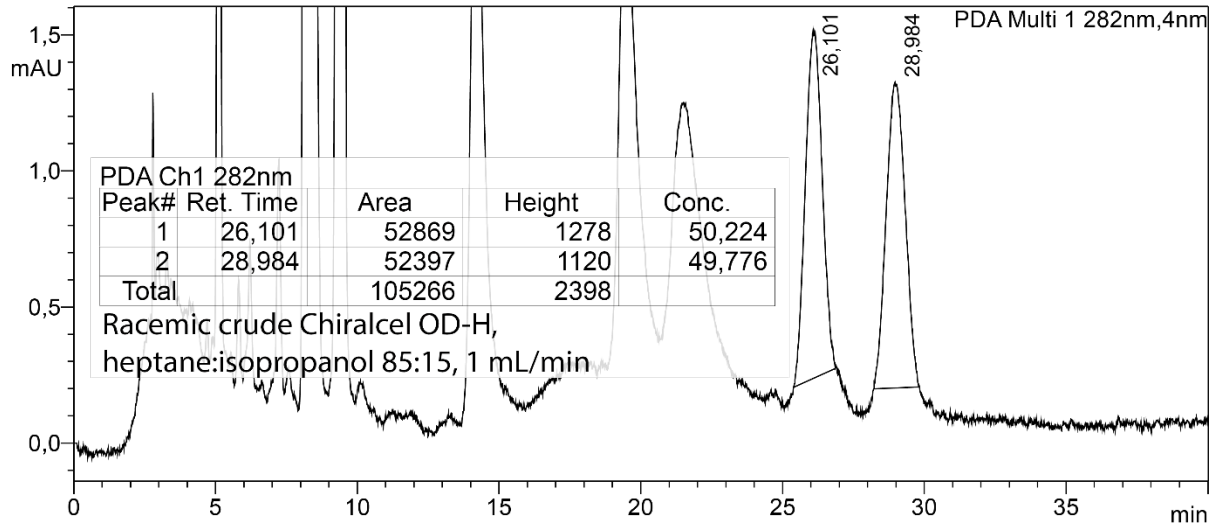

PDA Ch1 282nm

Peak#	Ret. Time	Area	Height	Conc.
1	26,101	52869	1278	50,224
2	28,984	52397	1120	49,776
Total		105266	2398	

Racemic crude Chiralcel OD-H, heptane:isopropanol 85:15, 1 mL/min

Artificial enzyme catalysed reaction: (Chiracel OD-H, heptane:isopropanol 85:15, 1 mL/min)

On account of abundant side-products evident in the racemic reaction, the enantioenriched reference compound chromatogram is shown instead for comparison.

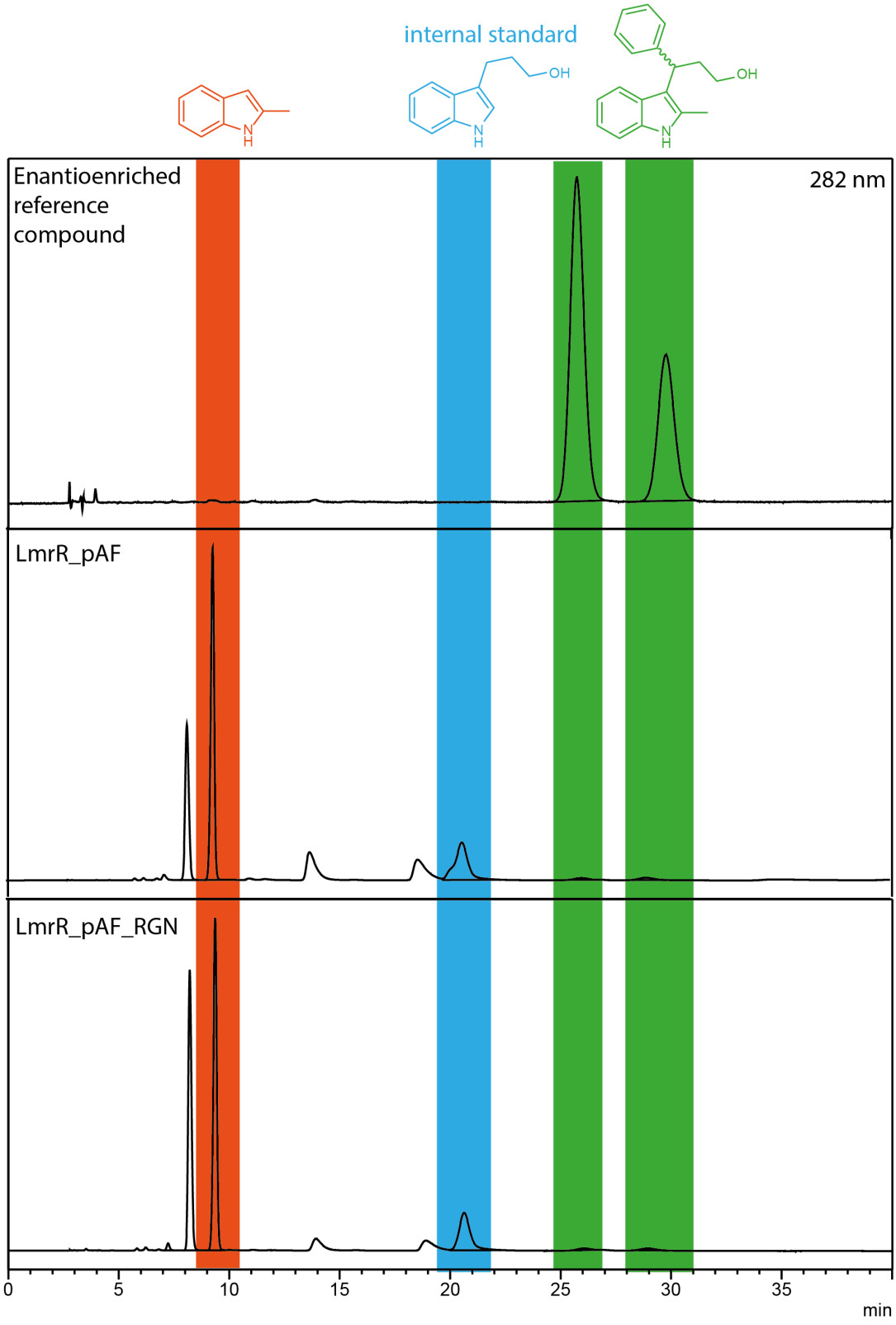

3-(1H-indol-3-yl)hexan-1-ol (3e)

Reference compound and racemic crude:

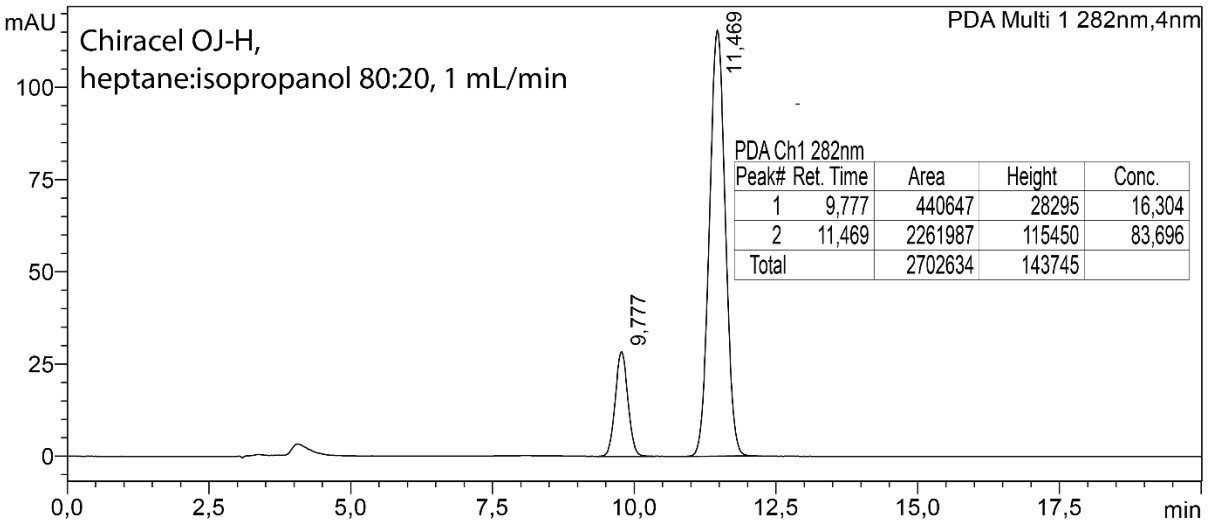

PDA Ch1 282nm

Peak#	Ret. Time	Area	Height	Conc.
1	9,777	440647	28295	16,304
2	11,469	2261987	115450	83,696
Total		2702634	143745	

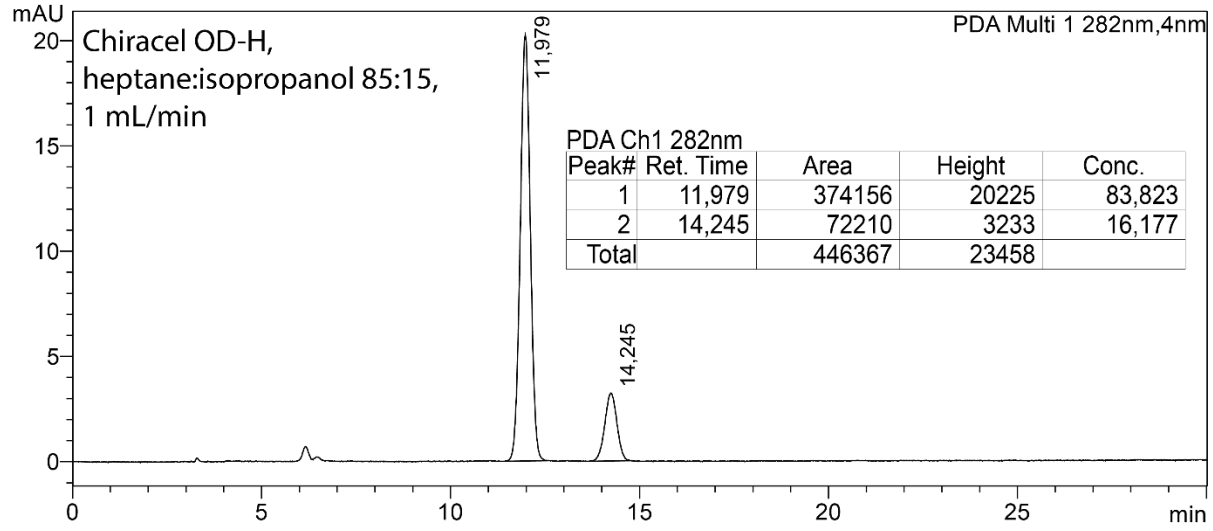

PDA Ch1 282nm

Peak#	Ret. Time	Area	Height	Conc.
1	11,979	374156	20225	83,823
2	14,245	72210	3233	16,177
Total		446367	23458	

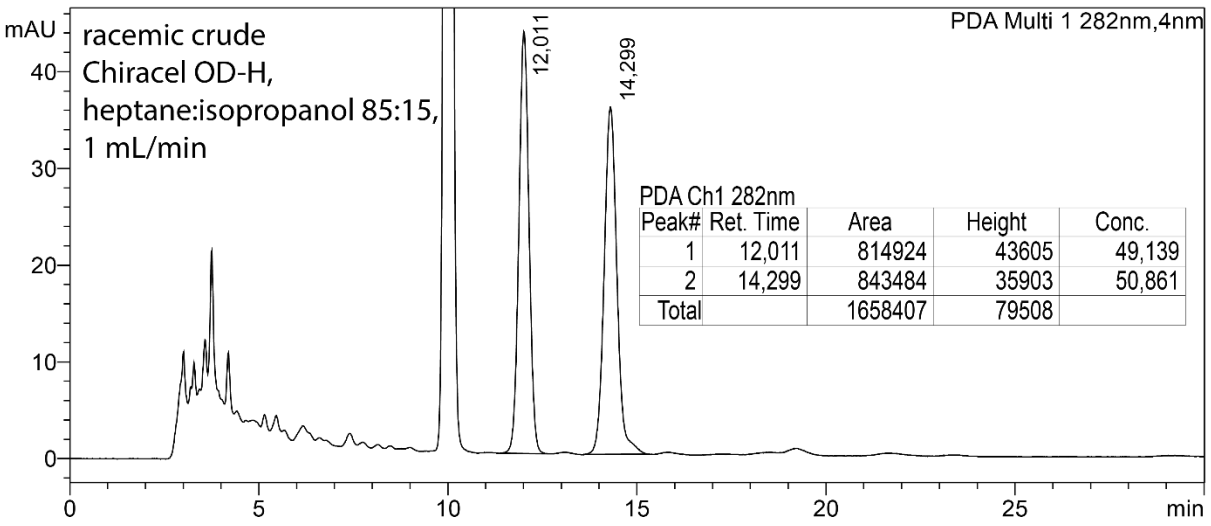

PDA Ch1 282nm

Peak#	Ret. Time	Area	Height	Conc.
1	12,011	814924	43605	49,139
2	14,299	843484	35903	50,861
Total		1658407	79508	

Artificial enzyme catalysed reaction: (Chiracel OD-H, heptane:isopropanol 85:15, 1 mL/min)

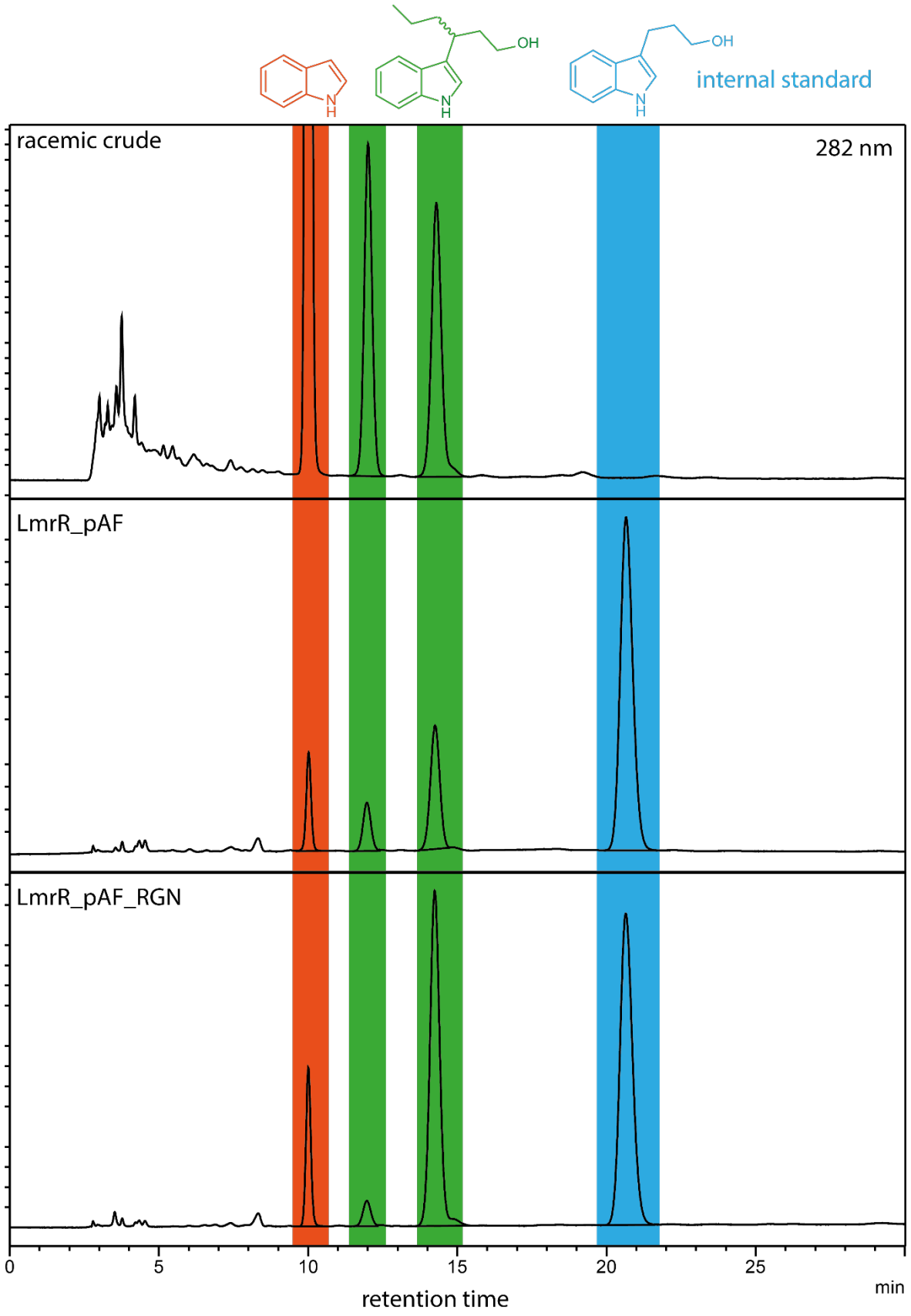

3-(5-methyl-1H-indol-3-yl)hexan-1-ol (3f)

Reference compound and racemic crude:

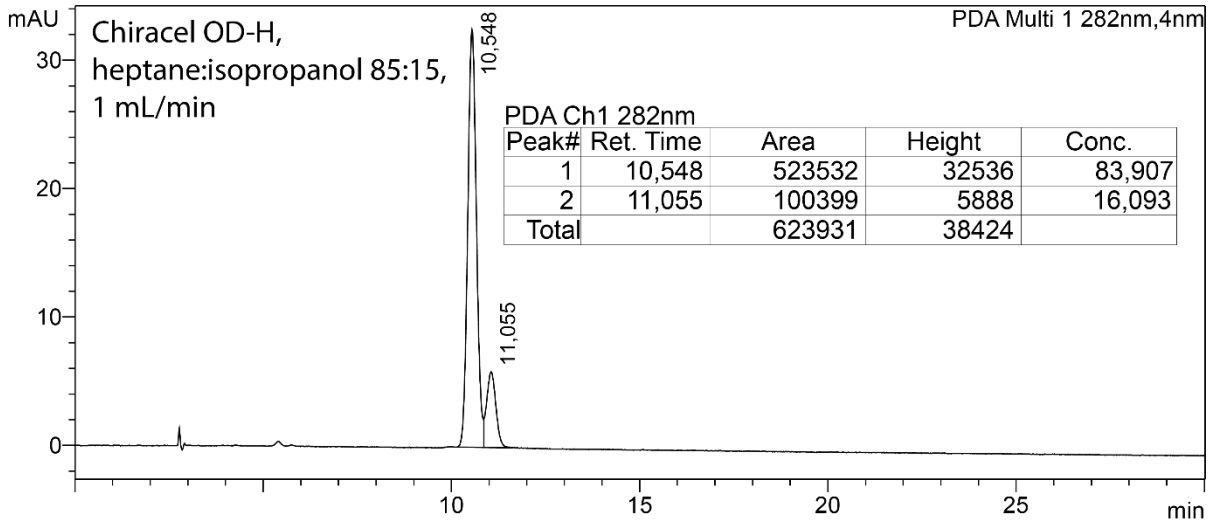

PDA Ch1 282nm

Peak#	Ret. Time	Area	Height	Conc.
1	10,548	523532	32536	83,907
2	11,055	100399	5888	16,093
Total		623931	38424	

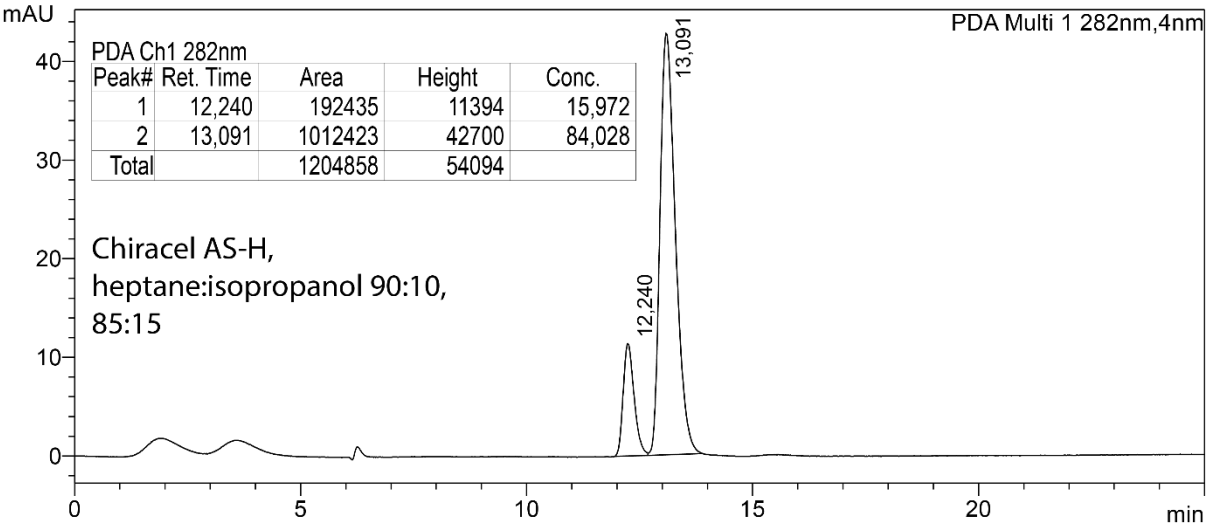

PDA Ch1 282nm

Peak#	Ret. Time	Area	Height	Conc.
1	12,240	192435	11394	15,972
2	13,091	1012423	42700	84,028
Total		1204858	54094	

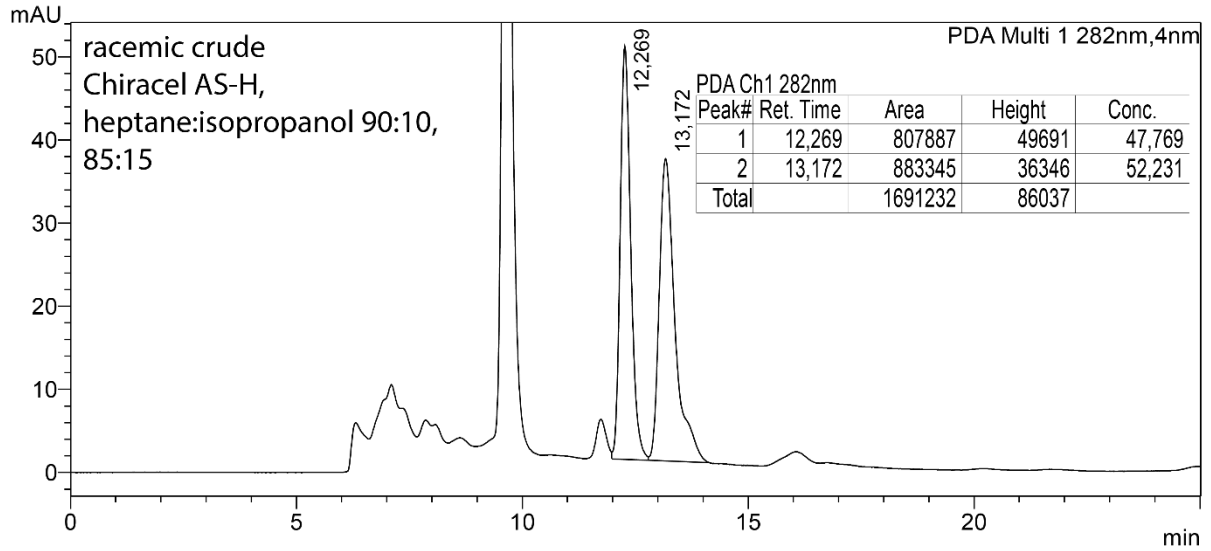

PDA Ch1 282nm

Peak#	Ret. Time	Area	Height	Conc.
1	12,269	807887	49691	47,769
2	13,172	883345	36346	52,231
Total		1691232	86037	

Artificial enzyme catalysed reaction: (Chiracel AS-H, heptane:isopropanol 90:10, 0.5 mL/min)

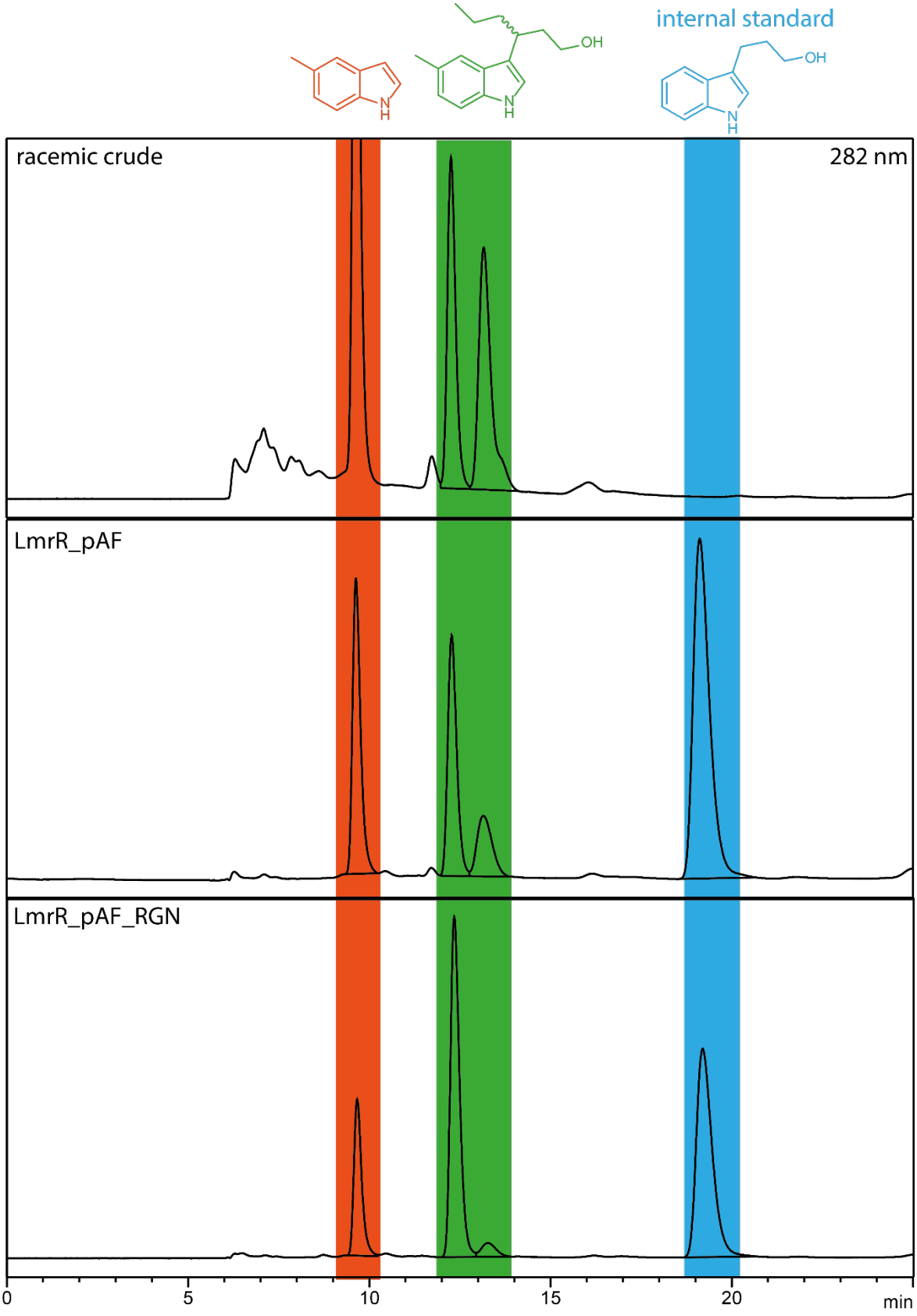

3-(5-methoxy-1H-indol-3-yl)hexan-1-ol (3g)

Reference compound and racemic crude:

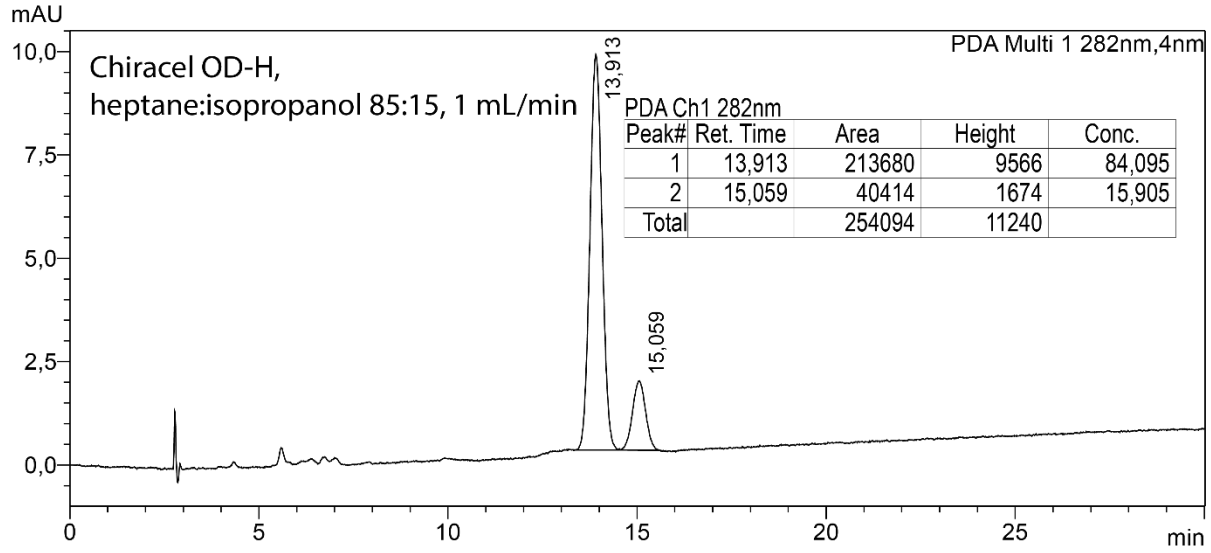

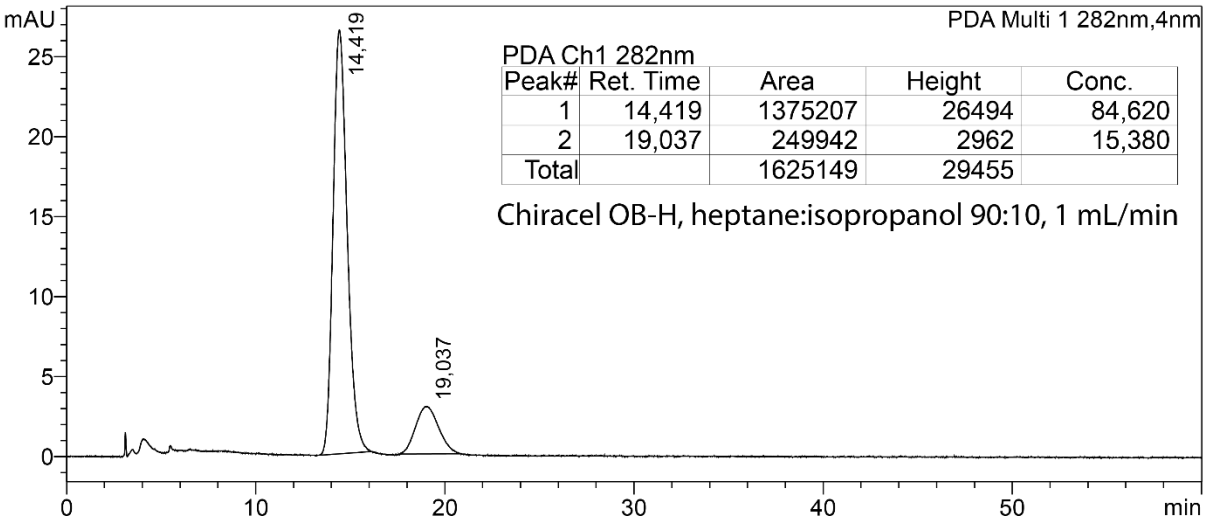

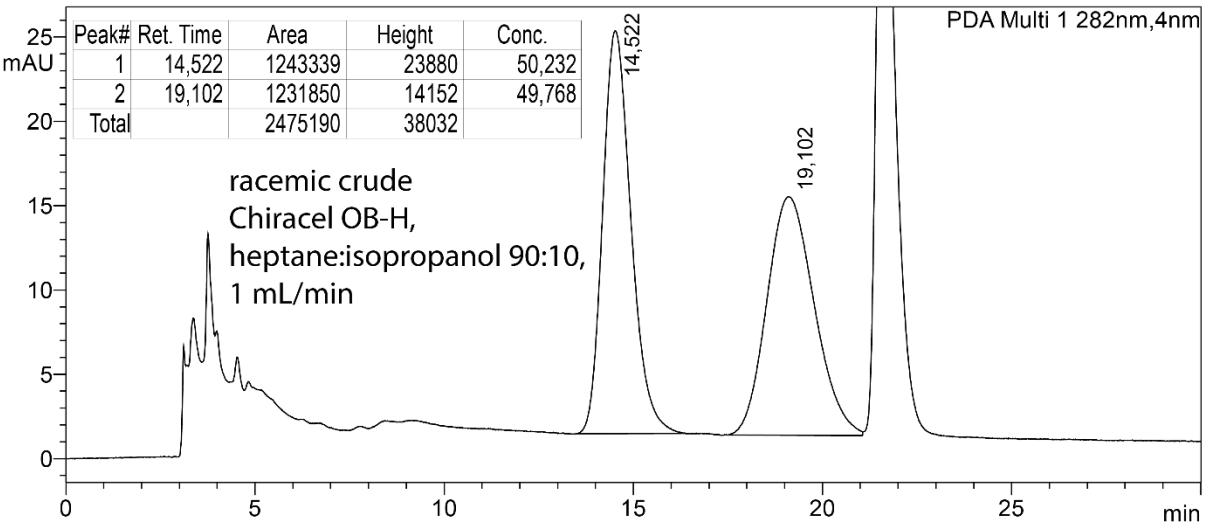

Artificial enzyme catalysed reaction: (Chiracel OB-H, heptane:isopropanol 90:10, 1 mL/min)

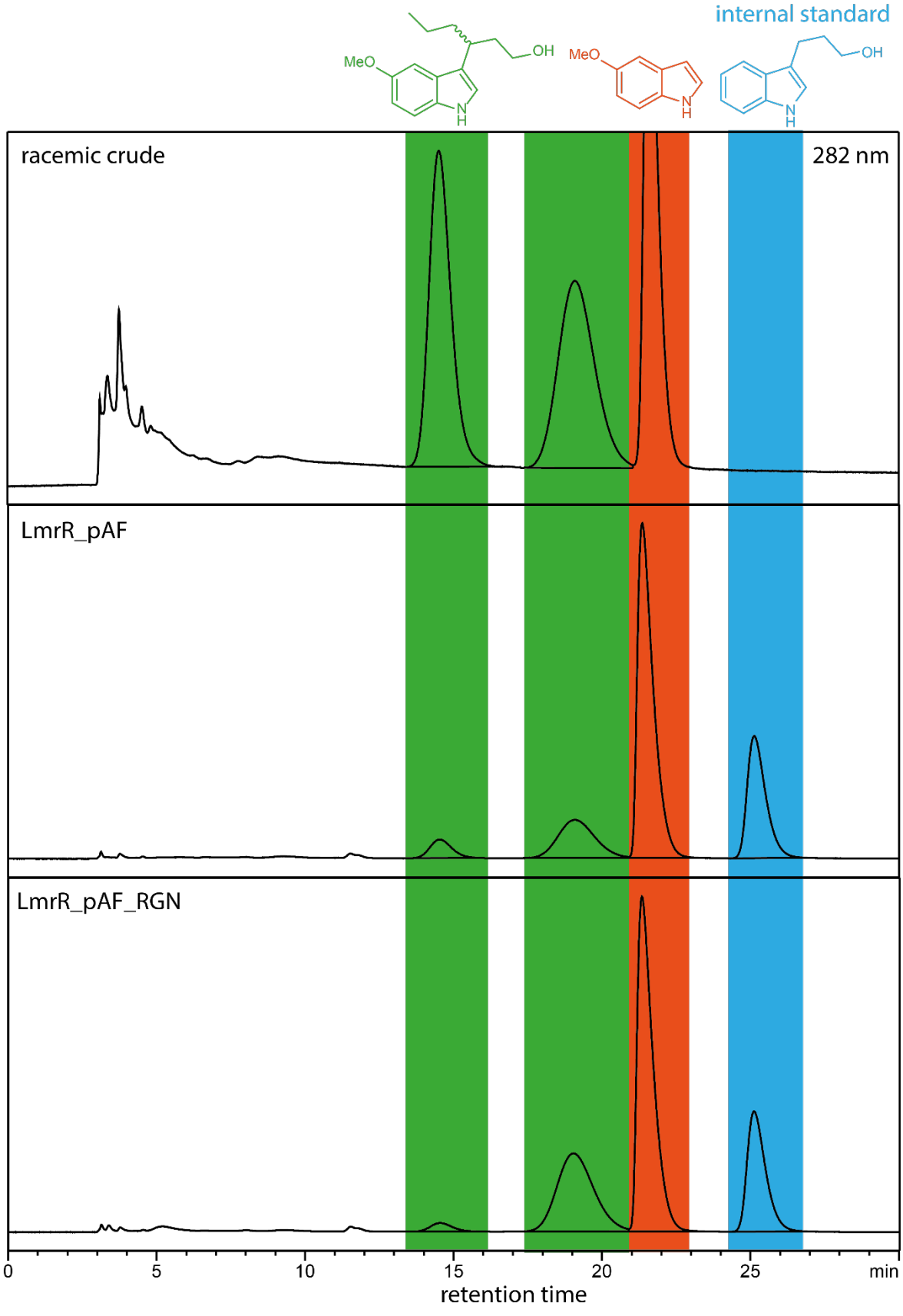

3-(5-bromo-1H-indol-3-yl)hexan-1-ol (3h)

Reference compound and racemic crude:

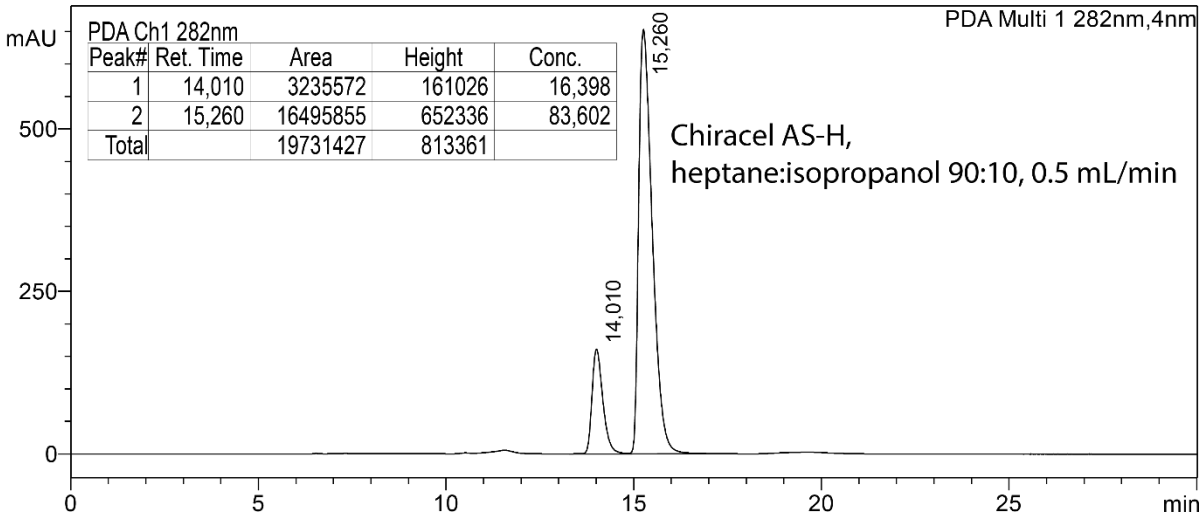

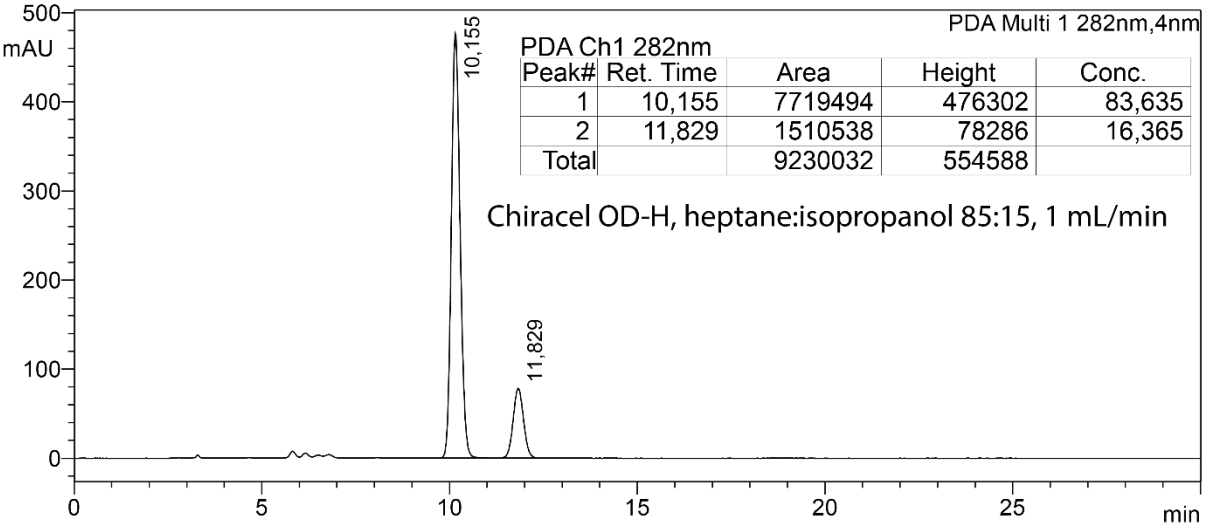

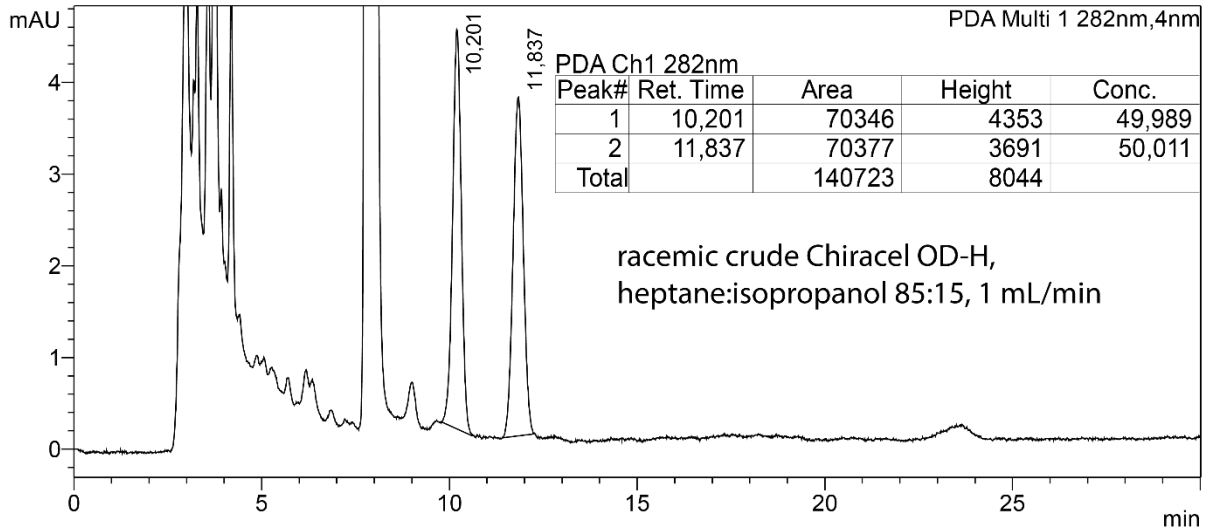

3-(5-methoxy-2-methyl-1H-indol-3-yl)hexan-1-ol (3i)

Reference compound and racemic crude:

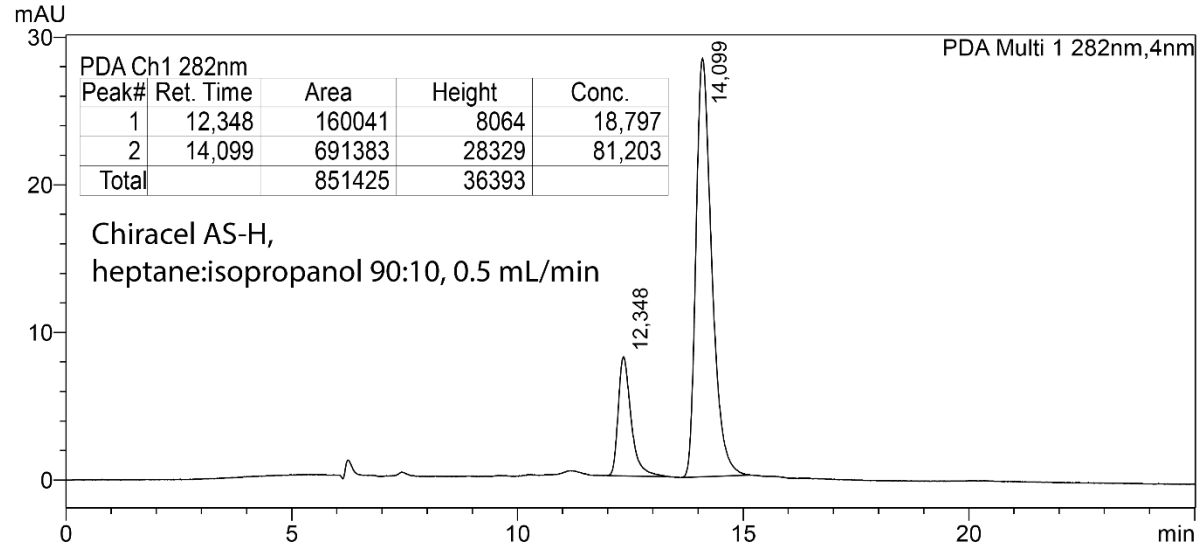

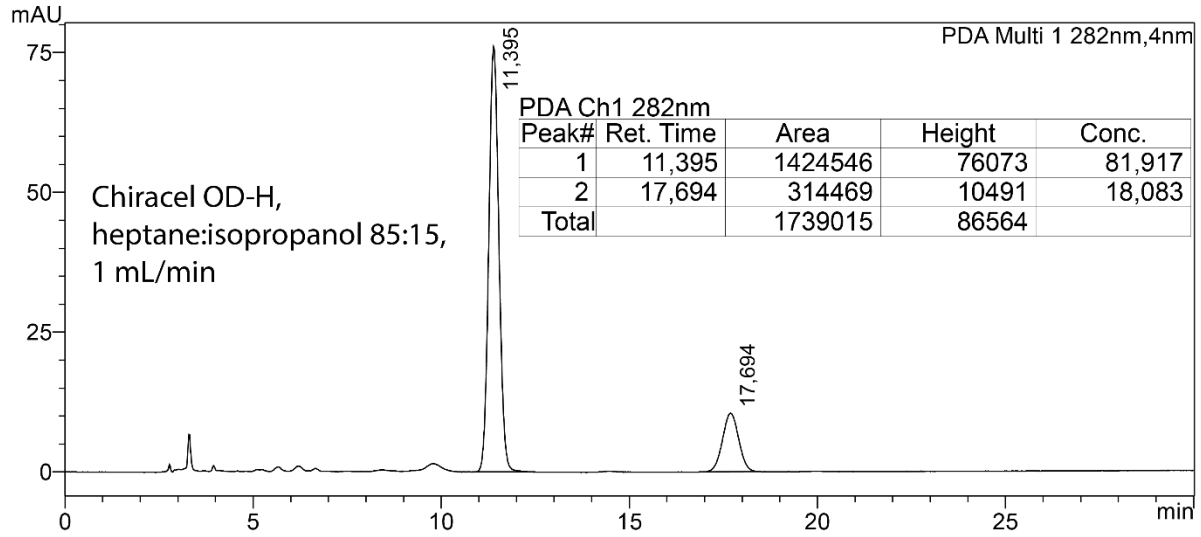

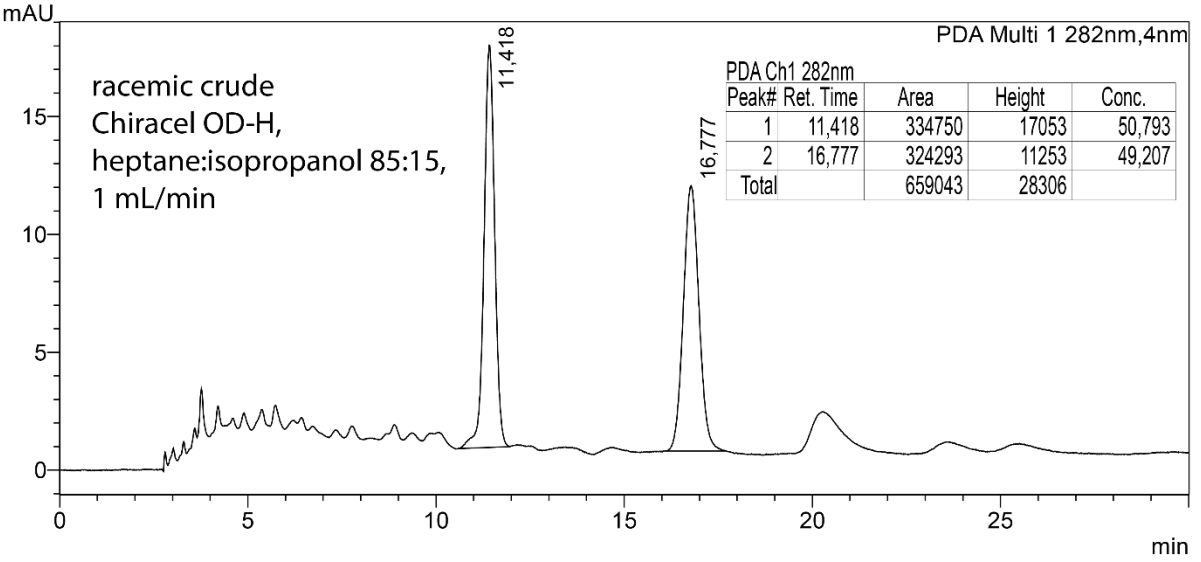

Artificial enzyme catalysed reactions: (Chiracel OD-H, heptane:isopropanol 85:15, 1 mL/min)

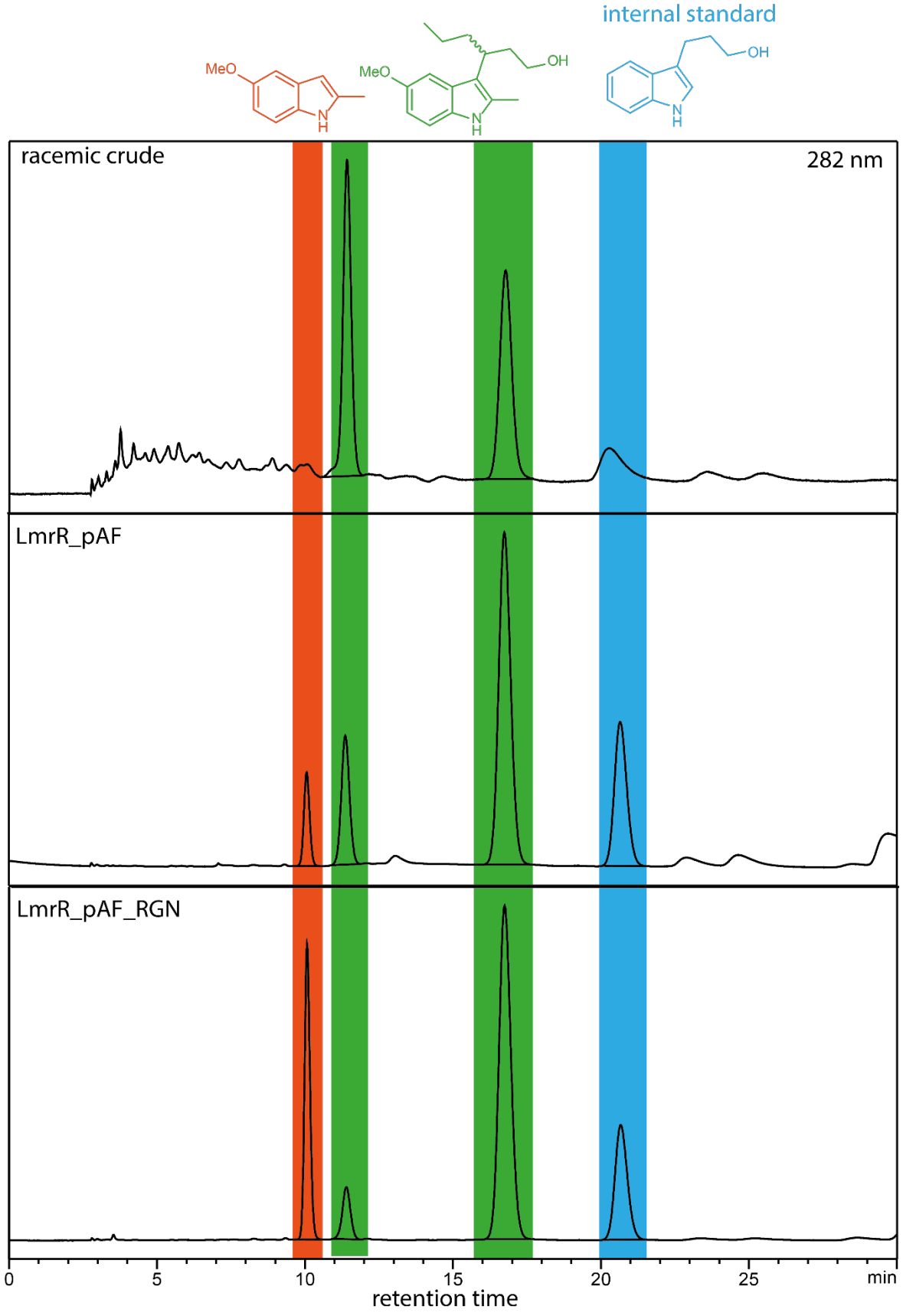

10. NMR Spectra

3-(2-methyl-1H-indol-3-yl)hexan-1-ol (3a)

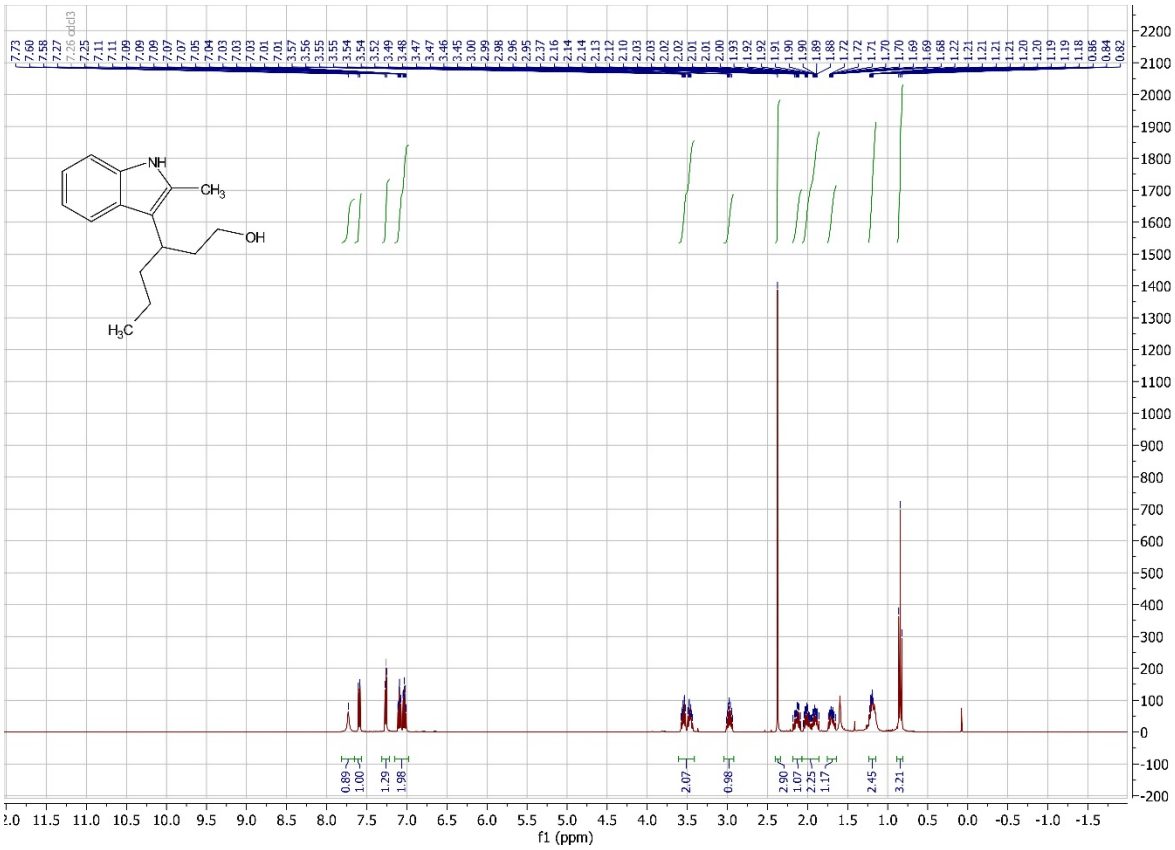

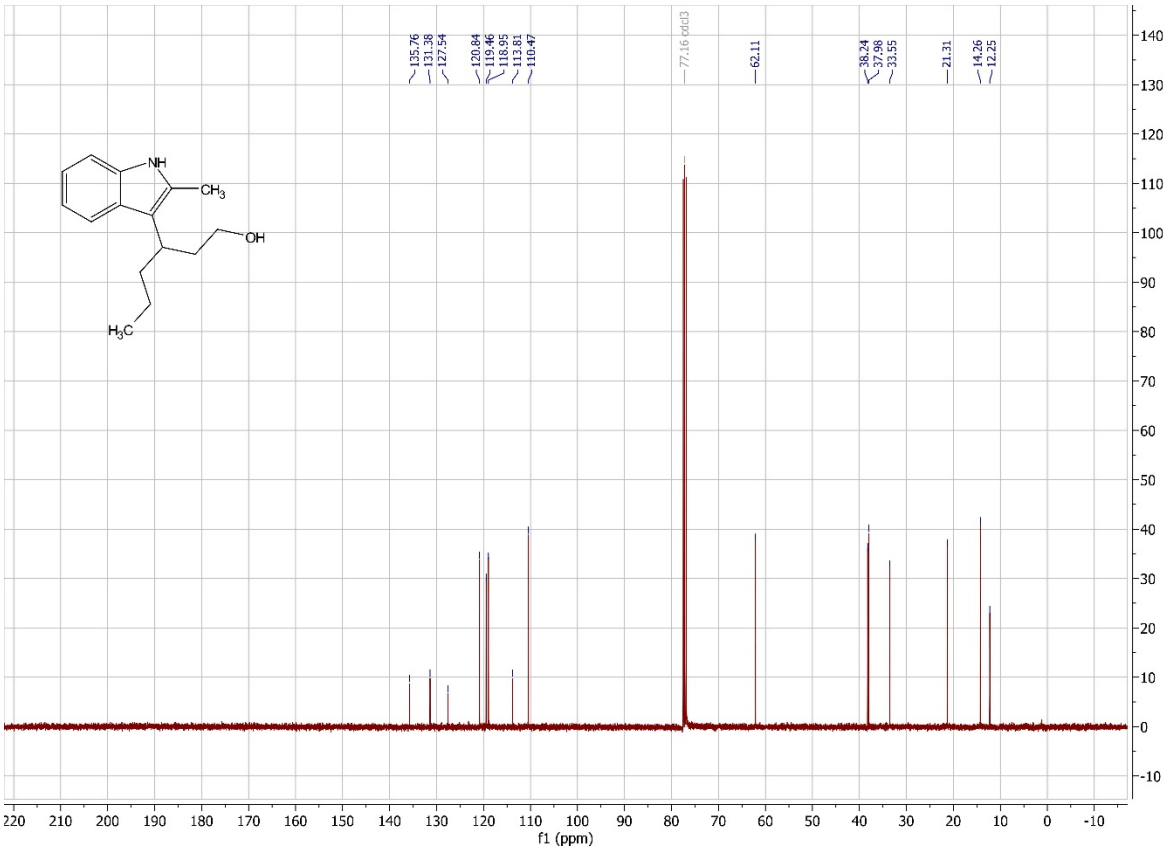

4-methyl-3-(2-methyl-1H-indol-3-yl)pentan-1-ol (3b)

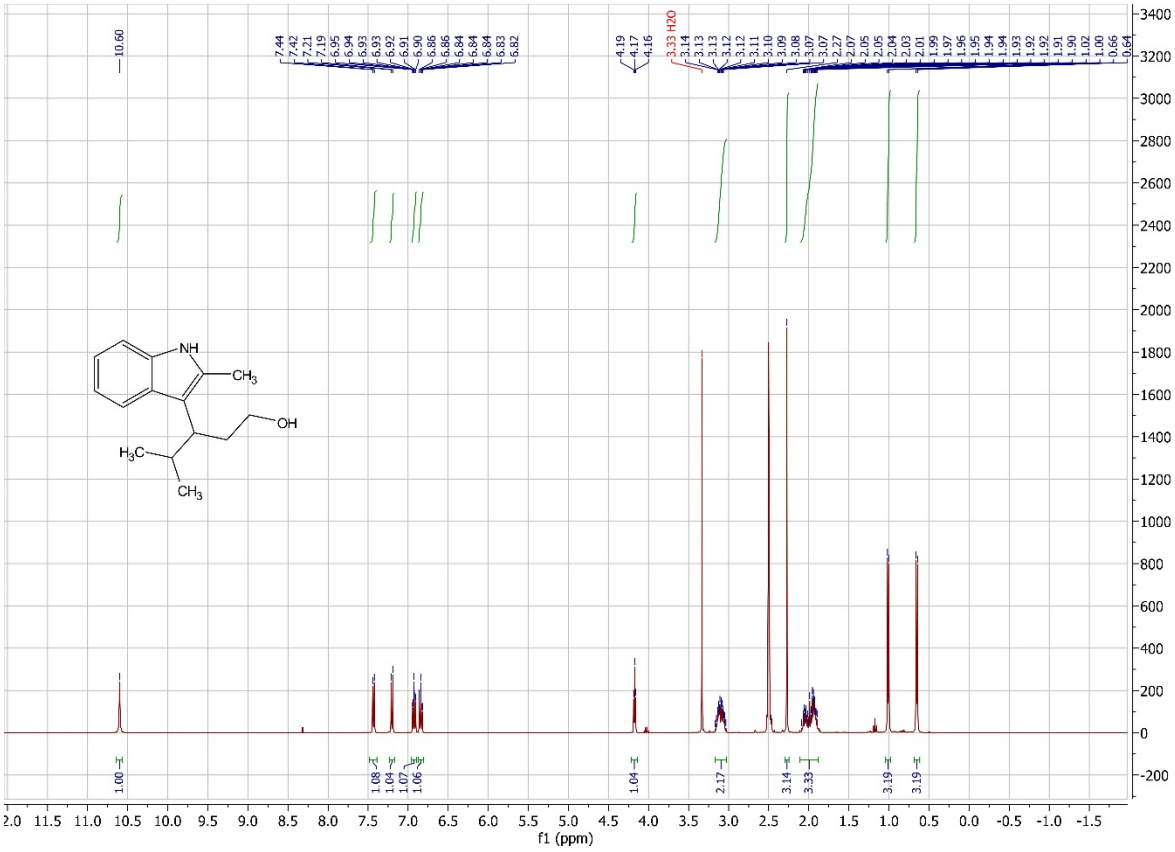

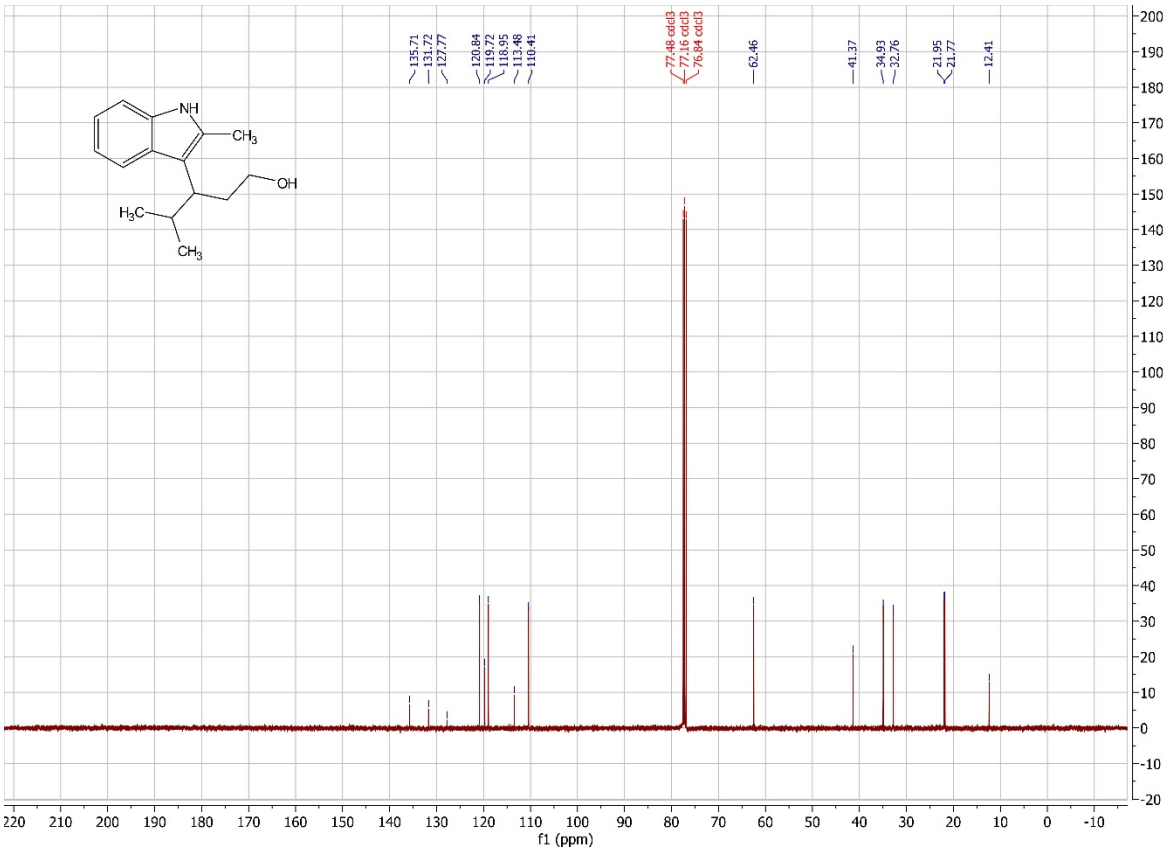

3-(2-methyl-1H-indol-3-yl)butan-1-ol (3c)

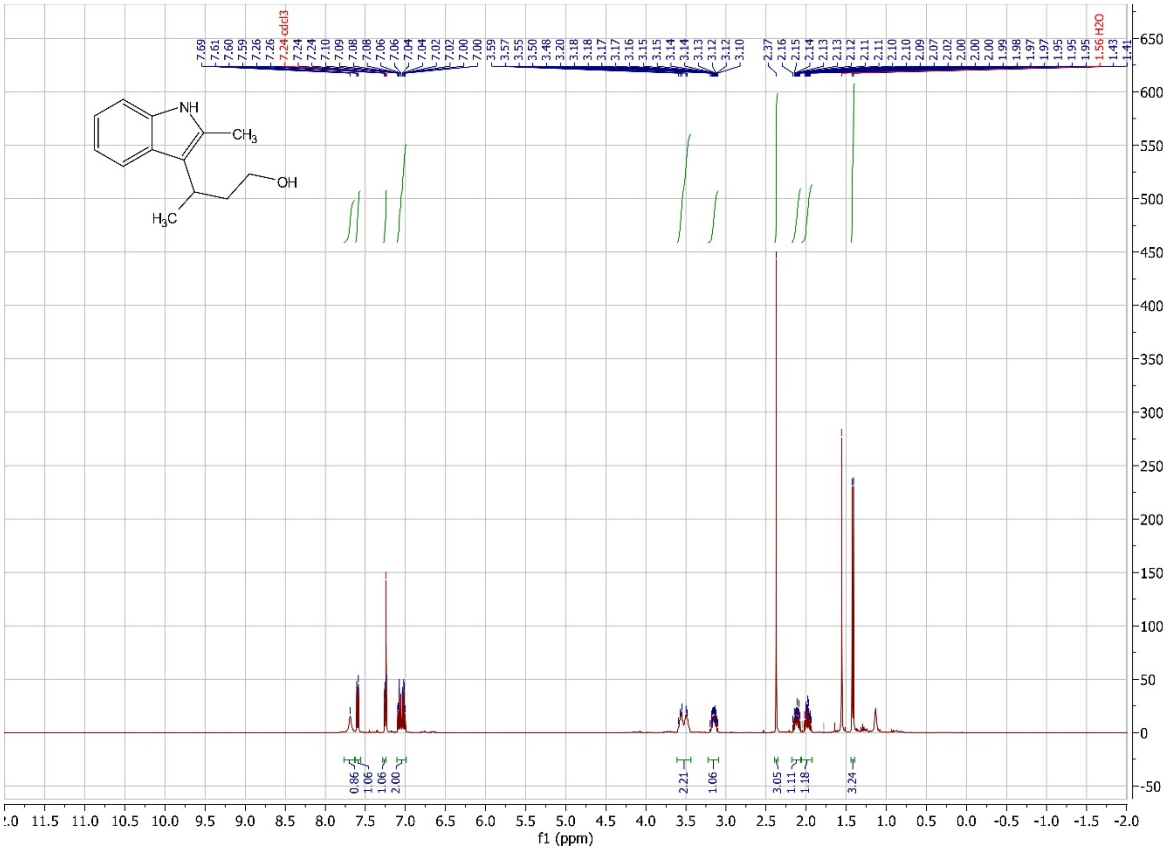

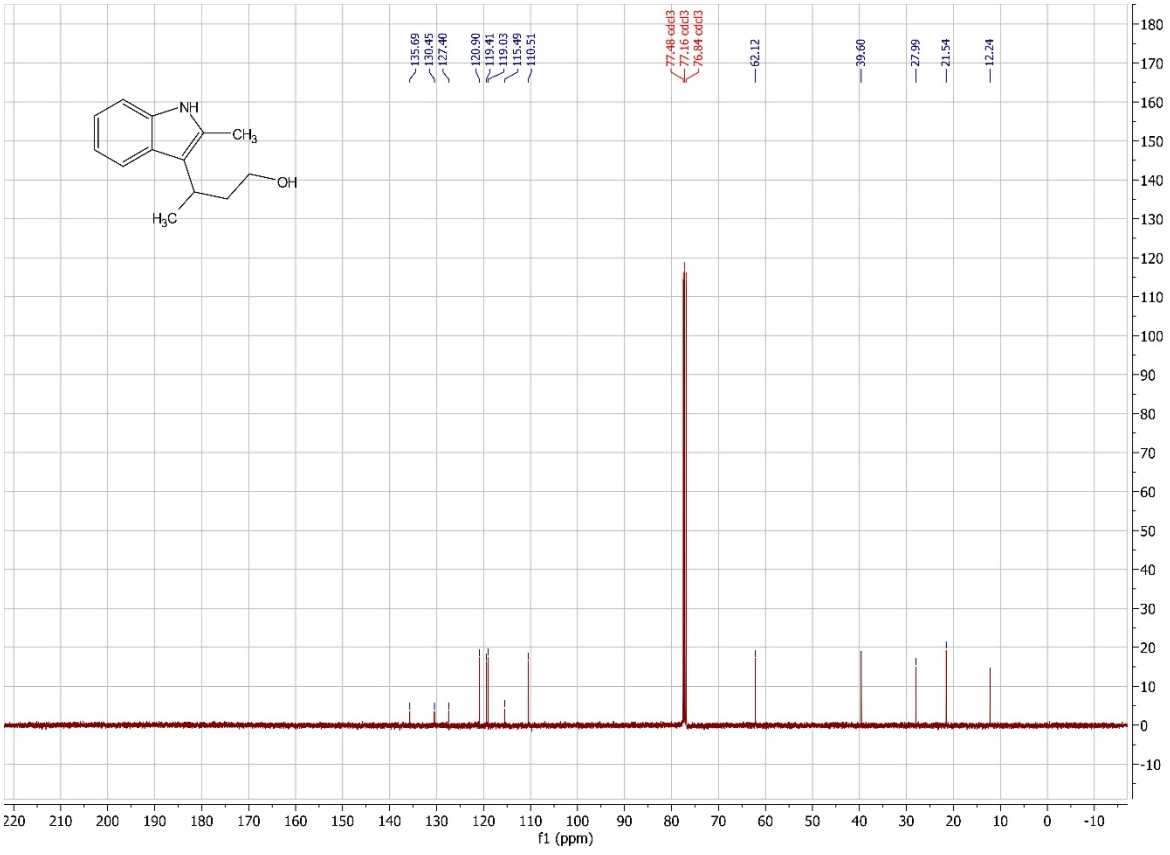

3-(2-methyl-1H-indol-3-yl)-3-phenylpropan-1-ol (3d)

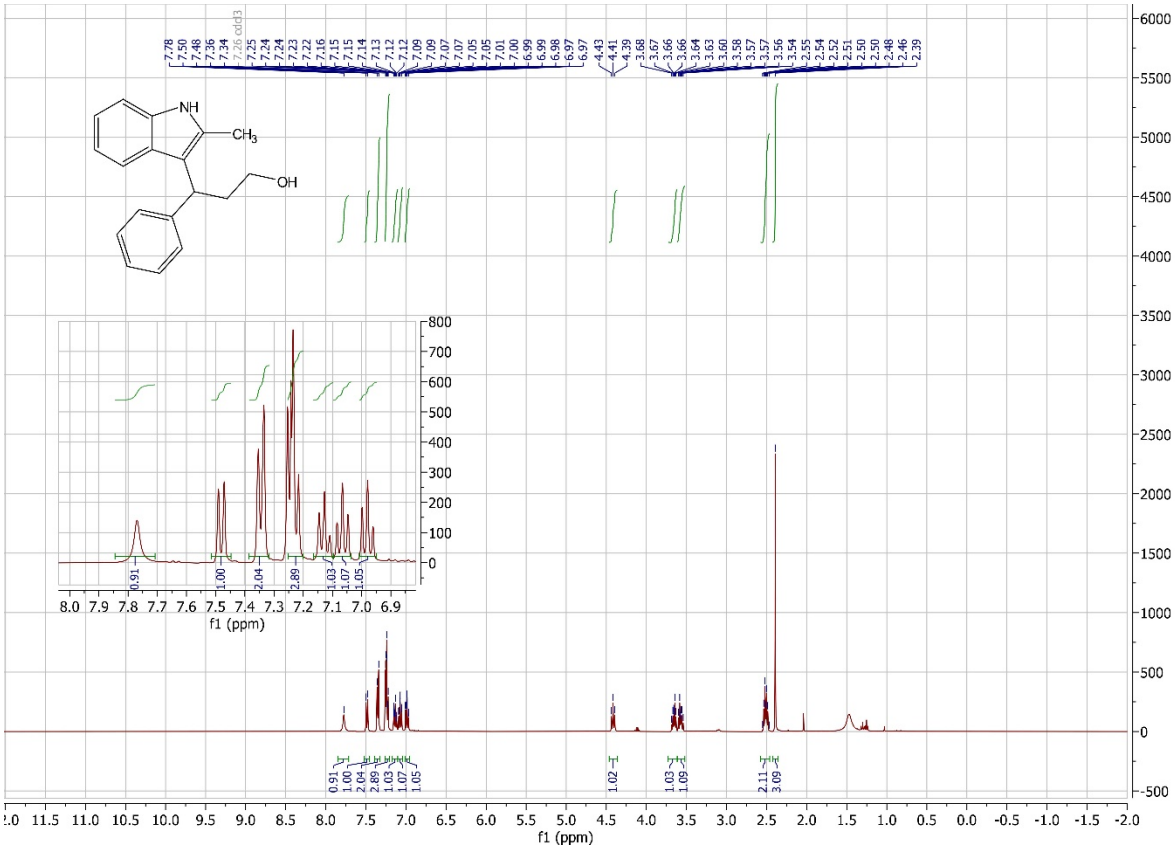

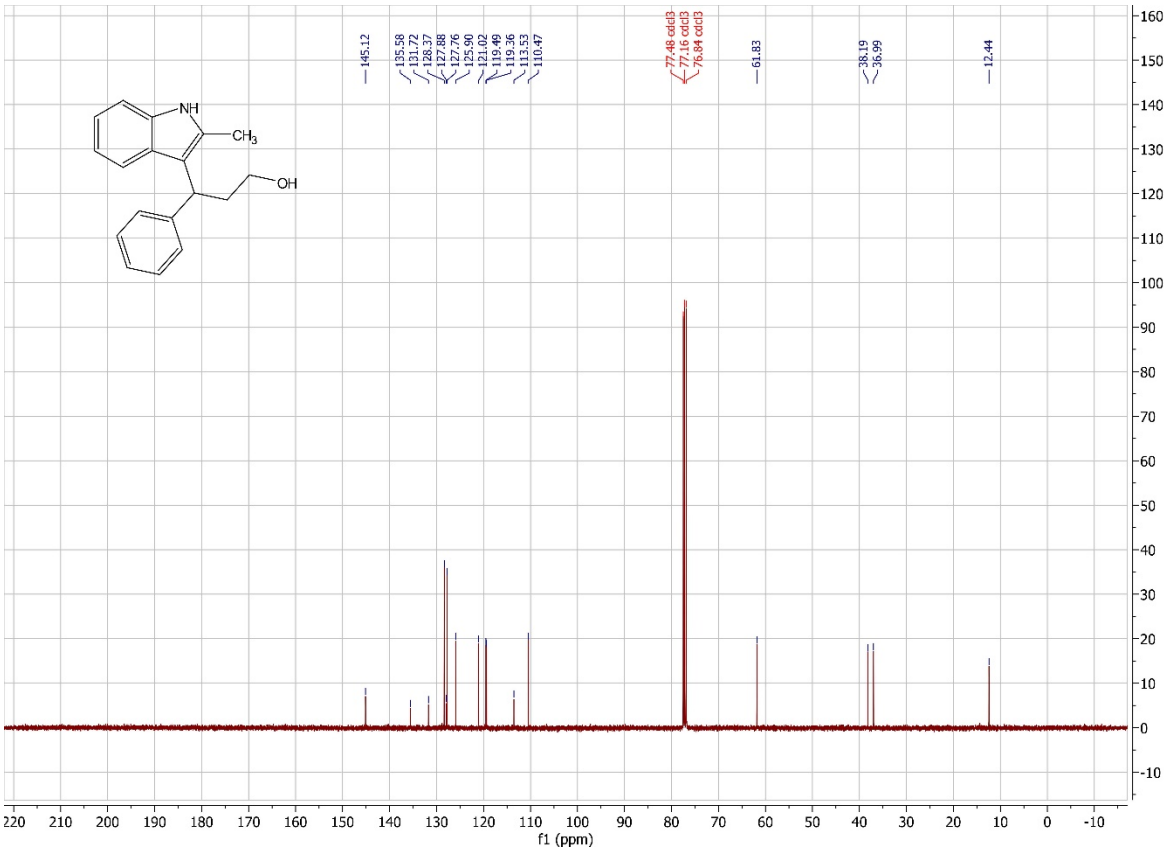

3-(1H-indol-3-yl)hexan-1-ol (3e)

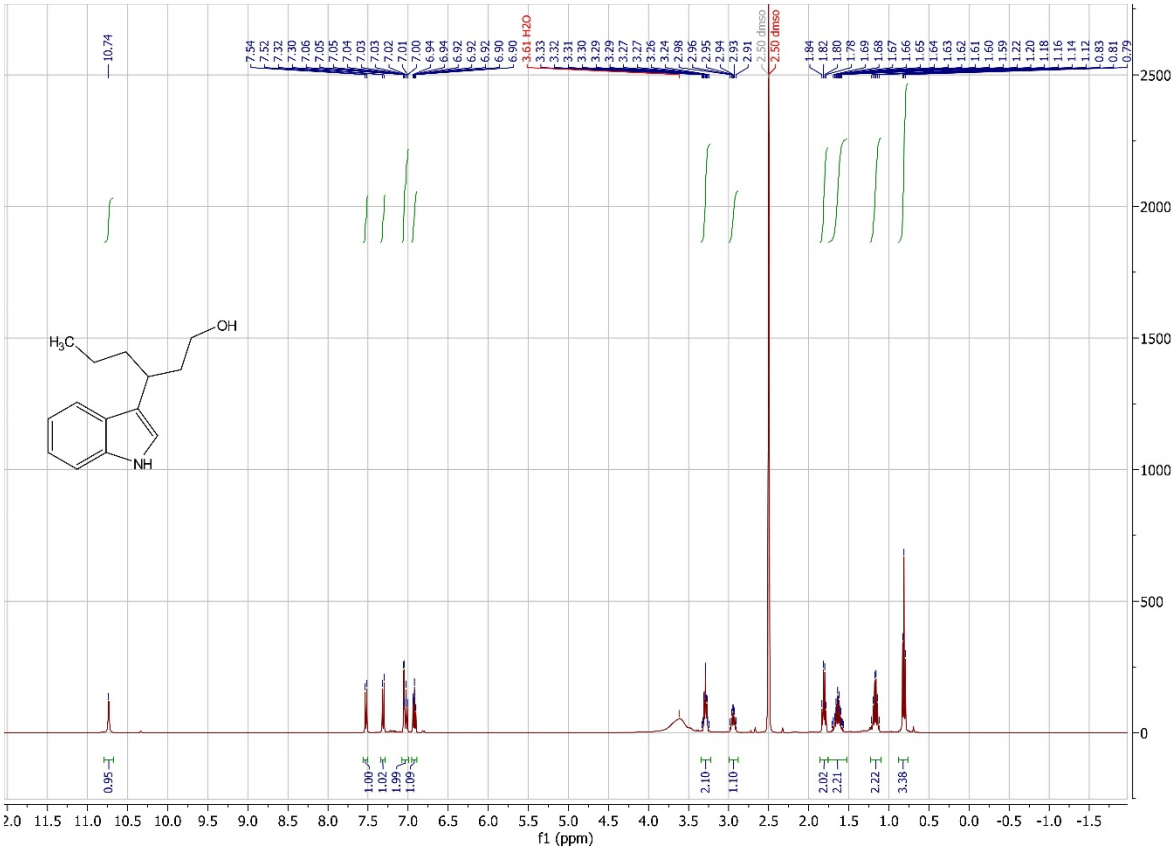

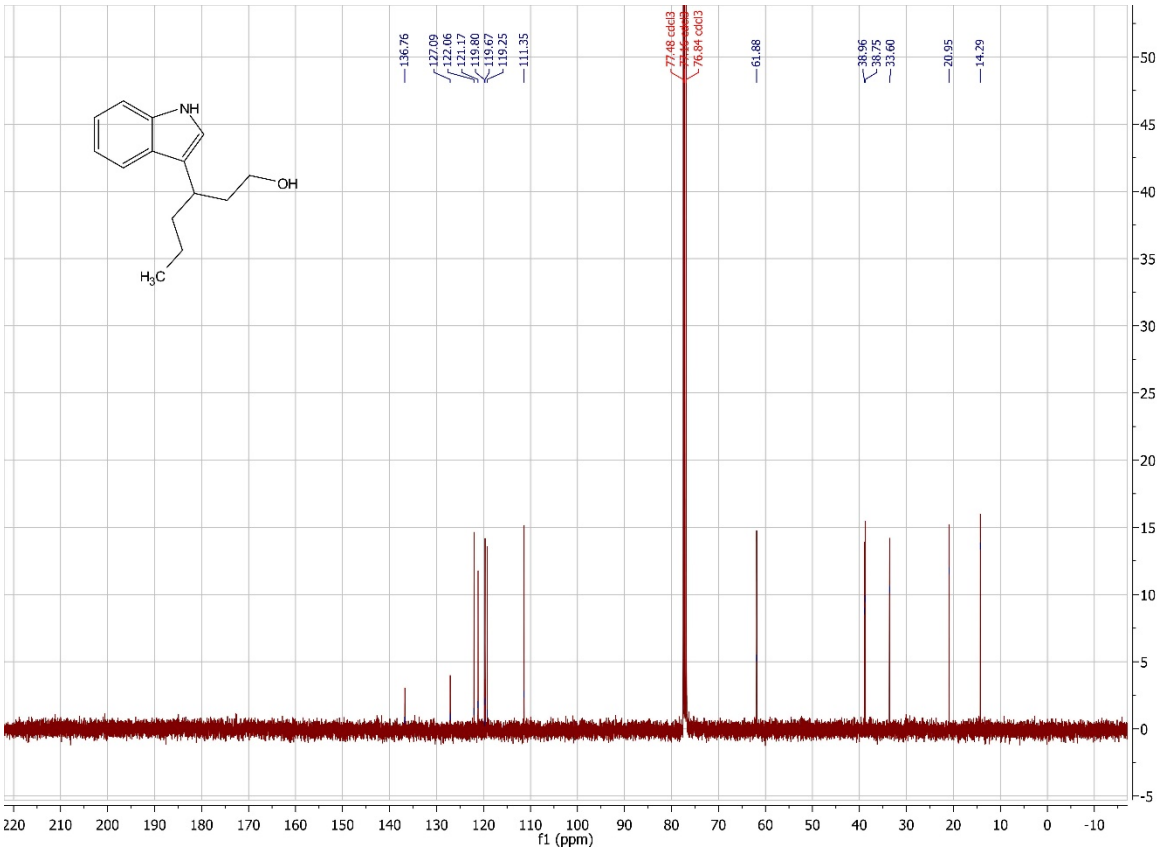

3-(5-methyl-1H-indol-3-yl)hexan-1-ol (3f)

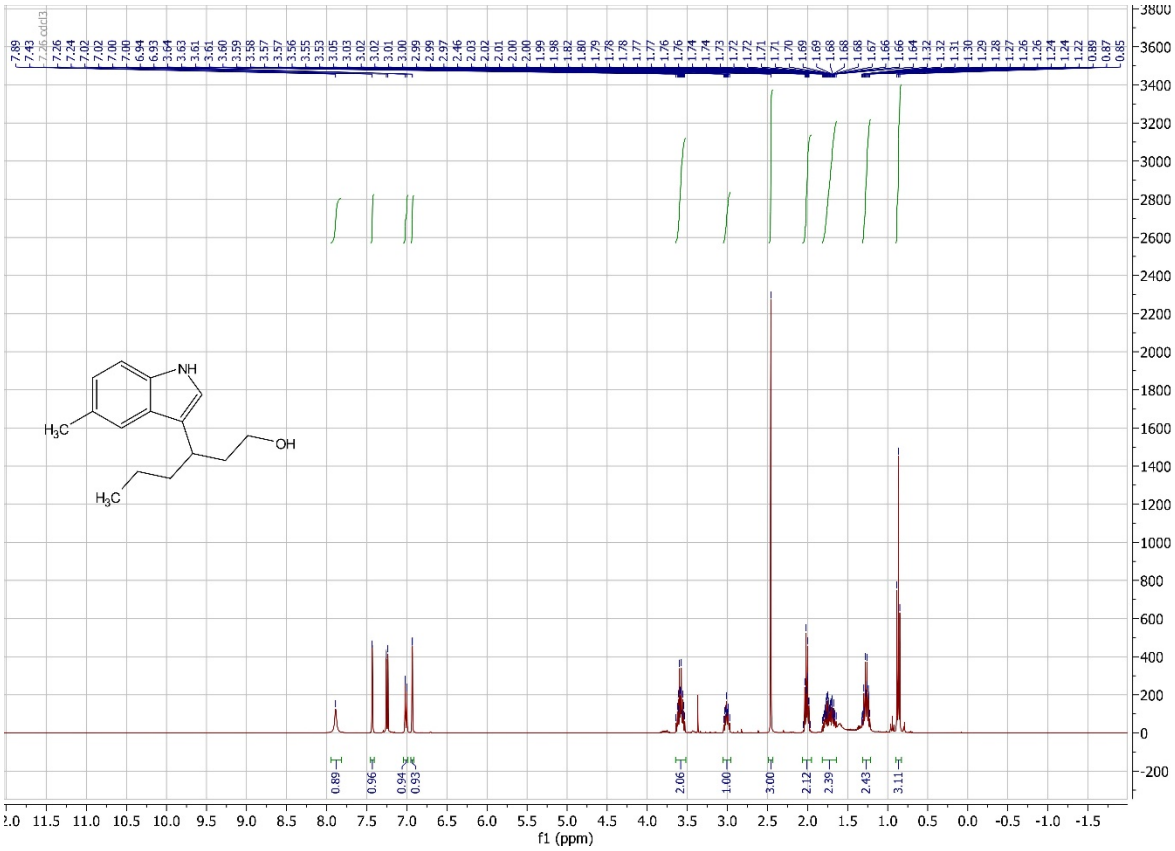

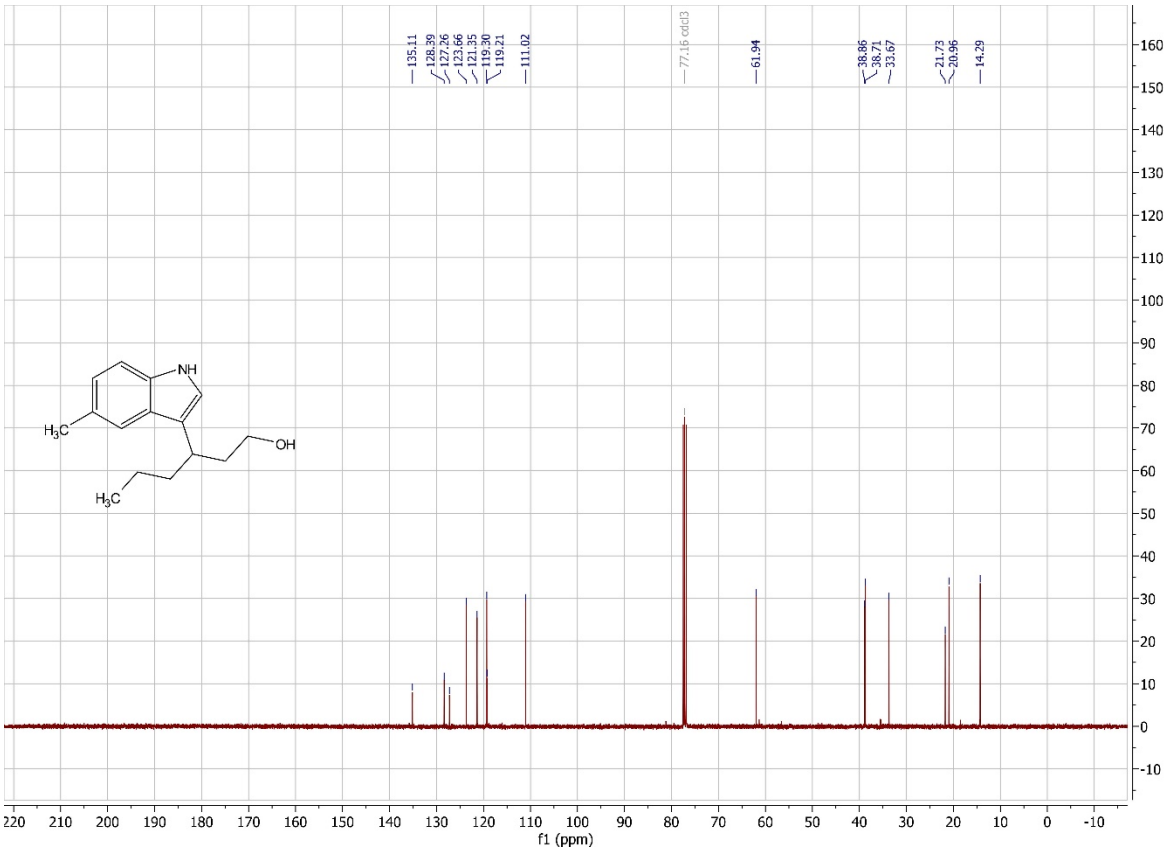

3-(5-methoxy-1H-indol-3-yl)hexan-1-ol (3g)

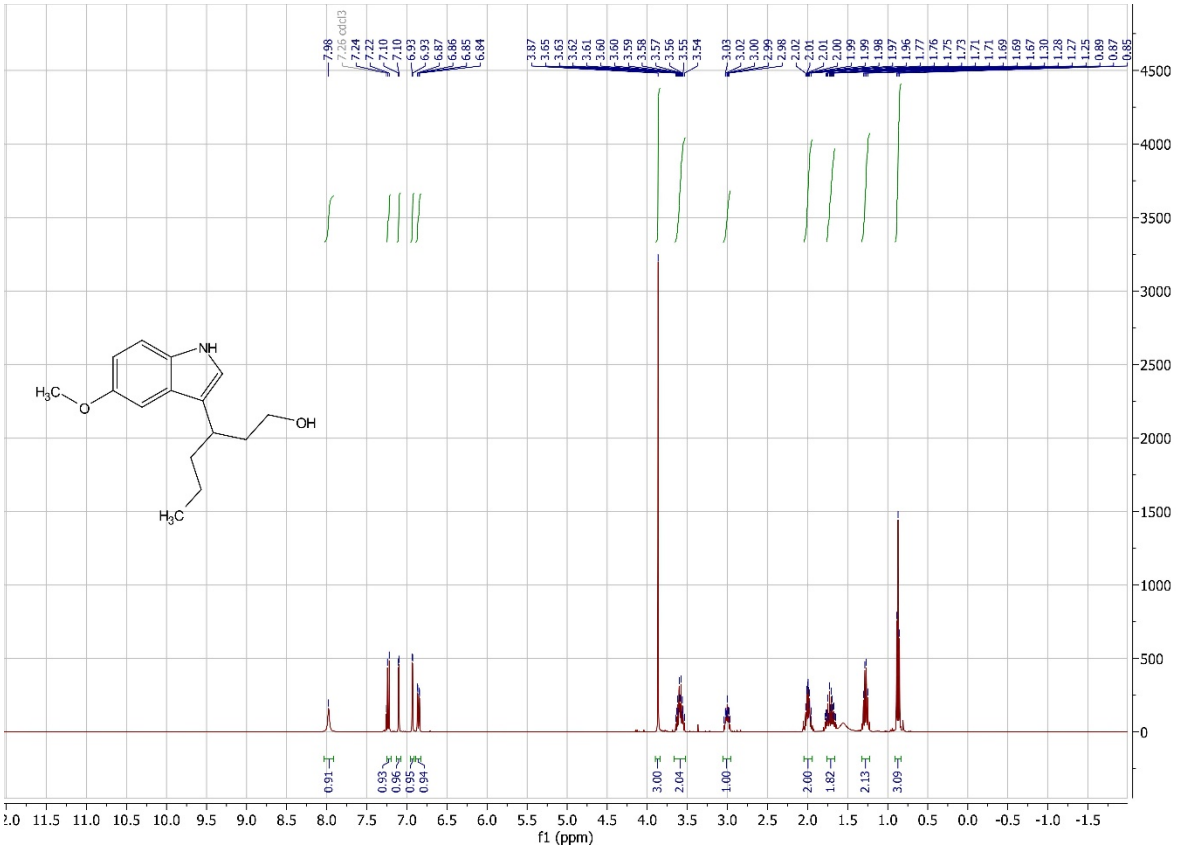

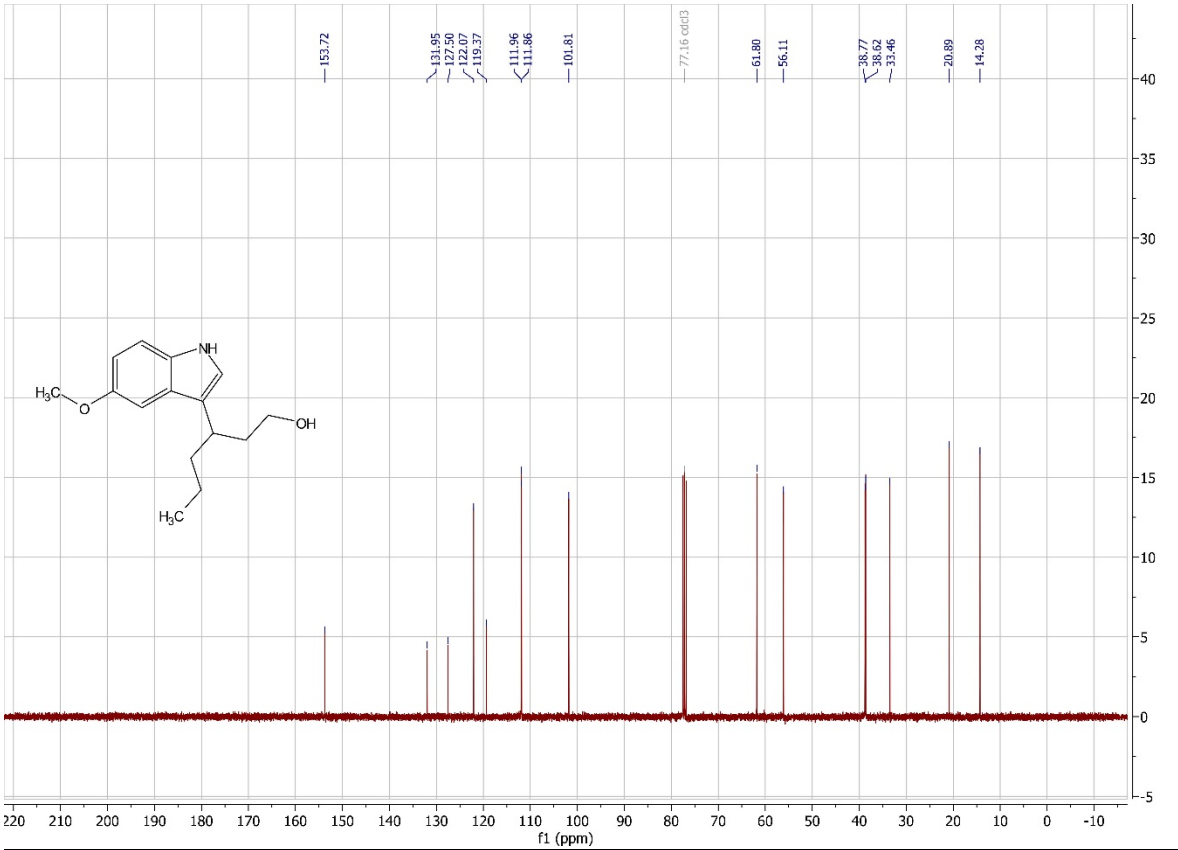

3-(5-bromo-1H-indol-3-yl)hexan-1-ol (3h)

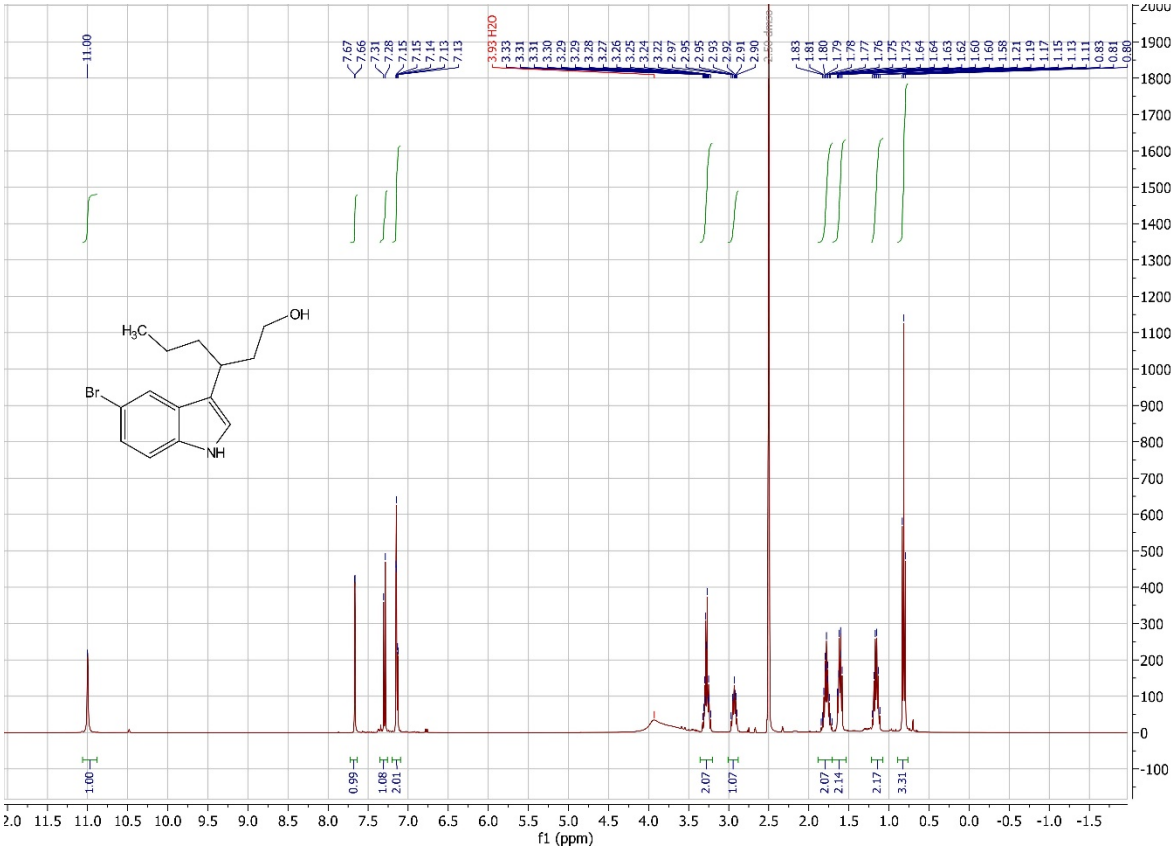

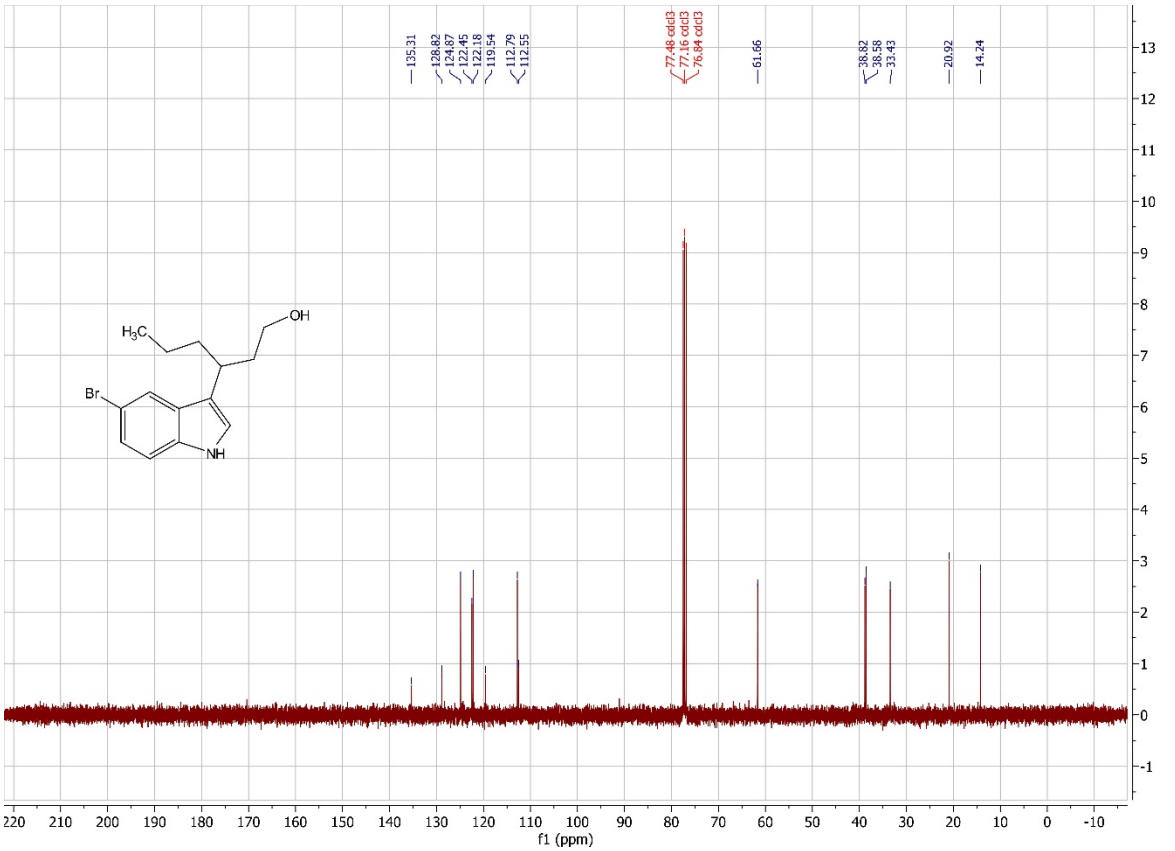

3-(5-methoxy-2-methyl-1H-indol-3-yl)hexan-1-ol (3i)

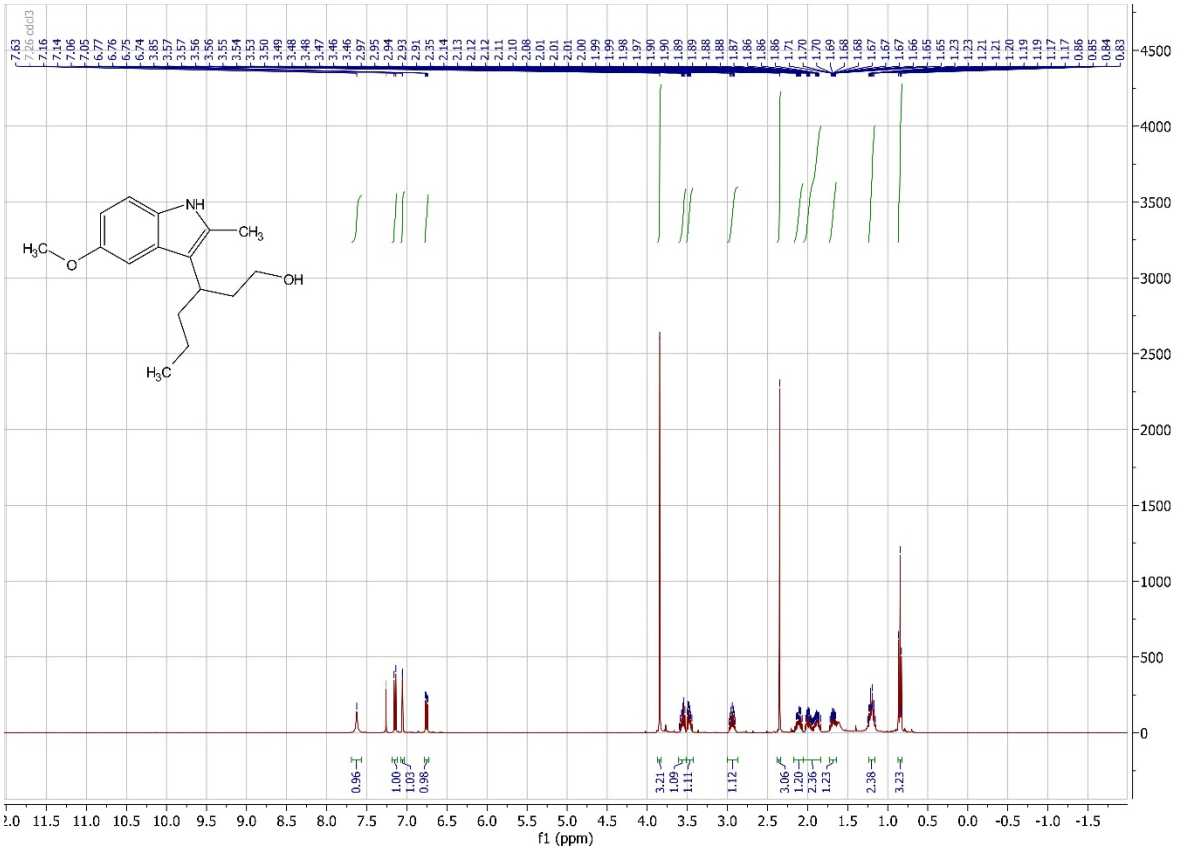

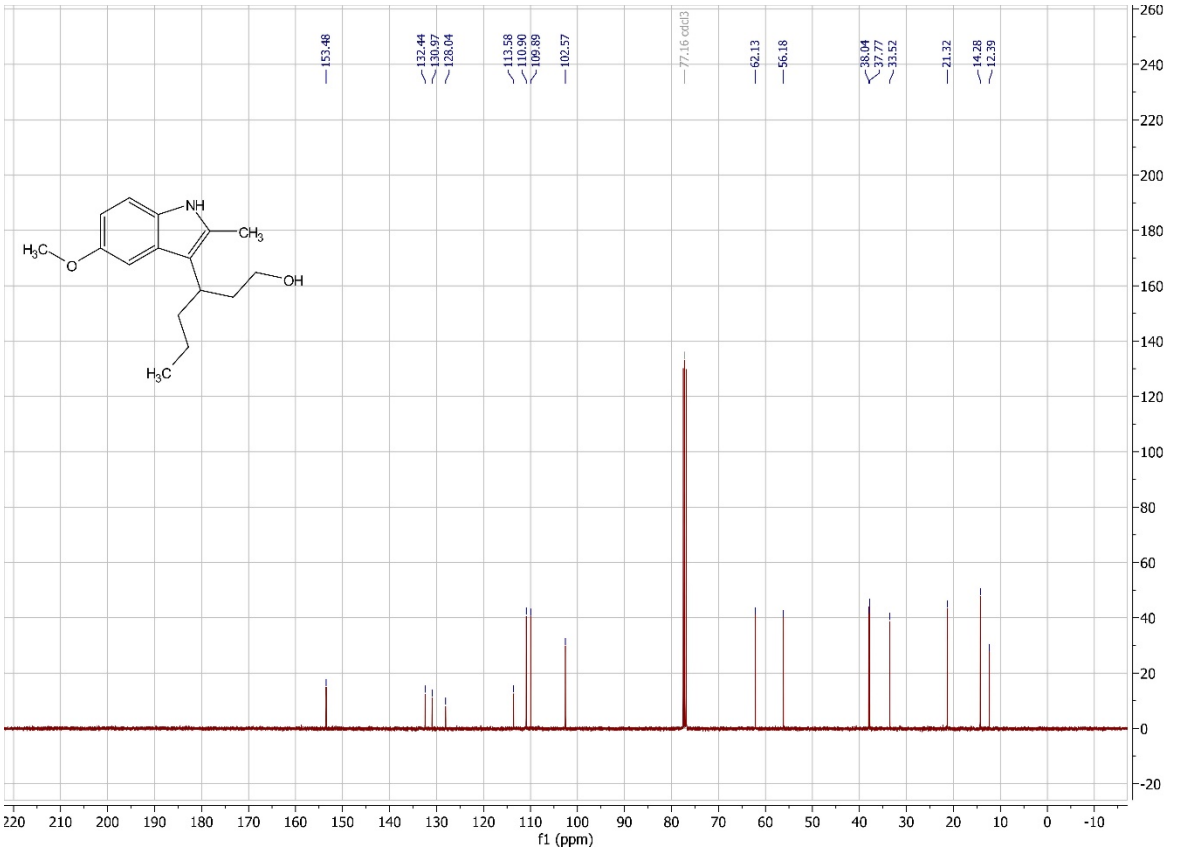

References

(1) Drienovská, I.; Mayer, C.; Dulson, C.; Roelfes, G. A Designer Enzyme for Hydrazone and Oxime Formation Featuring an Unnatural Catalytic Aniline Residue. *Nature Chemistry* **2018**, *10*, 946–952. https://doi.org/10.1038/s41557-018-0082-z.

(2) Chordia, S.; Narasimhan, S.; Lucini Paioni, A.; Baldus, M.; Roelfes, G. In Vivo Assembly of Artificial Metalloenzymes and Application in Whole-Cell Biocatalysis. *Angew. Chem. Int. Ed.* **2021**, anie.202014771. https://doi.org/10.1002/anie.202014771.

(3) Mayer, C.; Dulson, C.; Reddem, E.; Thunnissen, A.-M. W. H.; Roelfes, G. Directed Evolution of a Designer Enzyme Featuring an Unnatural Catalytic Amino Acid. *Angew. Chem. Int. Ed.* **2019**, *131* (7), 2083–2087. https://doi.org/10.1002/ange.201813499.

(4) Im, H. The Inoue Method for Preparation and Transformation of Competent E. Coli: "Ultra Competent" Cells. *Bio-101* **2011**, e143. https://doi.org/10.21769/BioProtoc.143.

(5) Sullivan, B.; Walton, A. Z.; Stewart, J. D. Library Construction and Evaluation for Site Saturation Mutagenesis. *Enzyme and Microbial Technology* **2013**, *53* (1), 70–77. https://doi.org/10.1016/j.enzmictec.2013.02.012.

(6) Denhart, D. J.; Mattson, R. J.; Ditta, J. L.; Macor, J. E. One-Pot Synthesis of Homotryptamines from Indoles. *Tetrahedron Letters* **2004**, *45* (19), 3803–3805. https://doi.org/10.1016/j.tetlet.2004.03.070.